JNC TJ7400 2002-004

割れ目系岩盤を対象とした地質構造のモデル化に関する研究

（核燃料サイクル開発機構　委託研究成果報告書）

2002年3月

埼玉大学　地圏科学研究センター

2002年3月

割れ目系岩盤を対象とした地質構造のモデル化に関する研究

長田昌彦*，渡辺邦夫*

要旨

割れ目系岩盤中の地下水流動は，ダム建設，トンネル掘削，岩盤内の水資源開発，廃棄物の地層処分などの地盤工学的な問題を取り扱ううえで非常に重要なものとなっている。地下水流動解析を実施するためには，割れ目系岩盤の水理地質学的なモデルを適切に構築しなければならない。割れ目系岩盤では，チャンネルと呼ばれる水みちを通して地下水が流動していることが認識されており，このチャンネルネットワークを実岩盤において適切に評価し，信頼性の高いモデルを構築することが重要である。

Part Iでは，岐阜県東濃地域（東西4 km x 南北6 km x 深さ3 km領域）を対象としてチャンネルネットワークモデルを構築し，地下水流動解析を実施した。ここでチャンネルネットワークモデルの構築には，MIUサイトで得られた4本の1000mボーリングデータ(AN1, MIU1, MIU2及びMIU3)を用い，解析には新たに改良を加えたDon-Chanモデルを使用した。これらの検討により，MIUサイトには6パターンの主要割れ目が発達すること，このモデル化による解析ではMIU2ボーリングに見られる月吉断層上下の水圧差をうまく表現できること，さらに地下水解析結果に与える境界条件の影響を明らかにしたなどの結論が得られた。

Part IIでは，割れ目系岩盤の水理地質学的なモデル化に際して，割れ目の方向・頻度分布のみからの推定ではなく，岩石の物性を含めた検討をすることによって，これまでの割れ目系岩盤のモデル化の信頼性向上が見込めるかを検討した。岩石コアの力学的な物性値を得るために，エコーチップ反撥試験装置を用いた。このような簡便で客観的な指標を導入することで，断層幅の推定や水みち近傍の局所的な情報の整理に有益な情報を取得することが可能であることがわかった。

本報告書は、埼玉大学地圏科学研究センターが核燃料サイクル開発機構の委託により実施した研究の成果である。
契約番号：1306A00410
核燃料サイクル開発機構担当部課室および担当者：
東濃地科学センター　地質環境特性研究グループ　三枝博光
*　埼玉大学地圏科学研究センター

March 2002

A study on Geological Modeling for Fractured Rock

Masahiko Osada*, Kunio Watanabe*

Abstract

The proper analysis of groundwater flow in a fractured rock mass is very important in many geotechnical fields such as dam construction, tunnel excavation, water resource development within the rock mass and deep underground waste disposal. For analysing groundwater flow, the proper hydrogeological modelling of a fractured rock mass is indispensable. It has also been pointed out in many previous studies that a large amount of groundwater flows through several selected seepage paths called channels that have developed in a fractured rock mass. It is therefore important to properly evaluate the channel network in an actual rock mass and to construct a reliable hydrogeological model of the rock mass before any groundwater analysis is performed.

In Part I, fractures model for the calculated area is made, channel network is generated and groundwater flow is calculated in the Tono area of Gifu, Japan. Calculated area is a real field site, a 4 km x 6 km x 3 km (EW, NS, vertical) region. Fractures data of four 1000 m boreholes (AN1, MIU1, MIU2 and MIU3), located in the MIU site, were used for constructing fracture model. Groundwater flows were calculated by using newly improved Don Chan Program. As the results, six fractures patterns were selected and major fractures directions were defined. The calculated piezometric head results at MIU2 borehole, where Tsukiyoshi Fault exists, were checked and compared with the measured piezometric head values at MIU2 borehole obtained by JNC. The effect of boundary conditions on the analysis of piezometric head distribution also makes clear by giving some kinds of boundary conditions. By this study, a new modelling technique for calculating groundwater flow in fractured rock mass could be proposed.

In Part II, the improvement of reliability in the hydrogeological modelling of a fractured rock mass is examined by considering not only the fracture directions and density but also the mechanical properties of rock. The Equotip Hardness Tester is used in order to estimate the mechanical properties of rock cores, which has a simple principle of measurement and is one of objective methods. It is seen by introducing this index that the useful information for fracture modelling can be obtained such as the estimation of the fault zone width and the mechanical properties around several seepage paths.

This work was performed by Geosphere Research Institute of Saitama University under contract with Japan Nuclear Cycle Development Institute.

JNC Liaison : Geoscience Research Group, Tono Geoscience Center Hiromitsu Saegusa

* Geosphere Research Institute of Saitama University

目次 【CONTENTS】

Part I

図リスト【LIST of FIGURES】

Part I

Part Ⅱ

表リスト【LIST of TABLES】

Part Ⅰ

Part Ⅱ

第1部における平成13年度成果と報告書概要

1 報告書第1部タイトル

Fracture modeling and groundwater flow analysis in the Tono area of Gifu, Japan

2 本年度研究の目的(第1部)

－調査と解析を総合化する割れ目モデル地下水解析法の確立を目指して－

岩盤浸透流解析には大きく分けて、岩盤を基本的に多孔体と近似し、有限要素法や有限差分法で解くものと、岩盤中の割れ目系を主要な水みちと考えて割れ目系を取り出してその中の流れを解く方法とがある。実際には、等価多孔体モデルのように、割れ目系を基礎として岩盤ブロックの透水係数を推定し、全体の流れを有限要素法などで解析する中間的な方法もあるが、大きく見れば上記のように大別しうる。

各々の方法では、解析に用いる情報が異なる。例えば後者の割れ目系モデルでは、当然、割れ目系の形態を妥当に表現することが大事となり、地質調査に要求される項目、調査の質も大きい。それに対して前者の多孔体モデルでは、岩盤全体にわたる透水係数や貯留係数の分布を把握あるいは推定することが大事となる。

従来の解析では、前者の多孔体モデルが使用されることが多かった。これは、解析に必要な透水係数などを測定・推定する方法が進んでいたことや、調査と解析を総合化したプロセスが明確であったこと、さらには、多くの異なった場所で解析が行われており、結果を相互に比較・検討しうることなどによるものである。これに対して割れ目モデルでは、下記の問題が長らく提起されていた。

- 実際の岩盤中には極めて多くの割れ目が存在している。事実上、解析ではすべての割れ目を取り扱うことはできないし、また割れ目の中には透水性が小さくまた他の割れ目との連結性が小さく、地下水流れにさほど寄与しないものもある。つまり、地下水流れに大きく寄与する割れ目(以下、主要割れ目と略記する)をどのように選別するかが明確でない。
- 選別された主要割れ目が、どの程度の広がり(以下、連続性と表現する)を持っているか検討されていない。
- 選別された主要割れ目の透水係数などの水理定数を推定する方法が明確になっていない。

これらの問題に対して総合的に処理するプロセスが明確でなければ、割れ目モデル解析の実際問題への適用が困難であると考える。この総合的プロセスを明確に提示することが、今回の研究目的である。このことをフローチャートで描いたものが次ページの図－1である。なお、研究にあたっては、核燃料サイクル開発機構、東濃地科学センターによって得られた、MIUサイトの4本のボーリング・データ(AN1,MIU1,MIU2,MIU3)を用いた。解析手法としては、核燃料サイクル開発機構と埼玉大学渡辺研究室が共同で開発したDon-Chanを用いた。

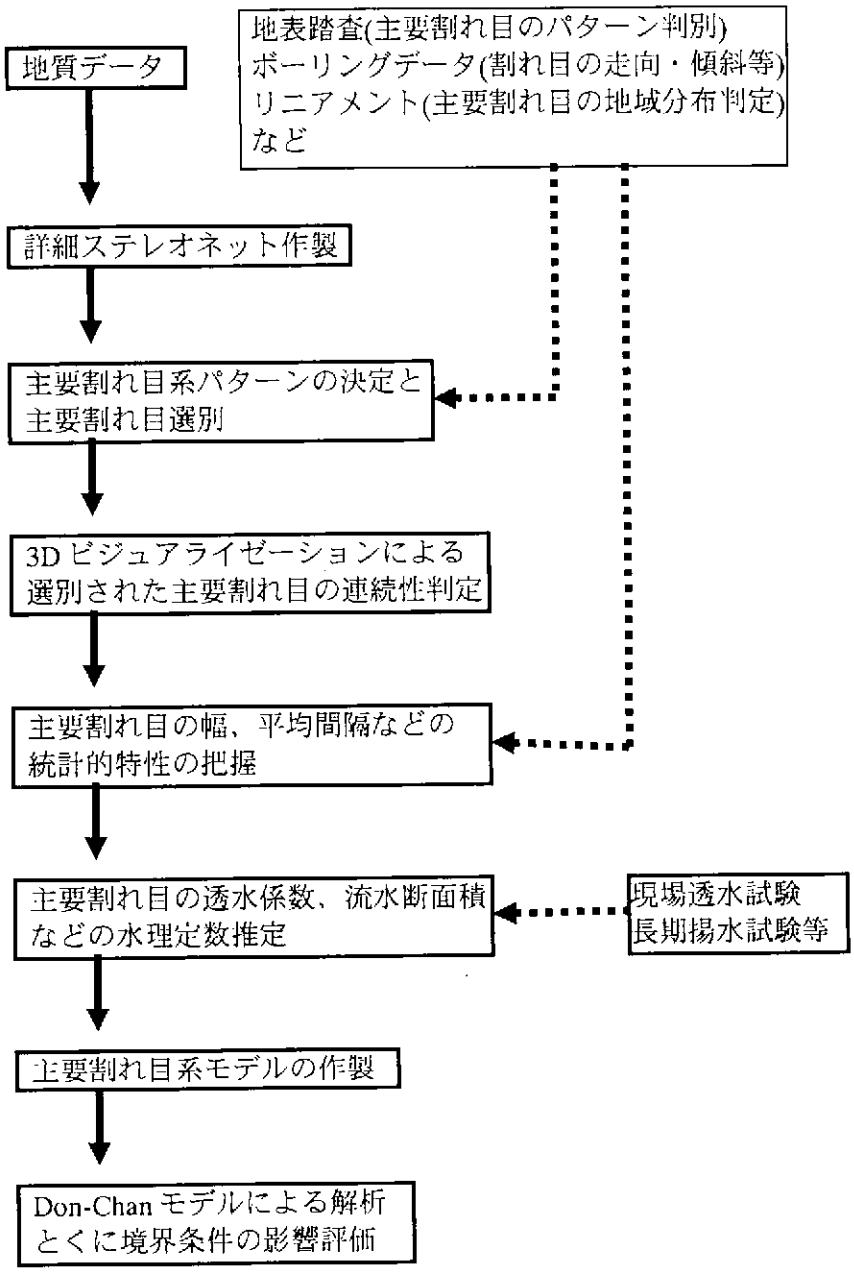

図－１　本研究第１部の研究の流れ

3　本研究の概要と得られた成果

前述したように、本研究は深部地下利用で問題となる岩盤割れ目系評価と地下水解析手法の総合化に取り組んだものである。研究の内容は、岐阜県東濃地域 MIU サイトで得られた４本の 1000m ボーリングのデータを整理し広域の割れ目モデルを組み立て、割れ目を主要流動経路とする地下水解析を行ったものである。解析に用いた手法は、核燃料サイクル開発機構と埼玉大学が共同で開発した Don-Chan モデルである。このモデルのパフォーマンスや妥当性はすでに明らかになっているが、解析に用いる割れ目ネット

ワークを現場のボーリングデータからどのように組み立てるかや実測データと対比など検討すべき課題が多かった。また、割れ目系データを３次元的に把握する可視化手法の開発なども重要な問題であった。本研究はそれらの課題に取り組んだものである。研究によって得られた主な結果と成果、新規性は以下である。

① 当該地域に発達する大量の割れ目の中から、とくに地下水流れに関与する主要割れ目のステレオネット解析に基づく選別方法を開発した。このため、5m 区間、1m づつスライドさせた 5m 区間、割れ目数が４本以上の 1m 区間の割れ目方向をステレオネットに投影した。ステレオネットに見られるパターンと、地表踏査結果を併せて行う主用割れ目選別法を提案した。この結果、MIU サイトには 6 パターンの主要割れ目が発達することがわかった。

② 各ボーリングで得られた主要割れ目の連続性を検討するために、割れ目系の３次元可視化手法を開発した。市販の Micro-AVS を用いてビジュアリゼーションを行った。その結果、主要割れ目の連続性がかなりあることを示した。このことは、逆に、主要割れ目選別の妥当性を示すものと考えられる。

③ 割れ目ネットワークモデルを構築し、地下水流動解析を行って現場の実測データと比較してモデル化手法と解析手法の妥当性を明らかにした。とくに、MIU2 ボーリングに見られる、月吉断層上下の水圧差をうまく表現できることがわかった。

④ 地下水解析結果に与える境界条件の影響を明らかにした。

4 今後の問題

本研究第１部によって、地質調査と解析を総合するプロセスがまとめられたと考える。しかしながら、今年度は総合化を目的とするあまり、詳細な検討ができなかった点もある。例えば、主なものとして、下記がある。

- 主要割れ目選別の妥当性を明確にするため、今回選別された割れ目が、新規の斜めボーリング MIU4 でも認められるかを詳細に検討する。
- 主要割れ目の水理定数推定方法などの妥当性を、MIU4 で行われる長期揚水試験など新規調査結果と併せて検討する。
- 今回の解析は定常状態を対象としたが、貯留係数など非定常地下水流れに関係する定数の推定法を開発し、妥当な非定常解析法を確立する。

これらについてさらに研究を進めて行きたい。

第2部における平成13年度成果と報告書概要

1 報告書第2部タイトル

花崗岩における水みちの構造的特徴に関する基礎研究

2 本年度研究の目的(第2部)

広域的な地下水流動を対象として割れ目系岩盤を水みちネットワークとしてモデル化する場合，まず概念モデルの構築が必要となると考えられる。ここでいう概念モデルとは，対象領域全体にわたって水みちとなる割れ目系がどのように分布しているかを表現するモデルを指す。例えば，報告書第1部ではボーリングコア情報から主要割れ目を取り出すことにより，水みちネットワークを構築している。これも一つの概念モデルであると考える。しかし，このようにして構築した水みちネットワークをボーリング掘削領域外へ拡張しようとした場合，主要割れ目がどこまで連続しているのかについては，どの程度信頼できる情報となっているか評価できないのが現状である。従って，このような概念モデルをさらに進化させていく必要がある。

概念モデルを進化させるには，何をすべきであろうか。理想的には，個々の割れ目の変形史を，それらを形成したときの力学的な枠組みの中で，紐解くことができれば，それに越したことはないが，これは量的にも時間的にも，あまりに現実的ではない。従って，まず対象とする概念モデルに対して，最も効果的な基礎情報を取得することが肝要である。問題は対象とする概念モデルに対して何が基礎情報となるかである。それには，これまでの地質調査方法，およびボーリングコア情報の取得方法を見直し，概念モデルを構築するために必要な基礎情報が何であるかをもう一度考え直すことが必要である。ただし割れ目系計測における不確実性のために，おそらく必要となる基礎情報は，対象とする概念モデルによっても異なるものとなる場合があることには注意すべきである。

第一部では，主要割れ目を抽出する過程において，スプレー構造やステップ構造などのせん断変位に起因する構造を拠りどころにしている。地圏科学研究センターで以前に実施された釜石鉱山やスウェーデン・エスポ地下実験場における坑道壁面調査からも，やはりせん断変位を有する割れ目系からの湧水量が多いという結果が得られている。従って，必要となる基礎情報のキーワードの一つはせん断変位を持つ割れ目である。

第2部の目的は，せん断変位を持つ割れ目を如何にして，ボーリングコア情報から取得するかについて基礎的な研究を行うことである。実施した検討項目は以下の通りである。

(1) BHTV データからの分岐割れ目の頻度分布
(2) コアロギングの一手法としてのエコーチップ反撥強度試験
(3) 断層破砕帯幅の認定方法
(4) 逸水を伴う水みち付近の特徴的な構造について

(5) 破面観察の利用

3　本研究の概要と得られた成果

(1) BHTV データからの分岐割れ目の頻度分布

ステップ・スプレー構造などのせん断に伴う割れ目が発達している場合，ボーリング孔内においても一つの割れ目から分岐している割れ目が観察される。ここでは，MIU1,2,3 孔における BHTV データを用いて，このような分岐する割れ目を抽出し，その頻度分布を求めた。その結果，割れ目系全体の頻度分布は岩相で異なり，biotite granite で 4 本／m，filsic granite で 7 本／m であるのに対して，分岐する割れ目の頻度分布は，岩相によらずほぼ一定しており，0.2 本／m 程度の値を示した。この結果の詳細な検討は今後の課題である。

(2) コアロギングの一手法としてのエコーチップ反撥強度試験

コア観察を行う場合，簡便で客観的な指標が必要である。また詳細なデータを得るためには，センチメートルオーダーの岩石物性の変化を捉える必要がある。ここではこの要求に応えるために，エコーチップ反撥強度試験の適用を試みた。エコーチップ反撥強度試験は，チップを岩石に衝突させて打撃速度と反撥速度を計測するもので，主に岩石の弾性的な性質を示す指標である。

適用性を検討するために，インタクトな biotite granite と filsic granite に対して試験を行い，良好な結果を得た。これらの岩相の相違は，この指標の絶対値の大きさとバラツキの幅として捉えられ，コアロギング手法として十分に適用できることがわかった。

(3) 断層破砕帯幅の認定方法

断層はせん断変位を有する割れ目の代表格である。せん断変位を有する割れ目の特徴を把握するためには，まず断層周辺でどのような岩石物性の変化が見られるのか検討しておく必要がある。さらに断層破砕帯幅の推定は，現在地質専門家の詳細な検討により行われているが，これを裏付けるための客観的な指標があることが望ましい。

ここでは，(2)のエコーチップ反撥強度試験を MIU2,3,4 が貫く月吉断層周辺で実施し，その傾向を検討した。断層周辺の岩石は，せん断に伴い破砕されている可能性があること，その後の熱水変質作用により脆弱化している可能性があること，さらに岩石の脆弱化に伴い，ボーリングコア周面も荒れている可能性があり，これらによりインタクト部よりもエコーチップによる指標が小さく表現されるものと考えられる。

測定結果は，予想通り断層周辺の指標値は小さな値を示した。断層破砕帯幅の推定方法を「エコーチップによる指標値が，どこを叩いてもインタクト部の値を示さない範囲」とすると，詳細な検討した断層破砕帯幅とほぼ一致する結果が得られた。この判断基準に従って，MIU－4 を貫く月吉断層の破砕帯幅は，659～677m 間の 18m となる。また断層の上盤側では断層主部から離れても付随する断層によって指標値が小さくなる箇

所が多く見られるのに対して，下盤側では指標値の戻りが早い傾向にあることがわかった。

(4) 逸水を伴う水みち付近の特徴的な構造について

MIU 孔では，掘削時にいくつかの深度で大量の逸水が発生している。これらの逸水箇所がせん断に伴うものであれば，断層破砕帯周辺で見られたエコーチップ値の低下が観察される可能性がある。また長年の間地下水の通り道となっていた場合には，その周辺で岩石物性に変化を生じ，セメント鉱物の溶出による脆弱化あるいは地下水に溶解していた成分の沈殿による固化を伴っている可能性もある。

ここでは，MIU－1 孔深度 201m と 980m，MIU－2 孔深度 223m における逸水箇所付近においてエコーチップ反撥強度試験を行った。浅い深度の逸水箇所では，指標値に大きな変化は見られなかったのに対して，MIU－1 孔の深い深度の逸水箇所では明らかに小さい指標値が得られており，月吉断層主部までは達していないものの，断層の影響を強く受けた上盤部分での逸水であることが明らかとなった。逸水箇所前後 20m における割れ目の頻度分布と比較すると，浅い深度の逸水箇所では低角度の割れ目が発達しているのに対して，深い深度の逸水箇所では高角度の割れ目が発達している。また浅い深度の指標値は，インタクト部の基準（MIU－1 孔：深度 500m 付近）とした値よりも大きな値となっている。このことは，同じ岩相であっても場所により岩石物性が異なる可能性を示している。

(5) 破面観察の利用

構造地質学的検討では，しばしばせん断変位の有無を破面の構造から判断する。コア観察を行う場合，すべての割れ目でこの有無を肉眼的に判断することは容易ではない。このような肉眼的に判断できない大きさのせん断に伴う構造をなんらかの方法で収集することにより，コアからせん断変位の情報を増やすことを目的として，肉眼的に条線の見られるサンプルを採取し，走査型電子顕微鏡（SEM）を用いて観察した。

ここでは一例を示すのみとなったが，SEM 画像において条線と見られる構造を特定することができた。この例では 0.25mm^2 程度の領域の表面粗さを 1μm の精度で計測できるならば，このような構造を捉えうることがわかった。

4　今後の問題

本研究第 2 部では，せん断変位を示す情報をコア情報から収集することを目的として，上記の各種調査を行った。エコーチップ反撥強度のような簡便で客観的な指標を導入することで，割れ目の方向・頻度分布のみからの推定ではなく，岩石の物性を含めた検討が行いうる可能性は示すことができた。今後，このような指標をボーリング孔全体のロギング方法として採用できるならば，より多くの情報が得られるものと考えられる。また破面観察は，一つ一つの試料を実験室に持ち帰り分析するよりも，局所領域における表面粗さ計測が可能な機器を導入して，現場でコアから直接情報を得ることが望ましい。

Part I

FRACTURE MODELING AND GROUNDWATER FLOW ANALYSIS IN THE TONO AREA OF GIFU, JAPAN

CHAPTER 1

INTRODUCTION

1.1 Background

Groundwater is the portion of the water beneath the surface of the earth that can be collected with wells, tunnels or drainage galleries or that flows naturally to the earth's surface via seeps or springs. Today, groundwater is a major source of water for many municipalities, industries, irrigation, suburban homes and farms. Groundwater has been an important water resource throughout the ages.

Fluid flow in rock mass occurs in two principal ways, flow in the pore network of the sedimentary rock connecting small spaces between particles (porous media flow) and flow along faults and fractures in rocks (fracture flow or channel flow). While igneous and metamorphic rocks (granites, gneisses, etc) yield reasonable amounts of groundwater only when fractured by faulting or weathering.

A fracture is made up of two surfaces that are wavy and rough. The two surfaces are in contact with each other in some points but are at a distance from each other at other points. The openings in the fracture are potential channels. These are only potential conduits because they have to be connected to other open sections in order to form a continuous network. When a hydraulic gradient is imposed over a fracture with a variable aperture, the water will seek out the easiest pathways. If there is a random but large variation in the transmissivity values in different places, the water will seek out a tortuous path, always avoiding those sections where the transmissivity is low. In such a case, most of the water may choose to flow along one path because it is the path with least resistance for that specific gradient.

The proper analysis of groundwater flow in a fractured rock mass is very important in many geotechnical fields such as dam construction, tunnel excavation, water resource development within the rock mass, and deep underground waste disposal. For analysing

groundwater flow, the proper hydrogeological modeling of a fractured rock mass is indispensable. It has been pointed out in many previous studies that a large amount of groundwater flows through several selected seepage paths called channels that have developed in a fractured rock mass (Bear et al., 1993). Tanaka et al. (1994) and Watanabe et al. (1994) studied the hydrogeological features in fractured granite in the Kamaishi Mine, Japan, and concluded that the intersections between conjugate fractures tend to be the highly permeable channels. There have also been several observations that indicate that fracture intersections form easy pathways (Abelin et al., 1987; Neretnieks, 1987b; Moreno and Neretnieks, 1988). It is important to properly evaluate the channel network in an actual rock mass and to construct a reliable hydrogeological model of the rock mass before any groundwater analysis is performed.

1.2 Objective and Aim of the Study

The channel network in an actual rock mass, presenting flow in fractures, must be properly modelled for the analysis of groundwater flow. In order to generate channel network, fractures model is needed. This study is intended to make fractures model for the calculated area, to generate channel network, to calculate and analyse groundwater flow in the Tono area of Gifu, Japan. For calculating groundwater flow based on channel network, we use Donnen-Saitama Channelling Model (Don-Chan Model).

In more detailed explanation, the objectives of this study are:

1. To make fractures model for calculated area by analysing fractures data of four 1000 m boreholes (AN1, MIU1, MIU2 and MIU3), located in the Mizunami Underground (MIU) site in Tono Area of Gifu, Japan and obtained by Japan Nuclear Cycle Development Institute (JNC). In the analysis of fractures data, the following steps were performed:

- Executing fractures patterns interpretations, selecting major fractures and determining major fractures direction based on stereographic projections of fractures orientation data read by Borehole Television (BTV) figures.
- Checking connection of fractures among observed boreholes

- Defining representative fractures patterns and major fractures directions after comparing with fractures in bore cores.
- Creating a fractures model and combining the fractured rock mass with the sedimentary rock.

2. To calculate and analyse groundwater flow by using Don-Chan Program. Calculated area is a 4 km x 6 km x 3 km region including the MIU site. The following steps were done:

- Generating the channel network of both fractured rock mass and sedimentary rock and calculating groundwater flow in this composite model by using Don-Chan Program
- Comparing the calculated result at MIU 2 borehole, where Tsukiyoshi Fault exists, with the measured values at MIU 2 borehole obtained by JNC.

1.3 Summary of Contents

The present thesis consists of six chapters. Brief presentation for each chapter is furnished as follows:

Chapter 1, is an introduction part and the importance of making fracture model is explained. The objectives and aims of the present study are briefly described.

Chapter 2, is concerning the literature review and problems that should be solved in this study. Rough structure of analysis to show the steps of study is also shown as the scope of study.

Chapter 3, presents basic idea of fracture modeling and groundwater flow analysis by using Don-Chan Model. Description of stereographic projection, procedure of major fracture selection based on borehole data, technique of fractures patterns selection, problems of fractures connection, calculation of fracture zone width and average distance between fractures are included. Basic concept of Don Chan Model and groundwater flow calculation by using Don Chan Model are also explained.

Chapter 4, presents the modeling of fractures in Tono Area. Area targeted in this study, fractures data, and boreholes information are explained in this chapter. Example of stereographic projections of fractures orientation data read by Borehole Television (BTV) and the interpretations are briefly described. Each fracture pattern in each observed borehole is shown in figures using 3-D visualization technique.

Chapter 5, is concerning about groundwater flow in a composite media. An example of Don Chan Model calculation is included in this chapter. Analysis of groundwater flow in calculated area surrounding MIU site in Tono Area of Gifu is presented followed by the discussion of calculations results.

Chapter 6, is the conclusions drawn from this study. Further improvement for future study is also presented.

Beside the mentioned chapters, an abstract is included in this thesis. In addition, contents, list of tables, list of figures and references are comprehended.

CHAPTER 2

LITERATURE REVIEW AND PROBLEMS SHOULD BE SOLVED

2.1 Literature Review

2.1.1 Important Geological Factors Affecting Groundwater Flow

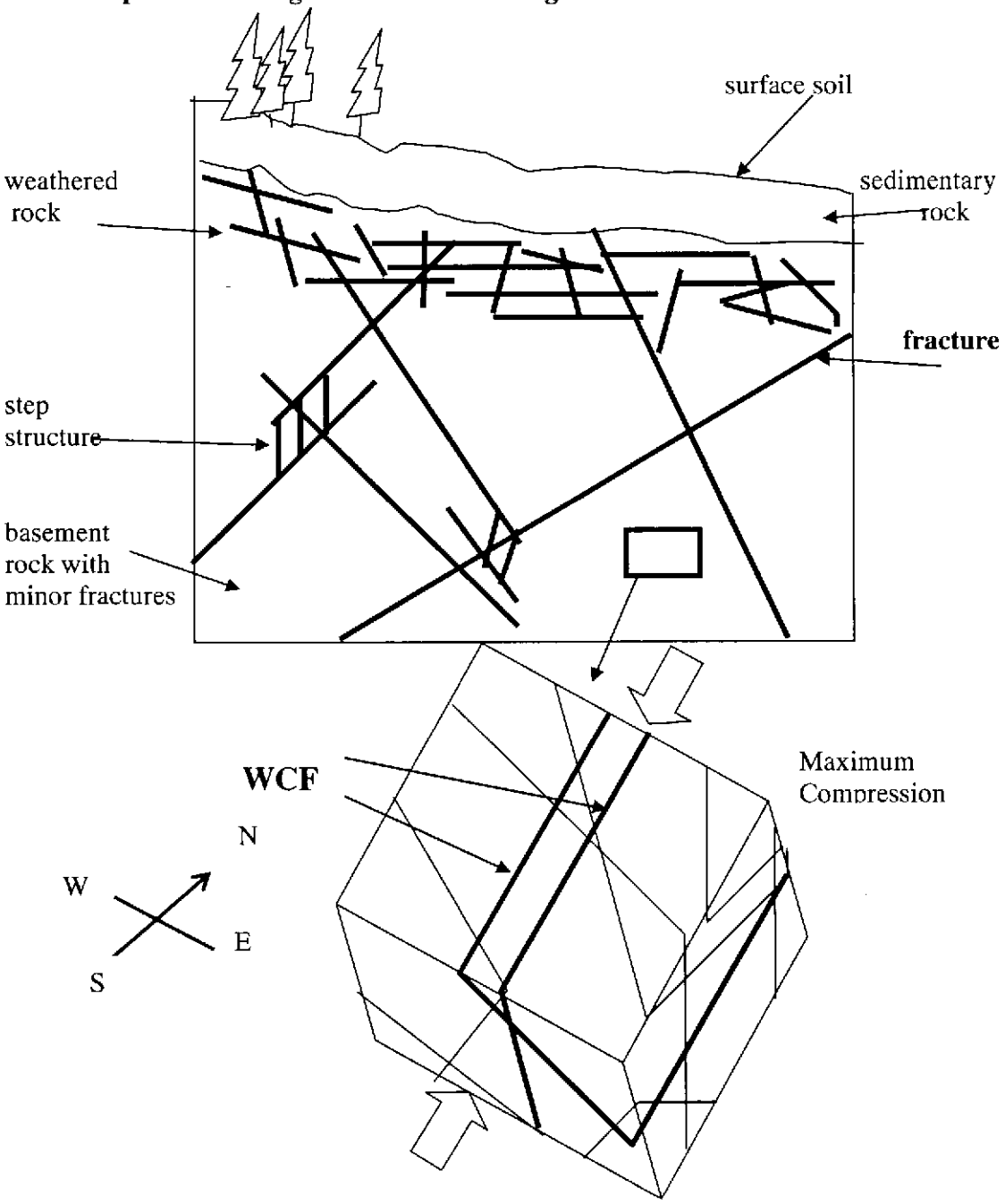

Figure 2.1.1 Overview of underground rock condition and water conducting features described in 2.1.

A. Fracture

a. Definition and Terminology

The term fracture is used for any discontinuity that is formed by discrete breaking of a rock body. Fractures are subdivided into joints, where no displacement has occurred, and faults where slip has displaced the walls along the discontinuity. The line where a fault plane cuts the outcrop (or the tunnel wall) is the fault trace. The fault trace terminates at the tip point, where displacement approaches zero.

On outcrop scale, faults are neither straight nor infinite in extension. In granite and other rock, increasing displacement along a fault also results in the growth of the fault trace (or, in two dimensions, of the fault surface area). Progressive deformation also leads to the linking of smaller faults into larger fault zones, a process called segment linkage. The linkage of adjacent faults in a fault step is achieved via splay cracks, which often occur in clusters of sub parallel single fractures. The final stage of this process results in fault zones, i.e. complex system of branching faults and diverging splays that form a large, interconnected system. The terminology is illustrated in the following figure:

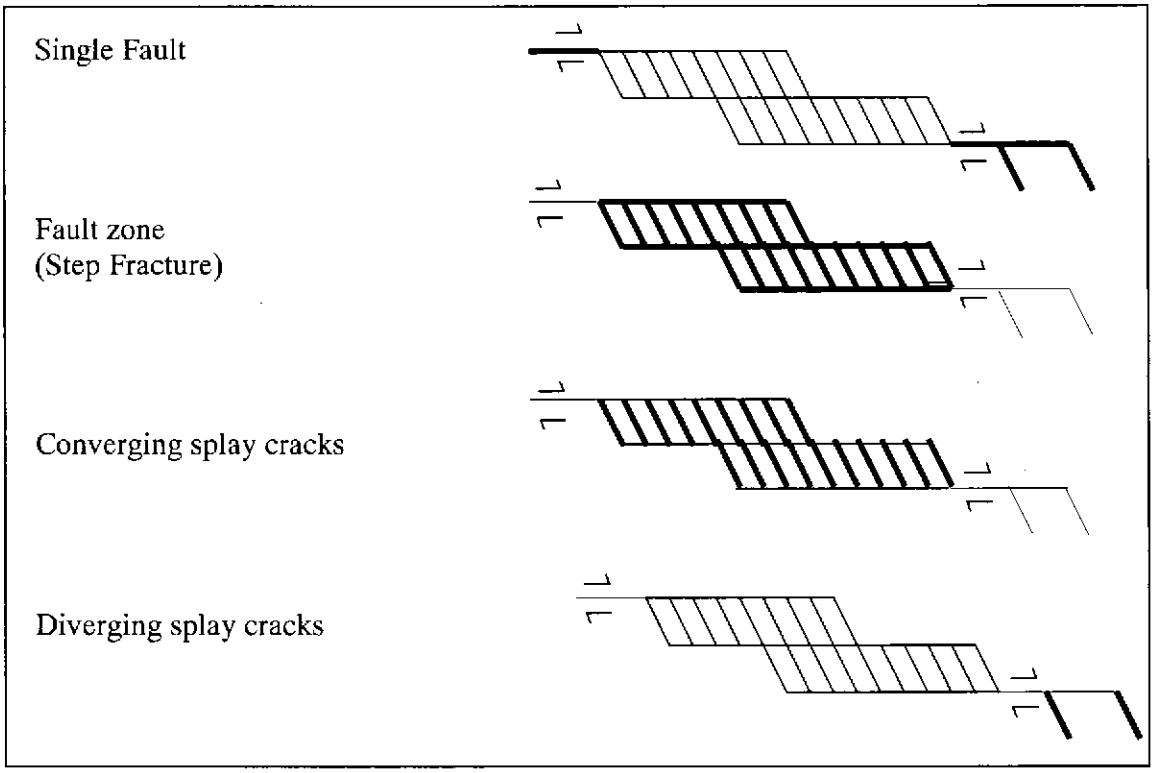

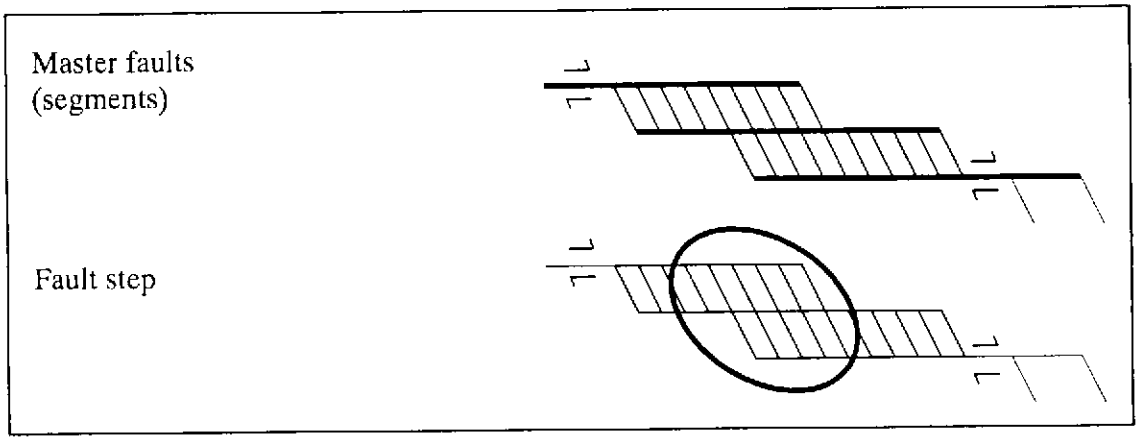

Figure 2.1.2 Terminology of fracture

b. Classification of Water Conducting Fractures

Referring to the investigations results on the outcrop scale in the classification and characterization of water-conducting features at ASPO, done by Mazurek, Bossart and Eliasson, a population of fractures can be classified into groups based on different criteria, such as geometric parameters of the fractures (fracture width, internal structure), deformation mechanism (faulting, jointing), host rock lithology or the origin (specific phases of deformation). The most striking variability among water-conducting features is their internal structure, namely the presence of one or several shear planes (master faults), fault steps, and the frequency of diverging and converging splay cracks. For these reasons, the anatomy of the faults is taken as the prime classification criterion.

In the initial classification scheme, all water-conducting faults were partitioned into the two principal structural groups "simple" and "complex" structures, using the number of master faults and frequency of splay cracks as discriminators. The classification scheme presented here is a further development. The simple and complex structures are subdivided into two or three subgroups, respectively. The new 5 types of water-conducting features are:

Simple features:

Type 1 – single fault (1 master fault, few splays)

Type 2 – swarm of single faults (2 or more master faults with splays, not connected)

Complex features:

Type 3 – fault zone (2 master faults with connecting splays)

Type 4 – fault zone with rounded geometries (2 master faults with connecting splays and lens-shaped geometry)

Type 5 – parallel fault zones with long connecting splays (2 or more master faults connected by splays)

Type 1 – *single fault*: Structure composed of 1, or for shorter distance 2, master faults without or with few splay cracks. Water flow is, with the exception of fault steps, restricted to a very small number of planes (often one single)

Type 2 – *swarm of single faults*: Although type 2 structures consist of two or more generally fairly smooth and planar master faults parallel to the main trend of the whole water-conducting feature, they are classified as simple structures. This is because they contain very few converging or diverging splay cracks, which are able to hydraulically connect the individual master faults. The flow regime in such a feature would be simpler than flow in a fault zone with more intricate fracturing (high density of converging splays). Munier and Hermanson (1993) denote fracture zones with an internal fracturing like this a "fracture swarm".

Type 3 – *fault zone*: Structure generally composed of 2 or more master faults and commonly more than 0.5 converging splay cracks/m (measured along the fault). Locally (for short distance), it may consist of only 1 master fault. Because the master faults and the converging splay cracks represent an interconnected system of fractures, water flow may occur along a number of different flow paths with different flow velocities, which results in enhanced longitudinal dispersion. The extreme cases are flow entirely within master faults and flow in splay cracks only.

Type 4 – *fault zone with rounded geometries*: This type is distinguished from the classic fault zone (type 3) by the rounded, lens-shaped or undulating fault geometries (large waviness). In terms of anatomy and the mechanistic understanding of fault

formation, type 4 is very similar to type 3. Two or more master faults and fairly many-curved splay cracks form rounded shear lenses and undulating, wavy fault planes. Although some type 4 features may contain only one master fault, the rounded shear lenses, and thereby intricate geometry of the brittle fracturing implies that they are classified as complex structures.

Type 5 – *parallel fault zones with long connecting splays*: Similarly to type 2, type 5 features consist of several smooth and planar master faults. The major difference to type 2 features is that the master faults are connected to each other by another set of smooth and planar fractures (interpreted as converging splay cracks). It could be argued that type 2 and 5 features are quite similar, the major difference being the connectivity of the master faults via long splays in type 5.

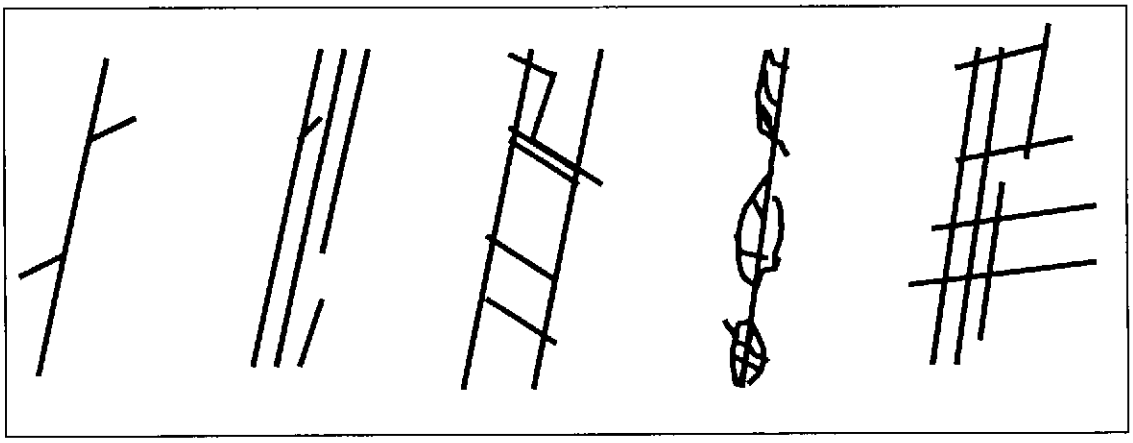

Type 1	Type 2	Type 3	Type 4	Type 5
Single Fault	Swarm of single faults	Fault zone	Fault zone with rounded geometry	Fault zone with long splays

Figure 2.1.3 Type of water conducting features

A fracture is approximated as shown in the following figure. The fracture is defined as the set of master fracture and splay fractures. Step fracture can store and transport water. Master fracture can flow water.

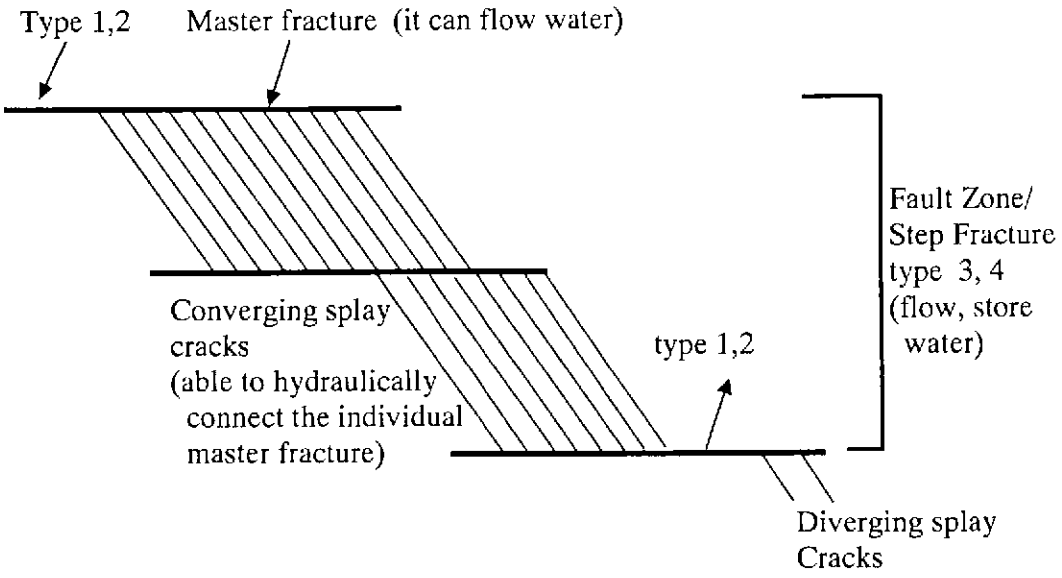

Figure 2.1.4 Model of a fracture and hydraulic features

Although there remains the possibility that the hydraulic nature is different with fracture type, the following features are taken into consideration when a hydrogeological map is reconstructed (Figure 2.1.4):

1. **Extremely high permeable and large storage features**
    - Step structure
    - Intersection line among fractures
2. **High permeable part**
    - major single fracture
3. **Low permeable part (groundwater barrier)**
    - Hydrothermaly altered big fault

c. Water Conducting Fracture in ASPO

Based on the previous study done by Martin Mazurek, Paul Bossart and Thomas Eliasson in December 1996, at the topic of Classification and Characterization of Water-Conducting Features at ASPO: Result of Investigation on the Outcrop Scale, some findings were obtained:

Hydraulically active and inactive faults

The fractures, which almost contain no water, are called tight fractures (hydraulically inactive faults). The fractures in which groundwater can easily pass through them are called open fractures or water conducting fractures (hydraulically active faults). It was observed that most NW-SE striking faults discharge into the tunnel, whereas many NE-SW directed faults are dry. This fact is also described by Munier (1993), who performed detailed fracture measurements in the rock laboratory. He separated the fractures into two groups, those, which are tight, and those, which are **open and permeable.** In spite of some spread, the data suggest that the orientations of water-conducting fractures are different from those of the tight fractures. During the excavation of the laboratory, grout injection into the tunnel front was applied in order to seal highly transmissive fractures. Most of these grouted, initially highly transmissive fractures are also striking in a NW-SE direction.

B. Rocks

Rocks are aggregates of one or more mineral. The nature and properties of a rock are determined by the minerals in it (particularly those essential minerals such as quartz, feldspar etc, which individually make up more than 95% of its volume) and by the manner in which the mineral are arranged relative to each other (the texture of the rock). The commonly used classification of rocks, however, groups rocks according to how they were formed, and is based upon this principle. It is a genetic classification of rocks, even though the criteria it uses to assign a rock to a particular category are the features readily observed, that is, mineral composition and texture. According to their manner of formation, rocks are of three main types.

Igneous rocks are formed from magma, which has originated well below the surface, has ascended towards the surface, and has crystallised as solid rock as its temperature fall down. Many different types of mineral occur in igneous rocks, but only about eight, namely quartz, orthoclase, plagioclase, muscovite, biotite, hornblende, augite and olivine, are normally present as essential constituents of a rock. Which of the eight are present is controlled primarily by the order of crystallisation from magma. Since the crystals

formed early have a higher specific gravity than the remaining liquid of the magma, they settle downwards or the two fractions, crystals and liquid, may be separated by some other process of differentiation to give rise eventually to several different types of rock.

Sedimentary rocks are formed by the accumulation and compaction of:

- fragments from pre-existing rocks which have been disintegrated by erosion
- organic debris such as shell fragments or dead plants
- material dissolved in surface waters (rivers, oceans,etc.) or ground water which is precipitated in conditions of over saturation

The sediment has been transformed into solid rock by compaction as it was buried and compressed by subsequent deposits. In many cases, minerals in solution in the ground water have been precipitated to act as natural cement, and bond the fragments together. The nature of a sedimentary rock, and its position in a scheme of rock classification, are partly dependent on these original conditions of transport and deposition.

The commonly used classification of sedimentary rocks uses the general type of material from which the rock was derived as its principal criterion, and is therefore a genetic classification. The three principal types of material are rock fragments, mineral material dissolved in water and organic debris.

Each defines a major group of sedimentary rocks. It is, however, convenient for most practical purposes to recognise the common chemical and physical properties of limestone, which are formed from each and all of the principal materials listed, and to describe them as a separate major group of sedimentary rocks. The four major groups of sedimentary rocks are:

- **Terrigenous sedimentary rocks** (sometimes referred to as clastic or detrital rocks, which are formed from rock fragments
- **Chemical sedimentary rocks**, which are formed from the precipitation of salts dissolved in water

- **Organic sedimentary rocks**, which are formed from the skeletal remains of plants and animals
- **Limestones and dolomites** which are sedimentary rocks consisting of more than 50% carbonate

Mineralogy of sedimentary rocks. The constituents of sedimentary rocks are fragments from pre-existing rocks and minerals. These may be fresh and unaltered, or may be alteration products of weathering, such as clay minerals. Quartz is the most common mineral, which is chemically stable and hard enough to resist abrasion as it is transported. *Textures of Sedimentary Rocks.* Chemical sedimentary rocks generally have a crystalline textures. The only important exception to this is oolitic limestone. The others are formed of fragments, and their textures are dependent on the sizes, shapes and arrangement of these fragments. If the rock has been formed from organic debris, then the fragments may consist of particles of shell or wood, but the texture can be described with the same terms as are used for other fragmental rocks.

Metamorphic rocks are formed from pre-existing rocks of any type which have been subjected to increases of temperature (T) or pressure (P) or both, such that the rocks undergo change. This change results in the metamorphic rock being different from the original parental material in appearance, texture and mineral composition. A recrystallisation of the original rock may occur if T and P are high.

C. Weathered Rock

The highly weathered rock is decomposed and brown in colour due to oxidation. There are several chemical and physical reasons for the occurrence of partial weathering. In the usual case, the infiltration of rainwater and the oxidation are needed in the process of weathering. Three processes of weathering and erosion at and near the surface transforms solid rock into unconsolidated rock waste. They are as follows:

The mechanical disintegration of a rock mass at the surface, as water, wind, ice and the rock fragments carried by them, buffet or press against it, or force it apart. It leads to a

physical disaggregation of the original rock mass into smaller particles. For example, freezing of water within a crack produces an expanded wedge of ice, which forces the walls of the crack apart.

The chemical reactions between the original minerals of the rock, the near-surface water and the oxygen of the atmosphere to produce new minerals which are stable under the conditions at the Earth's surface and remove other more soluble constituents. Chemical weathering of several common rock-forming minerals produces clay minerals. These are normally created by alteration and are said to be secondary minerals. The specific type of clay formed depends on the composition of the original mineral and the surface conditions where weathering is taking place. The change is not usually a direct or simple one. Other alteration products, which are not strictly clays, may be formed as intermediate stages of the weathering process, and one clay mineral may be transformed into another more stable one as condition change. For example, chlorite sometimes occurs as a primary constituent of rock, and sometimes as a secondary mineral formed by weathering. It is not a clay mineral, but does alter readily to clay.

The biological activity which produces organic acids, thus adding to the chemical reactions, and which may also be an agent assisting mechanical disintegration. Organic matter in soils is broken down by microorganisms to give water and either carbon dioxide or methane and small quantities of ammonia and nitric acid. An excessive accumulation of decaying organic matter will consume all the available oxygen and produce a reducing environment, for example, in lakes where circulation is poor. In these circumstances sulphides form, and pyrite is usually created.

The effectiveness of these processes in destroying the rock is dependent on its constituent minerals and its texture. For example, a mineral property, such as cleavage, influences how readily water and air can enter the mineral grain, and speed any reaction. The well developed cleavages of feldspar allow the change to clay minerals to take place within, as well as around, the mineral grain. In contrast, quartz is chemically inert and is a particularly stable mineral. The principal effect of weathering and erosion on it is to

reduce the size of each quartz grain by abrasion, though the hardness of quartz helps to preserve it from this type of attack as well.

Large cracks and fissures in the rock mass also facilitate the entry of water and air, and so assist weathering. The more fissures and other rock discontinuities that the rock possesses, the greater is the surface area exposed to chemical reaction, and hence the faster weathering takes place.

2.1.2 Groundwater Movement

A. Darcy's Law

Groundwater in its natural state is invariably moving. This movement is governed by established hydraulic principles. The flow through aquifers, most of which are natural porous media, can be expressed by what is known as Darcy's law. The experimental verification of Darcy's law can be performed with water flowing at a rate Q through cylinder of cross-sectional area A packed with sand and having piezometers a distance L apart. Total energy heads or fluid potentials, above a datum plane may be expressed by the Bernoulli Equation:

$$p_1/\gamma + v_1^2/2g + z_1 = p_2/\gamma + v_2^2/2g + z_2 + h_L \qquad (2.1.1)$$

where, p = pressure, γ = the specific weight of water, v = the velocity of flow, g = the acceleration of gravity, z = elevation, h_L= head loss. Because velocities in porous media are usually low, velocity heads may be neglected without appreciable error. Hence, by rewriting, the head loss becomes

$$h_L = [p_1/\gamma + z_1] - [p_2/\gamma + z_2] \qquad (2.1.2)$$

Therefore, the resulting head loss is defined as the potential loss within the sand cylinder, this energy being lost by frictional resistance dissipated as heat energy. It follows that the head loss is independent of the inclination of the cylinder. Now, Darcy's measurements

showed that the proportionalities $Q \sim \partial h$ and $Q \sim 1/\partial x$ exist. The volumetric flow of groundwater is calculated using Darcy's law:

$$\boxed{Q = - KA\, \partial h/\partial x = qA} \qquad (2.1.3)$$

where, Q = the volumetric flow rate [$L^3\ T^{-1}$] in the x direction, A = the cross-sectional area for flow, K = the hydraulic conductivity [LT^{-1}], $\partial h/\partial x$ = the gradient in hydraulic head (hydraulic gradient), q = the specific discharge (flow rate per unit area [LT^{-1}]).

The statement that the flow rate through porous media is proportional to the head loss and inversely proportional to the length of the flow path, is known universally as Darcy's law.

The minus sign indicates that fluid moves in the direction of decreasing hydraulic head. The specific discharge is sometimes referred to as the Darcy flux, Darcy velocity, or bulk velocity. It is referred to as the Darcy velocity because it assumes that flow occurs through the entire cross section of the material without regard to solids and pores. Actually, the flow is limited to the pore space only so that the average interstitial velocity or the pore water velocity V [LT^{-1}] is related to the specific discharge by:

$$\boxed{V = q/n} \qquad (2.1.4)$$

where n is the effective porosity.

To define the actual flow velocity, one must consider the microstructure of the rock material. In water flowing through sand, for example, the pore spaces vary continuously with location within the medium. This means that the actual velocity is non-uniform, involving endless accelerations, decelerations and changes in direction. Thus, the actual velocity depends on specifying a precise point location within the medium.

In applying Darcy's law, it is important to know the range of validity within which it is applicable. Darcy's law is valid for laminar flow, a condition met in the great majority of

hydrogeologic settings. The Reynolds number (N_R) has been employed to establish the limit of flows described by Darcy's law. Reynolds number is expressed as:

$$N_R = UL / \nu \qquad (2.1.5)$$

where U = darcy velocity, L = average grain size and ν = kinematic viscosity. Experiments show that Darcy's law is valid for $N_R<1$ and does not depart seriously up to $N_R = 10$. This, then, represents an upper limit to the validity of Darcy's law. Fortunately, most natural underground flow occurs with $N_R<1$, so Darcy's law is applicable. Deviations from Darcy's law can occur where steep hydraulic gradients exist, such as near pumped wells, also, turbulent flow can be found in rocks such as basalt and limestone that contain large underground openings.

Applications of Darcy's law enable groundwater flow rates and directions to be evaluated. The dispersion, or mixing, resulted from flows through porous media produces irregularities of flow that can be studied by tracers. Groundwater velocities vary widely depending on local hydrogeologic conditions. In media with lower hydraulic conductivity, groundwater velocities are corresponding lower. Usually, velocities tend to decrease with depth as porosities and permeability also decrease. Velocities can range from negligible (all groundwater within the hydrologic cycle should be regarded as in continuous motion, although it must be granted, some of it flows at extremely small rates) to those of turbulent streams in underground openings within basalt and limestone. Mechanisms such as well and drains act to accelerate flows.

B. Hydraulic Potential and Fluid Flux

Groundwater flows through interconnected void spaces, along micro cracks between grain boundaries and in larger-scale fractures. Groundwater moves in response to differences in fluid pressure and elevation. The driving force is measured in terms of hydraulic head, h [L], where:

$$h = z+(p/\rho g) \qquad (2.1.6)$$

where, z = the elevation of the measurement point above datum, p = the pressure of a fluid with constant density ρ and g = the acceleration due to gravity.

Hydraulic head, also referred to as the piezometric or potentiometric head, is equal to the mechanical energy per unit weight of the fluid. Contribution from kinetic energy to hydraulic head can be neglected in almost all cases because groundwater velocities are so low. Groundwater flows from regions where the hydraulic head is higher toward regions where it is lower. By convention, pressure is expressed in terms of values above atmospheric pressure (gauge pressure). Defining the pressure head as:

$$\boxed{h_p = p/\rho g} \qquad (2.1.7)$$

leads to

$$\boxed{h = z + h_p} \qquad (2.1.8)$$

Contour maps of hydraulic head are used to infer directions of subsurface fluid flow since flow will be everywhere normal to the head contours in an isotropic medium. Fluid flow is in the same direction as the hydraulic gradient.

C. Transmissivity

The term transmissivity, T is widely employed in groundwater hydraulics. It may be defined as the rate at which water of prevailing kinematic viscosity is transmitted through a unit width of the saturated aquifer under a unit hydraulic gradient. It follows that the unit of transmissivity is m^2/day.

It should be emphasized that transmissivity is specifically defined for two-dimensional, horizontal analysis, having the aquifer thickness included within their values. In the case of horizontal flow through a layer of thickness b, one derived parameter commonly used is transmissivity, T, $[L^2T^{-1}]$. It is the product of hydraulic conductivity (K) and the layer thickness/saturated thickness of the aquifer (b).

$$\boxed{T = K\,b} \qquad (2.1.9)$$

D. Hydraulic Conductivity

The hydraulic conductivity is a measure of the ability of the soil to transmit water and depends upon both the properties of the soil (medium) and the fluid. Total porosity, pore-size distribution, and pore continuity are the important soil characteristics affecting hydraulic conductivity. Fluid properties affecting hydraulic conductivity are viscosity and density.

For practical work in groundwater hydrology, where water is the prevailing fluid, hydraulic conductivity K is employed. A medium has a unit hydraulic conductivity if it will transmit in unit time a unit volume of groundwater at the prevailing kinematic viscosity through a cross section of unit area, measured at right angles to the direction of flow, under a unit hydraulic gradient. The unit is m/day, indicating that hydraulic conductivity has unit of velocity.

The hydraulic conductivity of a soil or rock depends on a variety of physical factors, including porosity, particle size and distribution, shape of particles, arrangement of particles, and other factors. In general, for unconsolidated porous media, hydraulic conductivity varies with particle size. Clayey materials exhibit low values of hydraulic conductivity, whereas sands and gravels display high values.

E. Permeability

The permeability of a rock or soil defines its ability to transmit a fluid. This is a property of the medium only and is independent of fluid properties. To separate the effects of the medium from those of the fluid and to avoid confusion with hydraulic conductivity, which include the properties of groundwater, the intrinsic permeability (k) is defined in the following expression:

$$K = k\rho g/\mu \qquad (2.1.10)$$

where, K = hydraulic conductivity, k = permeability, is a property of the medium only $[L^2]$, g = acceleration of gravity, ρ = fluid density, μ = dynamic viscosity of the fluid.

Thus, intrinsic permeability possesses units of area. The following table shows representative ranges in hydraulic conductivity and permeability for a variety of sediment and rock types.

Table 2.1.1. Representative Values of Hydraulic Conductivity and Permeability

Sediment or Rock Type	**Hydraulic Conductivity m/day**	**Permeability m^2**
Clays	$10^{-7} - 10^{-3}$	$10^{-19} - 10^{-15}$
Silts	$10^{-4} - 10^{0}$	$10^{-16} - 10^{-12}$
Fine to Course Sands	$10^{-2} - 10^{+3}$	$10^{-14} - 10^{-9}$
Gravels	$10^{+2} - 10^{+5}$	$10^{-10} - 10^{-7}$
Shales (matrix)	$10^{-8} - 10^{-4}$	$10^{-20} - 10^{-16}$
Shales		
(fractured and weathered)	$10^{-4} - 10^{0}$	$10^{-16} - 10^{-12}$
Sandstones (well-cemented)	$10^{-5} - 10^{-2}$	$10^{-17} - 10^{-14}$
Sandstones (friable)	$10^{-3} - 10^{0}$	$10^{-15} - 10^{-12}$
Salt	$10^{-10} - 10^{-8}$	$10^{-22} - 10^{-20}$
Anhydrate	$10^{-7} - 10^{-6}$	$10^{-19} - 10^{-18}$
Unfractured igneous and		
metamorphic rocks	$10^{-9} - 10^{-5}$	$10^{-21} - 10^{-17}$
Fractured igneous and		
metamorphic rocks	$10^{-5} - 10^{-1}$	$10^{-17} - 10^{-13}$

F. Hydraulic Properties of a Porous Medium (Porosity)

Porosity is defined as the fraction of void space per unit volume of porous medium. Porosity is a dimensionless number less than 1, although it is frequently reported as a percentage. Effective porosity includes only that void space that forms part of the interconnected flow paths through the medium and excludes void space in isolated or dead-end pores.

Primary porosity refers to the void space between grains while secondary porosity is due either to fracturing or to chemical dissolution of the mineral framework. Although

fracture porosity may be in the order of 0.1 percent or less, a well-connected fracture network can have a large impact on hydraulic conductivity.

2.1.3 Flow System Characteristics for Selected Geologic Settings

The hydraulic properties of crystalline rock are strongly dependent upon the presence and extent of fracturing. Faults are fractures along which shear displacement has occurred. Joints are openings in which there has been no movement parallel to the fracture plane. Joints typically have lengths on the order of centimetres to tens of meters and occur in sets defined on the basis of the orientation of joint planes. Because of these preferred orientations, the hydraulic properties of fractured rocks are commonly anisotropic.

Breakdown of the rock matrix, and a greater amount of fracturing can create a zone where the permeability is two to three orders of magnitude higher than in the parent rock. Fractured media at a local scale can be extremely heterogeneous. Fracture properties controlling fluid flux include the number of fractures, spacing, fracture length, orientation of fracture set and fracture aperture. It should be recognized, however, that there might be a weak correlation between fracture density and permeability. Fractures that are steeply dipping are poorly sampled with vertical boreholes. Their presence and abundance may become apparent only during hydraulic testing. Alternatively, inclined boreholes could be considered.

Effective permeability of crystalline rock typically decreases by two or three orders of magnitude in the first several hundred meters below ground surface, as the number of fractures decreases and fracture close under increasing overburden pressure.

A. Groundwater in Igneous and Metamorphic rocks

Solid pieces of fresh metamorphic and plutonic igneous rocks have porosities of less than 3 percent and most commonly less than 1 percent. The few pores that present are small and generally are not interconnected. As a result, permeability is so small that they can be regarded as zero in almost all practical problems. Appreciable porosity and permeability, however, are developed through fracturing and weathering of the rock. The

aquifer tests indicated that permeability values parallel with the strike of the beds were two or three times the average permeability.

Fractures those are not associated with pronounced faults produce only a small increase in the overall porosity of rocks. Well yields suggest that permeability produced by fracturing of unweathered rock within a few hundred feet of the surface generally range from 0.001 to 10.0 darcys. Microscopically, the permeability varies from nearly zero in the solid rock to as much as several hundred darcys along highly fractured zones. Owing to the single orientation of most water-bearing fractures, the permeability of the rock as a whole is strongly anisotropic.

Effect of weathering may extend more than 300 feet into bedrock in regions of intense weathering. Depths of weathering of from 5 to 50 feet, however, are normally encountered. Hydrated minerals in weathered rock at the surface will form loose aggregates, which have porosities in excess of 35 percent. The porosity decreases with depth to zones in which the original rock-forming minerals are only partly altered. In the last few feet above fresh bedrock, the minerals are only slightly hydrated, but this is enough to produce differential expansion between mineral grains, which in turn creates a porosity of 2 to 10 percent. Well yields suggest that permeability values in the lower part of the weathered rock are roughly an order of magnitude greater than in the unaltered rock.

The average permeability of metamorphic and plutonic igneous rocks decreases rapidly with depth. This decrease is a combined effect of overburden and the tendency of surface disturbances to penetrate only a short distance into bedrock. Joints, faults and other fractures will tend to close at depth because of the weight of overlying material. Some openings, which are of interest to hydrogeologists can, therefore, exist at all depths. Water flow into some mines and tunnels, which are hundreds, and in some cases thousands of feet below land surface indicates that openings at great depths are large enough to supply water to wells.

Surface disturbances that produce rock permeability include landslides, rock falls, chemical weathering, root and frost wedging and various activities of man. Landslides and rock falls affect only the uppermost part of the bedrock and produce local deposits of rock debris, which can be important zones of rapid groundwater recharge and if saturated, good aquifers

B. Groundwater in Sedimentary Rocks

Shale, claystone, siltstone and other fine-grained detrital rocks account for roughly 50 % of all sedimentary rocks. Next in abundance are sandstones, then carbonate rocks and finally several minor types including conglomerate, gypsum, chert, tillite, salt and diatomite. The minor types constitute less than 2 percent of all exposed sedimentary rock.

Most fine-grained detrital rocks have relatively high porosities but very low permeability values. Siliceous shale, some claystones and most argillites will develop closely spaced joints if the rocks are near the surface. Also, if these rocks are involved in faulting, fractures that stay open at considerable depths may develop. Most commonly, however, the fine-grained rocks will be barriers to the movement of water.

The pore space in many fine-grained sedimentary rocks provides storage for vast quantities of water. Water stored in shales and similar rocks should always be considered in making groundwater inventories, particularly if differential hydraulic heads are great enough to induce drainage. Owing to the capillary effects, however, gravity drainage will be most important in the coarser sediments or in fractured zones.

Porosity of fine-grained sediments decreases with depth of burial and to some extent with age, although the relation is neither simple nor universal. Newly deposited fine muds will have porosities of between 50% and 90%. Compaction will force the pore water out of the fine material into adjacent permeable beds of sand so that porosities at depths of several hundred feet will be generally less than 50%. At depths of several thousand feet the porosity will be less than 30% and most commonly less than 25%. Extruded pore

water will not contribute a significant volume of water to aquifers under natural conditions because of the slow rates of compaction of the fine-grained sediments.

Sandstone

Porosity of sandstone ranges from less than 5% to a maximum of about 30%. The amount of pore space in an individual sample is a function of sorting, grain shape, packing and degree of cementation. Of these variables, cementation is the most important. Common cementing materials are clay minerals, calcite, dolomite and quartz.

Permeability values of sandstones are one to three orders of magnitude lower than permeability values of corresponding unconsolidated sediments. For example, medium-grained sand generally has permeability between 1000 and 30000 millidarcys, but values for the corresponding medium-grained sandstones generally range from 1 to 500 millidarcys. Some of the reduction in permeability values between sands and corresponding sandstones is caused by a closer packing of grains in the rock, but most must be owing to the restriction of pore space by the presence of cement. There is some correlation between porosity and permeability in sandstones of similar texture and lithology. The large number of variables influencing permeability, nevertheless, makes impossible the prediction of permeability on the basis of porosity alone.

Carbonate rocks

Limestone and dolomite, the two common carbonate rocks, originate from a large number of different sedimentary deposits such as inorganically precipitated limey muds, shell fragments, talus deposits, calcite sand, reef masses and accumulations of the remains of small planktonic organisms. The original porosity and permeability of many of these sediments are modified rather rapidly after burial.

Original porosity is relatively high in most young limestone. Permeability is generally low except in rocks such as breccias and coquina in which the large pores are not filled initially with cement. Permeability may range from less than one millidarcy for clay-rich dense limestone to several thousand darcys for partly cemented coarse breccia.

Intermediate values of 10 to 500 millidarcys are more common, however, for limestone having some original porosity. Dense crystalline limestone will generally have a permeability of less than one millidarcy.

Fractures and secondary solution openings along bedding planes and zones of primary porosity probably transmit the most water. The important conclusion concerning the permeability values of some younger carbonate rocks is that a search must be made for zones of secondary porosity produced through fracturing and solution. Zones of primary porosity, although permeable enough to be of interest to the petroleum industry, are not good aquifers. Primary porosity of the rock as a whole is significant in as much as it provides storage space for groundwater, which is released slowly to the more permeable zones. Sedimentary rocks all have a certain amount of stratification that produces some anisotropy in the vertical direction as compared with the horizontal direction.

2.2 Methods of Fracture Model Construction

Groundwater flow in actual rock mass is partly depend on the rock type, weathered zone, fractures existence and type. In the groundwater flow calculation, specific nature of area should be modelled. In the fractured rock mass, fracture model must be created for calculating groundwater flow. For generating fracture model, major fractures selection must be performed. There are some methods for construction of fracture model. Surface inspection, borehole data analysis, lineament taken by remote sensing system should be used to construct fracture model. Figure 2.2.1 shows some methods of fracture model construction.

Fracture Data

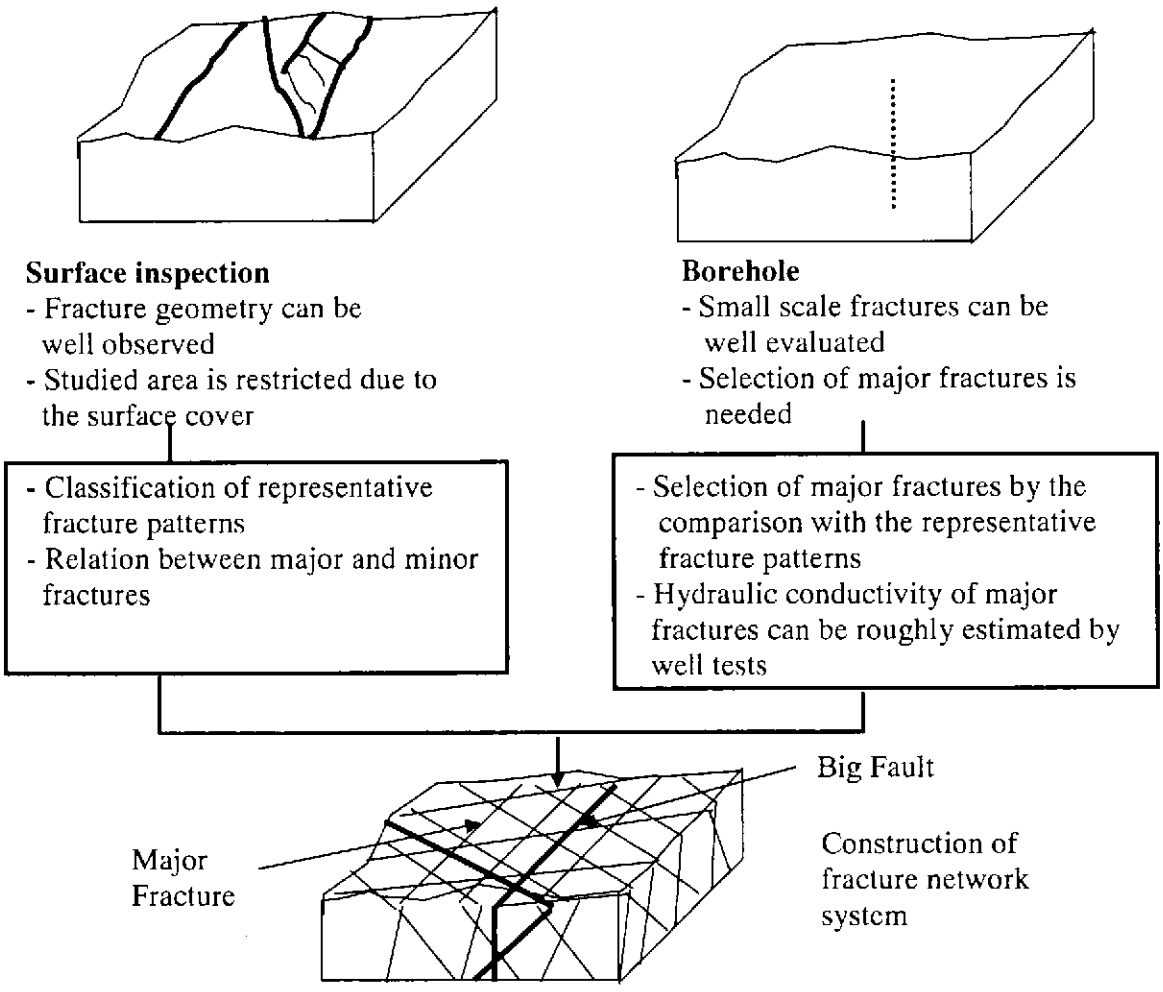

Figure 2.2.1 Methods of Fracture Model Construction

In the selection of major fractures, surface inspection should be done. By doing this field survey, actual major fractures can be observed and the geometry of selected major fractures can be figured out. The major fractures should have step structure. Small fractures in step fractures and direction of major fractures can be observed. We can estimate the direction of major fractures. In this field measurement, we can get clear relation between major and secondary fractures. Furthermore, the field survey results are compared with stereographic projections interpretation results of fractures orientation data read by Borehole Television (BTV). This is to check whether major fractures observed in boreholes are same with major fractures in the field.

Nevertheless, all surface of Tono Area are covered with soil so that it is difficult to find fractures patterns by doing field survey. Although results of surface inspections should be used, it is difficult to be executed in Tono Area due to dense forest and thick soil covers. It was considered how to construct fractures model by using limited number of data. Therefore, in this study, boreholes data were mainly used for constructing fracture model. The major fractures selection was performed by evaluation and interpretation the stereographic projections of fractures orientation data read by Borehole Television (BTV). The selected major fractures were also checked by comparing with the lineament data taken by remote sensing sytem.

2.3 Problems Should be Solved

In the procedure of fracture modeling and groundwater calculation, boreholes data are mainly used as the basic information. Problems should be overcome in this study are summarized as follows:

a. Treatment of borehole data

- Interpretation of the fractures patterns and major fractures directions based on the stereographic projections of fractures orientation data read by Borehole Television (BTV) figures.
- Determination of the fractures patterns and major fractures directions after observing and comparing with fractures in bore cores.

b. Fracture Modeling

- Making a fractures model after selecting fractures patterns and defining major fractures directions, combining with sedimentary rock and completed by actual data such as hydraulic conductivity.
- Determination of boundary conditions

c. Calculation of Groundwater Flow

- After completing fracture model and combining with sedimentary rock, groundwater flow is calculated in this composite model (fractured and sedimentary rock mass).

d. Validation of Model

- Calculations results of the model are compared with the measurements results obtained by Japan Nuclear Cycle Development Institute (JNC), to validate the fractures model.

2.4 Scope of the Study

This study has focused on fracture modeling and groundwater flow analysis based on boreholes data taken in the actual field. There are two major procedures in borehole treatment:

1. Stereographic projections
   - to find clear patterns of fractures
2. Bore cores inspection
   - to check and compare the fractures patterns interpreted from stereographic projections with the fractures in bore cores

Three types of boreholes division were used for making stereographic projections which are of every 5 meter, every 5 meter with sliding 1 meter and every 1 meter, to make clear the gradual change of fracture pattern around every major fracture, to check the relation between fracture pattern and hydraulic conductivity and the scale (width) of major fracture. The whole frame of this study is roughly presented in Figure 2.4.1. Detailed explanation of this figure is given in the following chapters.

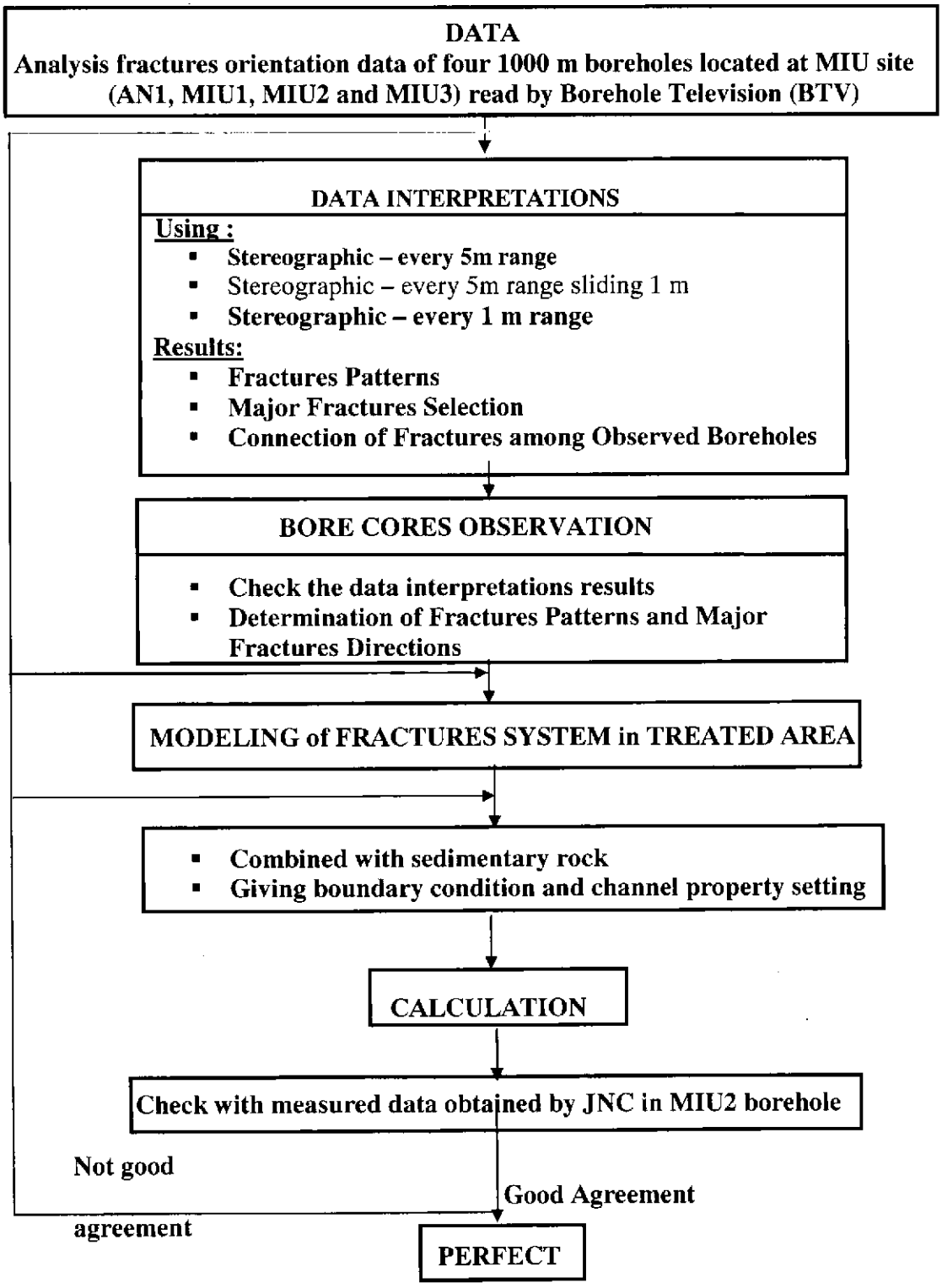

Figure 2.4.1 Scope of the Study

CHAPTER 3

BASIC IDEA OF FRACTURE MODELING AND GROUNDWATER FLOW ANALYSIS BY USING DON-CHAN MODEL

3.1 Stereographic Projection

Fracture direction can be projected at the lower or upper hemisphere. The basic idea of stereographic projection is shown in Figure 3.1.1 and 3.1.2. As well known, fracture in 3-Dimensional space can be projected on 2-Dimensional projection surface. The method is sub-divided into two techniques, Wulff Diagram (Figure 3.1.3) and Equal-Area Projection or Schmidt Diagram (Figure 3.1.4).

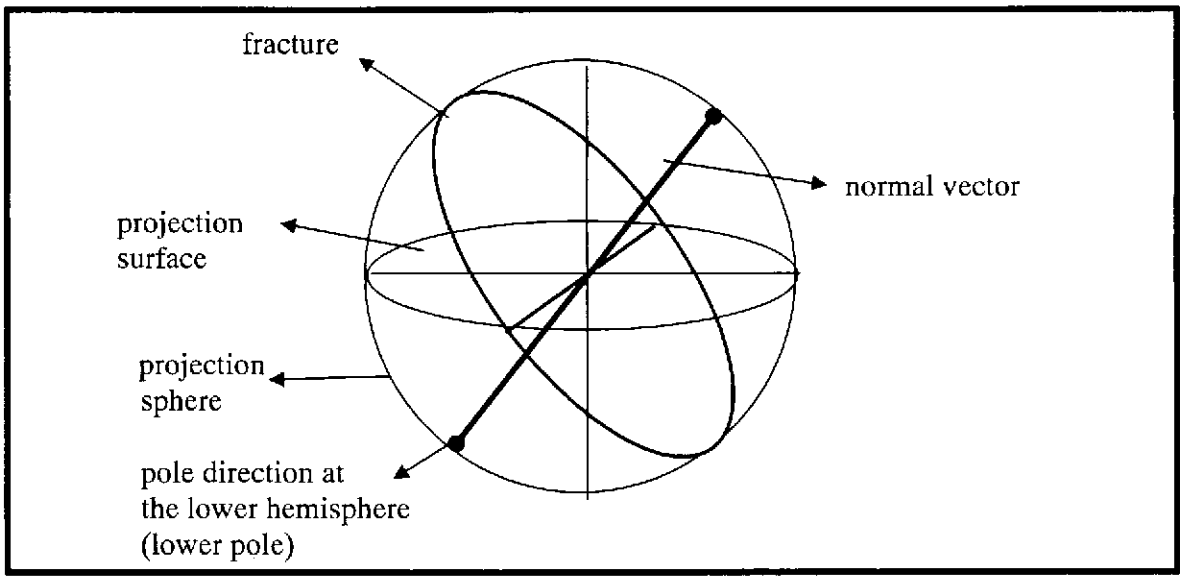

Figure 3.1.1 Stereograph projection showing lower hemisphere projection point

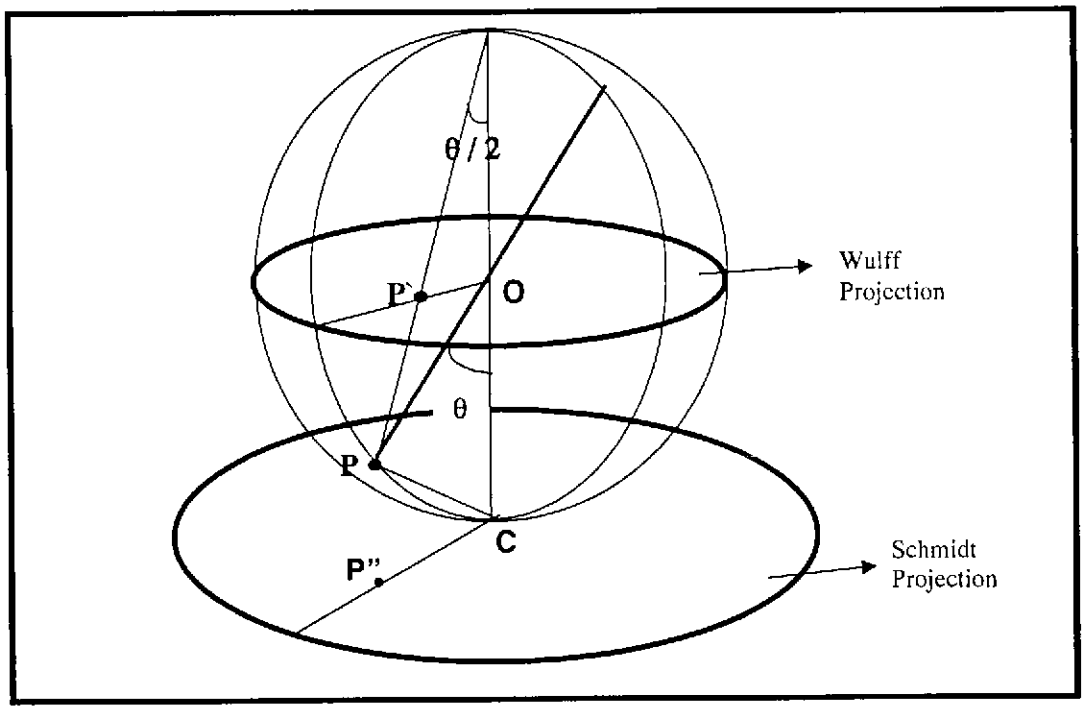

Figure 3.1.2 Stereographic projection by using Wulff Diagram and Schmidt Diagram

a. Stereographic Projection and Wulff Diagram

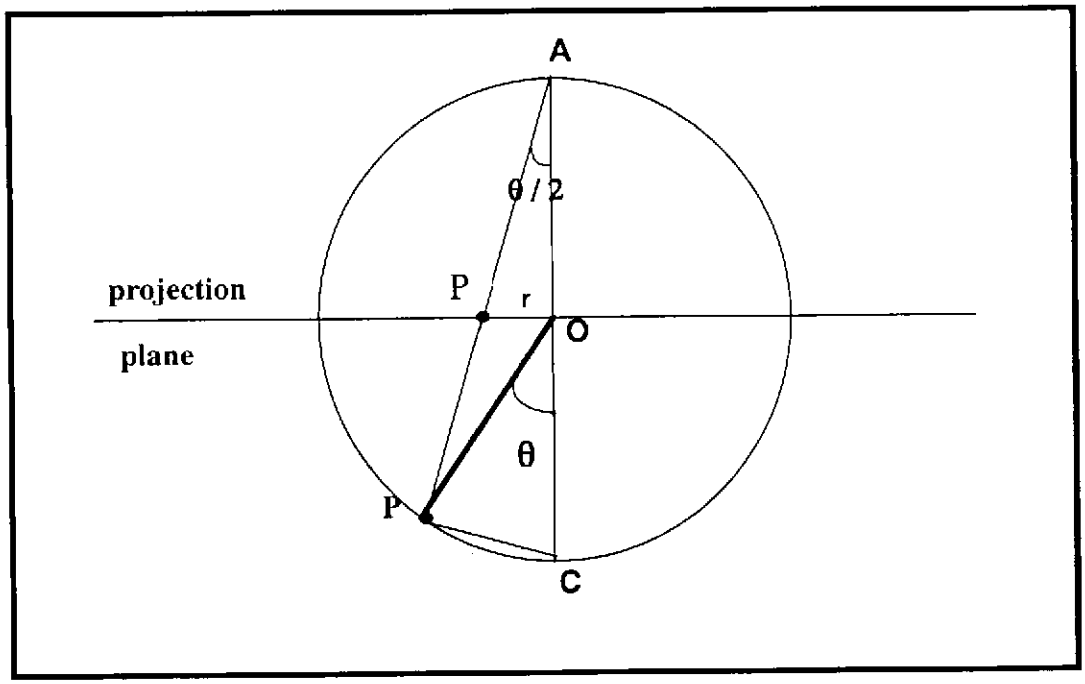

Figure 3.1.3 Stereographic Projection and Wulff Diagram

The equal-angle stereographic or simply stereographic projection, is illustrated above. The projection plane is the horizontal xOy plane to which the center O of the sphere belongs. The projection P' of the fracture pole P is the intersection of the line joining the upper point A of the vertical diameter to the fracture pole P with the xOy plane. In the 2D polar coordinates of plane xOy, the coordinates of P' are:

$$\textbf{Polar distance: } r = \tan(\theta / 2) \qquad (3.1.1)$$

An advantage of the stereographic projection is that it presents no distortion; a small circular area drawn anywhere on the reference sphere is represented by a very nearly circular area in the stereographic projection. However, an area of a given size on the reference sphere is represented in the stereographic projection by an area the size of which increases conspicuously with the distance from the center of the projection circle. Plotting the poles according to a stereographic projection produces a Wulff diagram.

b. Equal-Area Projection and Schmidt Diagram

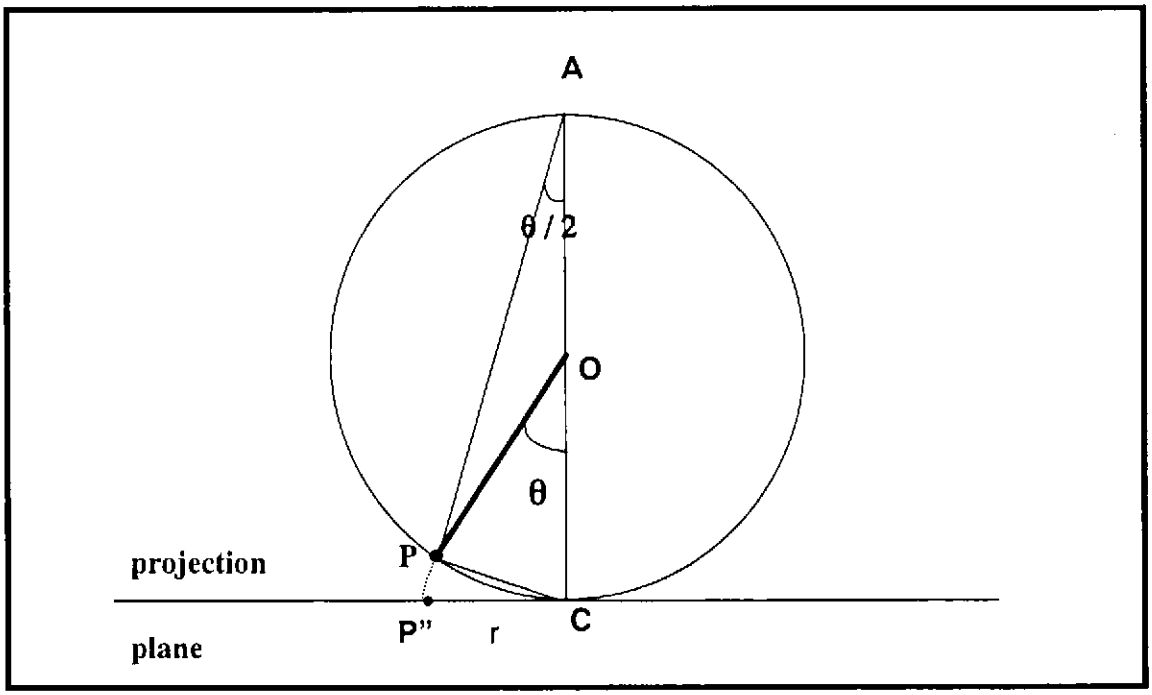

Figure 3.1.4 Equal-Area Projection and Schmidt Diagram

The Lambert equal-area or simply equal-area projection is illustrated above. The projection plane is the plane tangent to the lower point C of the vertical diameter of the reference sphere. The vector joining C to the fracture lower pole P is rotated in its vertical plane in such a way as to become a vector CP" in the projection plane. In the 2D polar coordinates of the projection plane centered on C, the coordinates of P" are:

$$\textbf{Polar distance: } r = 2\sin(\theta / 2) \qquad (3.1.2)$$

Two equal areas in the projection represent two equal areas in the reference hemisphere. This feature is advantageous in the statistical study of the fracture density. A counterpart of this projection lies in the distortion, which is greatest at the circumference of the projection circle. Plotting the fracture poles according to this projection is called a Schmidt diagram. For a lower-hemisphere projection, the left-hand poles represent eastward dipping fractures, whereas right hand poles represent westward dipping fractures. In case of an upper-hemisphere projection, the diagram would be transformed according to symmetry around the center of the projection circle, and hence, the opposite applies.

Steps in making stereographic projection

Based on the above explanation, we can use either Schmidt or Wullf diagram. In this calculation, Schmidt diagram is used.

$$r = CP'' = CP = 2 \sin(\theta/2) \qquad (3.1.3)$$

In order to create stereograph projection, it is necessary to convert strike and dip angle of a fracture into X and Y coordinate values.

$$\textbf{Coordinate X} = r \cos\alpha = 2 \sin(\theta/2) \cos\alpha$$

$$\textbf{Coordinate Y} = r \sin\alpha = 2 \sin(\theta/2) \sin\alpha$$

where: $r = CP'' = CP = 2R \sin(\theta/2)$

θ = dip angle

(3.1.4)

3.2 Major Fractures Selection Based On Borehole Data

The procedure of major fractures selection based on borehole data is shown by the following figure:

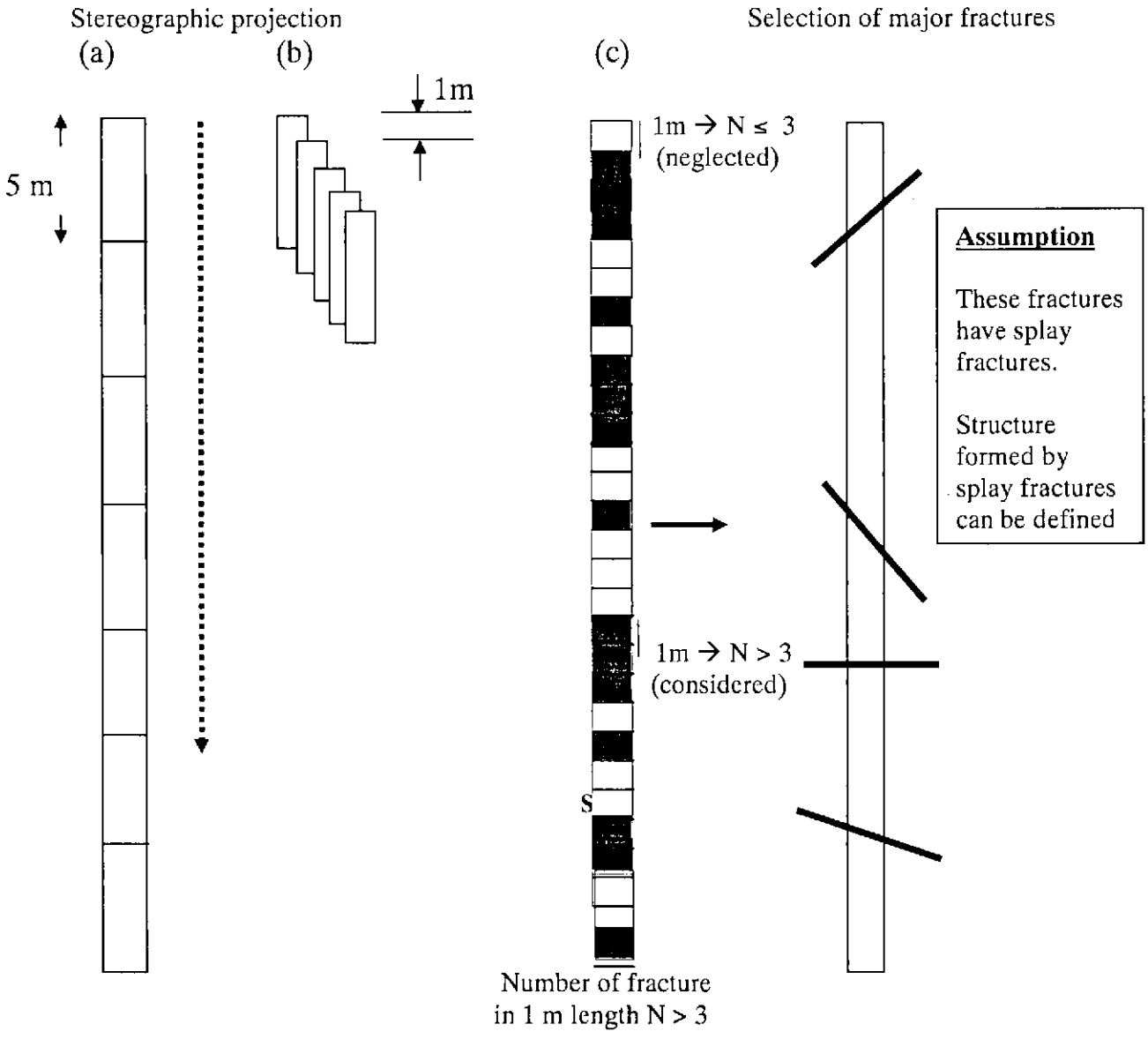

Figure 3.2.1 Procedure of major fractures selection

Stereographic projections in every 5 meter borehole depth were made to have rough interpretation about the fractures patterns. The length 5 meter of stereographic projection was decided with considering length of insitu test. Length 5 meter has been being used for common test such as hydraulic conductivity measurement. By making stereographic projection in every 5 meter length, it is possible to compare with hydraulic test data.

Stereographic projections in every 5 meter borehole depth with sliding 1 meter were drawn for making clear the gradual change of fracture pattern around every major fracture and for getting relation between fracture pattern and hydraulic conductivity.

Stereographic projections in every 1 meter borehole depth were made to check the scale (width) of major fractures.

3.3. Technique for Fractures Patterns Selection

Figure 3.3.1 and Figure 3.3.2 show the technique for selection of fractures patterns by using stereographic projection. As explained before in the literature review 2.1., a fracture is imposed of step structure, single fracture part and diverging splay fracture part (Figure 3.3.1). In the step structure, many splay fractures were created in the course of the shear displacement as shown in Figure 3.3.2. Those splay and master fracture in the step structure are extending in the vertical direction of the displacement so that the pole directions of those fracture should be arranging in a great circle in the stereographic projection. From this fact, the step structure can be defined by stereographic projection. On the other hand, for simple fracture part and terminal part, pole directions are plotted on a part of this great circle (see Figure 3.3.1).

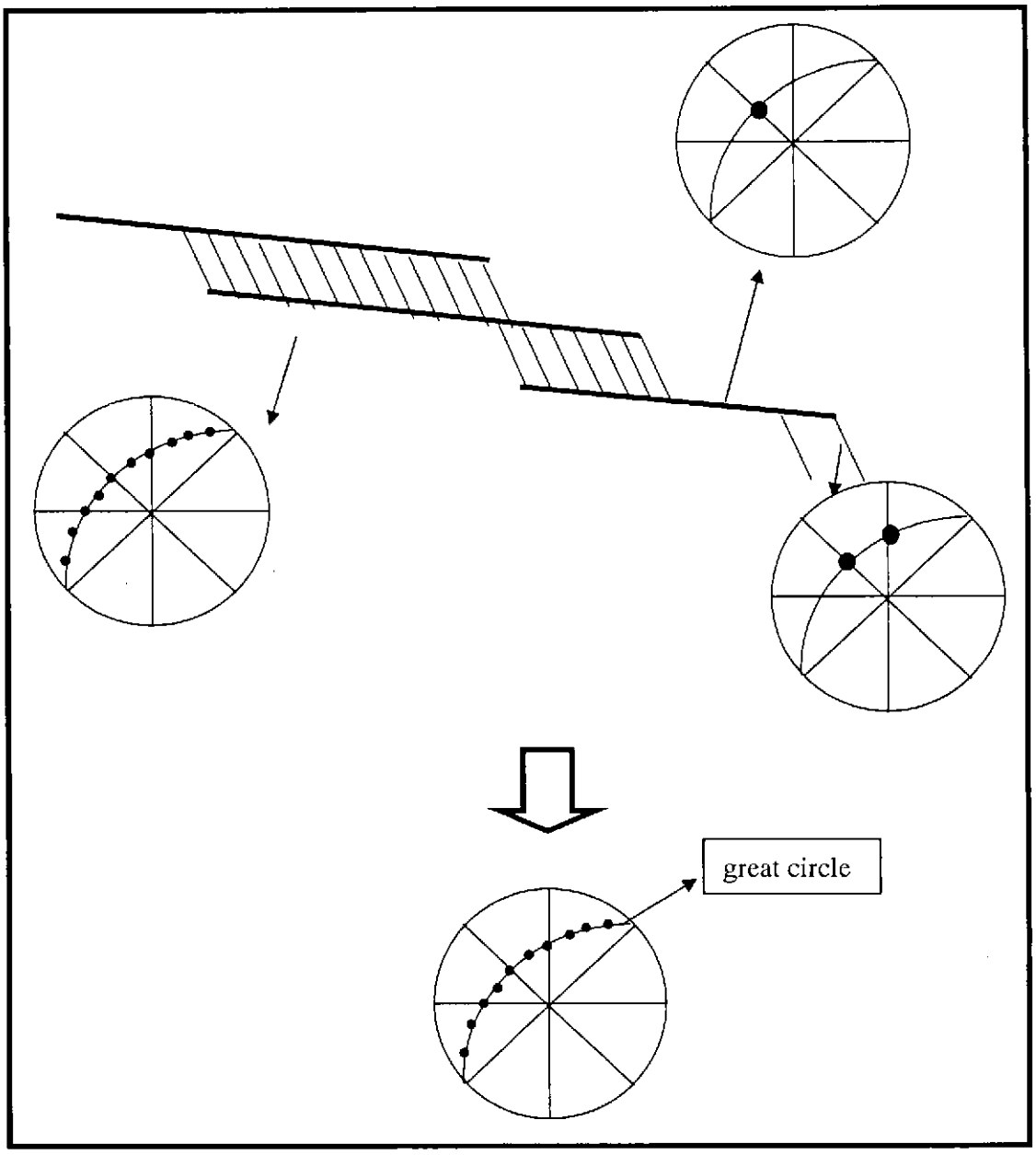

Figure 3.3.1 Stereographic projection of a step structure

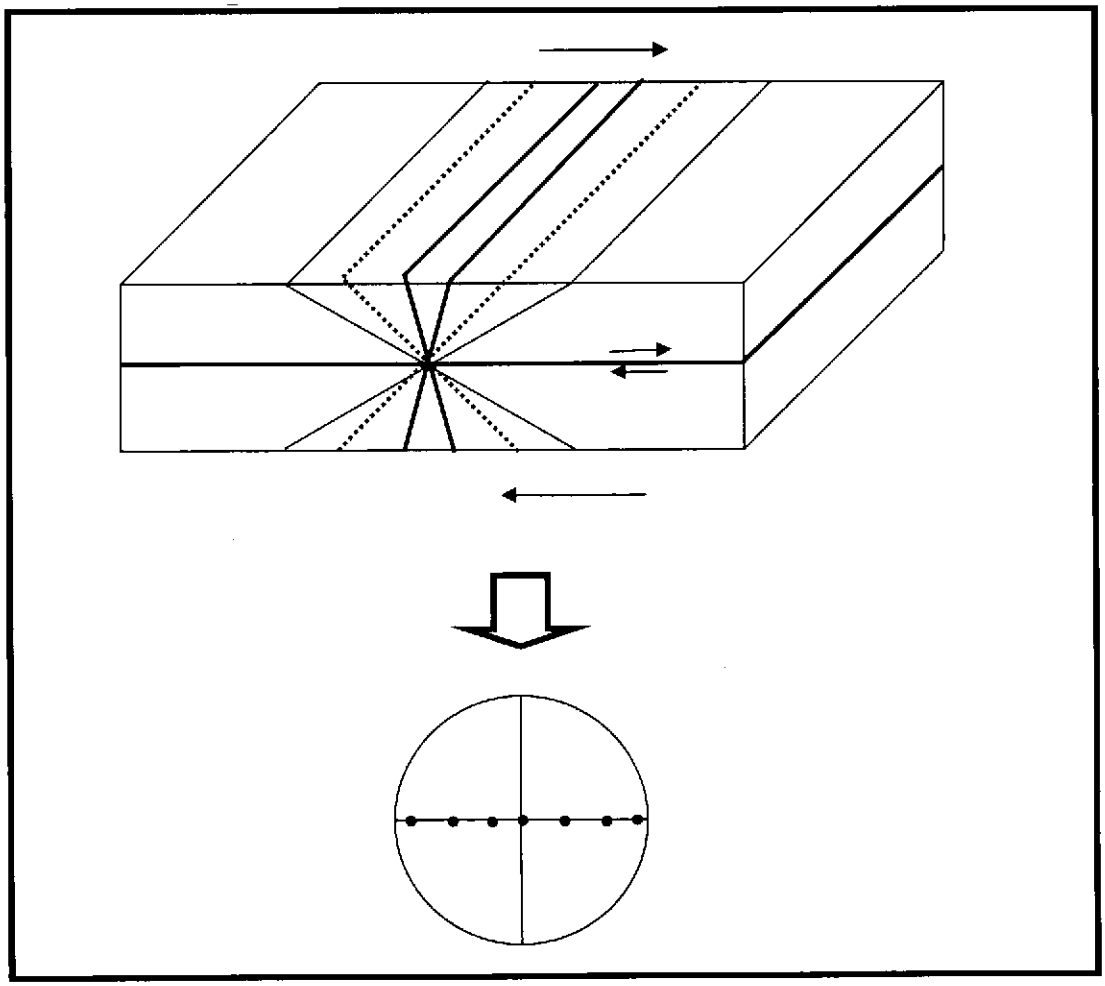

Figure 3.3.2 Stereographic projection of fractures created in step structures

3.4 Fracture Zone Width

From a fracture pattern, major fracture was selected. The major fracture zone width was calculated as follow:

Fracture Zone Width (*FZW of one fracture*)
- FZW fracture 1, FZW fracture 2, FZW fracture 3.....FZW fracture n.

Pattern X

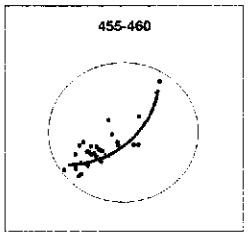

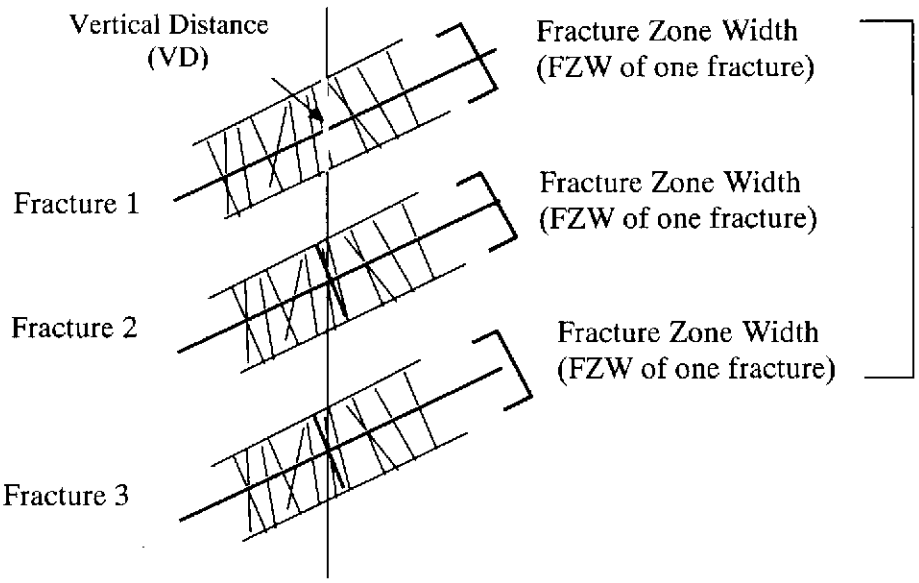

Pattern X

a. Average zone vertical distance in each borehole = Avg VD =

$$\frac{VD\ 1 + VD\ 2 + VD\ 3 + \ldots\ldots + VDn}{n}$$

b. Average zone vertical distance in pattern X = Avg VD PatternX

$$\frac{Avg\ VD\ AN1 + Avg\ VD\ MIU\ 1 + Avg\ VD\ MIU\ 2 + Avg\ VD\ MIU\ 3}{4}$$

c. Fracture zone width of each fracture in pattern X = *FZW of one fracture*
Avg. VD PatternX * sin (90 – dip angle)

Fracture Zone Width of a Representative Fracture (*FZW of one Repr. Fr*)

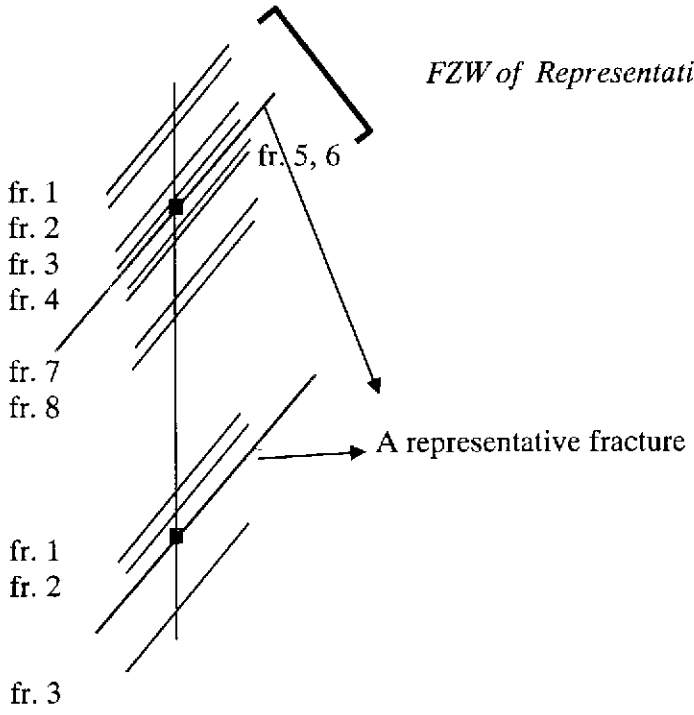

Pattern X

a.Average numbers of fractures create 1 representative fracture in pattern X = Avg FRC create one Repr. Fr =

$$\frac{\Sigma \text{ FRC create 1 Repr. fr in AN1} + \Sigma \ldots\text{in MIU 1} + \Sigma \ldots\text{in MIU 2} + \Sigma \ldots\text{in MIU 3}}{\text{total numbers of data}}$$

b.Fracture zone width of a representative fracture in pattern X = *FZW of one Repr. Fr* =

Avg FRC create one Repr. Fr * FZW of one fracture

3.5 Connection of Fractures

Considering continuity of fractures, uncertainty problems of fractures connections rise, such as:

1. Step fractures are not widely distributed (partial development of step fracture along major fracture)

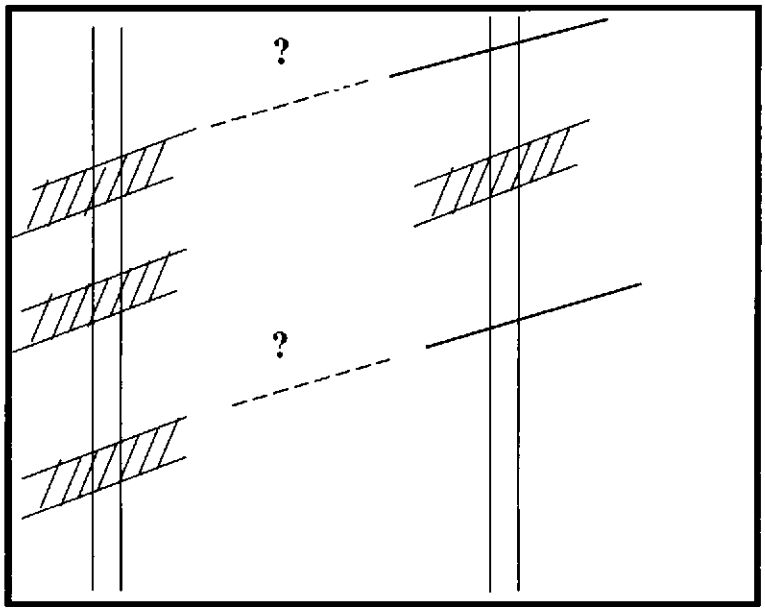

After six fractures patterns were decided, connections between the same fractures patterns were checked. The connection of each fracture pattern among observed boreholes was analysed.

2. Spatial change of direction of major fracture

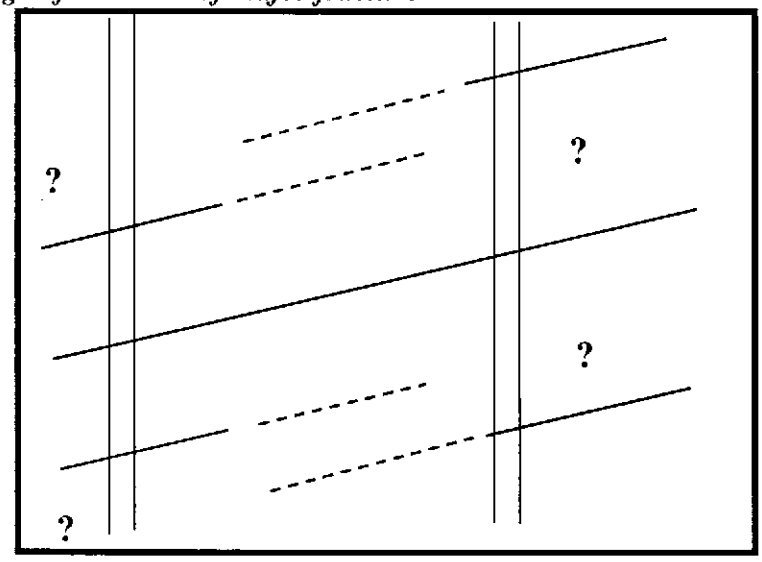

Therefore, in this study,. fracture modeling was executed by applying statistical method, calculating average distance (spacing) between fractures of each pattern.

Calculation of average distance between fractures is shown as follow:

Fracture Generate Interval (Average Distance between Fractures) = *FGI*

Pattern X

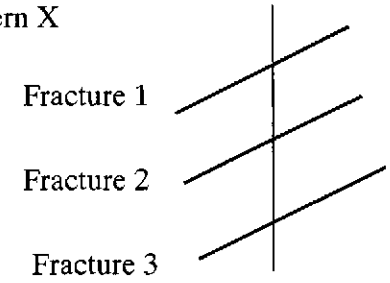

a. <u>Low angle fracture</u>

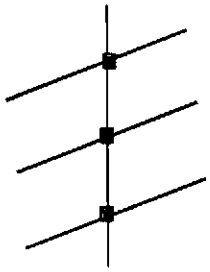

Fracture generate interval

b. <u>High angle fracture</u>

- Since high angle fracture will create many fractures in the model, it is necessary to make 1 representative fracture for some adjacent high angle fractures.

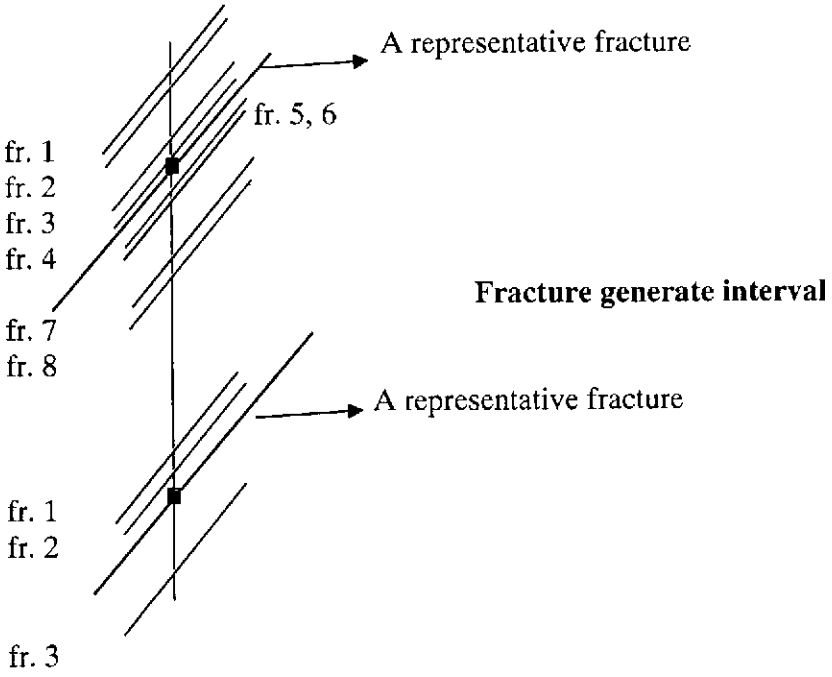

a. A representative fracture depth (symbol = ■) = Repr. FD =

$$\frac{\text{depth of fracture 1 + depth of fracture 2 + ... + depth of fracture n}}{\text{n}}$$

b. Fracture generate interval (average distance between fractures) = *FGI* =

Pattern X

$$\frac{\Sigma \text{ FGI AN1} + \Sigma \text{ FGI MIU1} + \Sigma \text{ FGI MIU2} + \Sigma \text{ FGI MIU3}}{\text{Total number of data}}$$

3.6 Basic Concept of Don Chan Model

The proper analysis of groundwater flow in a fractured rock mass is very important in many geotechnical fields such as dam construction, tunnel excavation, water resource development within the rock mass, and deep underground waste disposal. For analysing groundwater flow, the proper hydrogeological modeling of a fractured rock mass is indispensable.

It has been pointed out in many previous studies that a large amount of groundwater flows through several selected seepage paths called channels that have developed in a fractured rock mass (Bear et al., 1993). Tanaka et al. (1994) and Watanabe et al. (1994) studied the hydrogeological features in fractured granite found in the Kamaishi Mine, Japan, and concluded that the intersections between conjugate fractures tend to be the highly permeable channels.

It is important to properly evaluate the channel network in an actual rock mass and to construct a reliable hydrogeological model of the rock mass before any ground water analysis is performed. The estimation of the locations and the hydraulic conductivities of those channels in an actual rock mass, however, are very difficult, so that the general technique of how to construct a hydrogeological model has not yet been established.

The channel might have been created during a long history of geotectonic movement that includes the creation, the propagation, and the reactivation of fractures, and may be

closely related to the geological features of the fractures system. Basic study of the relation between the geological structure and the channel is important in creating the proper techique for hydrogeological modelling.

Bossart and Mazurek (1991) studied, in detail, the geometry and hydraulic features of fractures that developed in the Grimsel Test Site constructed in the Alpine region of Switzerland. It was found that the fractures created or reactivated during the brittle deformation stage were the major conduits of groundwater flow. Munier (1993) examined the fracture system that developed in the vicinity of the Aspo Hard Rock Laboratory in Sweden, and concluded that groundwater mainly flows through selected fractures that have been generated or reactivated within geologically recent time. These studies have clearly shown that the geological history of a fractured rock mass must be taken into consideration when a hydrogeological model is constructed.

It was observed that fractures created or reactivated in recent age (around 10.000 or 100.000 years before) were filled with water. These young-aged fractures can be as water conducting fractures (WCF). While, older fractures were completely filled with mineral such as clay, CaCO3. It is almost impossible for water to flow through such fractures.

Mazurek et al. (1995) reported on the hydrogeological features of the rock mass around the Aspo Hard Rock Laboratory. It was concluded that the fractures running parallel to the maximum stress axis formed the hydraulically active fractures and can act as channels for groundwater flow. The importance of the splay fractures on the behaviour of groundwater flow was also pointed out, with reference to the concept discussed in Martel and Pollard (1989). These studies have clearly pointed out that the hydraulic nature of a rock mass is closely related to the geological features and the earth pressure conditions.

Many small fractures are concentrated at the step structure, at the end points of single fractures, and the intersections between fractures. From the fact that highly weathered regions are mostly located at these features, it is thought that these features produce the

highly permeable zones. The concentration and deformation of these small fractures may create open space within these features. The open spaces allow for large hydraulic conductivity. This is possible reason that the highly weathered regions are located at the features.

Based on the previous study about fractured granite in Hinachi Area, Japan, it was concluded that the average hydraulic conductivity of highly weathered areas, estimated from porosity, is 10^4 to 10^5 times larger than fresh granite. The highly weathered areas, located at the geological features (such as the step structure, the end points of single fractures, and the intersections between fractures) and thought to be an indication of highly permeable regions, act as channels for groundwater flow. The channel network in an actual rock mass, presenting flow in a fracture, must be properly modelled for the analysis of groundwater flow. For analysing groundwater flow based on channel network, we use Donen-Saitama Channeling Model (Don-Chan Model).

3.6.1 Model of Region

In the Don-Chan Model, region shape model must be created. This region shape model is a region of rock mass where fractures are created. To make the region shape model, input data must be given, such as: total domain number, total boundary plane number, total number of geological domain, domain type, regular mesh interval, boundary type, total number of plane component point, coordinate of plane component point.

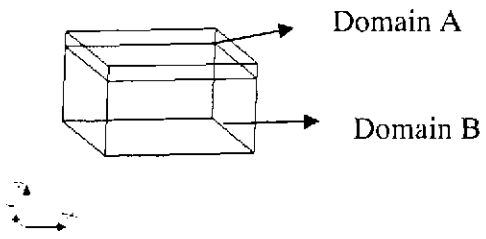

Figure 3.6.1 Model of a region. Case of the combination of two different domains.

3.6.2 Model of Fracture

Figures below schematically illustrate the concept of modeling process. Combination of two different fracture system is roughly presented.

- The figures represent rock masses having fractures.
- Fractures are approximated by network of fractures planes. To generate a fracture, input data are needed, such as: fracture type, water barrier fracture width, permeability, process/history of fracture, strike and dip angle, distance between channel

➢ A rock mass having four fractures

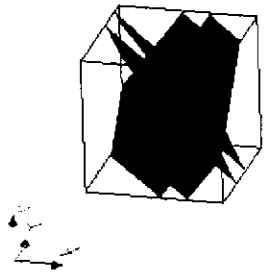

Figure 3.6.2 a. Model of fractures

➢ A rock mass having three fractures and same direction (parallel fractures)

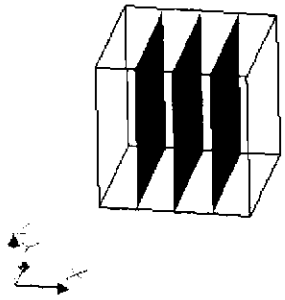

Figure 3.6.2 b. Model of fractures

- Network of fractures planes are combined to each other

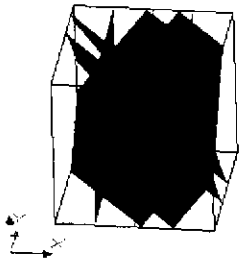

Figure 3.6.2 c. Model of fractures. Combination of four fractures (3.6.2 a) and three parallel fractures (3.6.2 b)

- Groundwater can flow through the fractures. To account for the flow through these fractures, a regular network of small channels is assumed to be located on every fracture, as shown by yellow colour lines, and create two dimensional channel networks (Figure 3.6.3).
- It is assumed that the orientation of an individual channel on each fracture is either horizontal or vertical.
- When the hydraulic conductivity of each fracture is anisotropic, the channel directions are selected by the principal directions of the permeability tensor of the fracture.
- Intersection lines among fractures (red colour lines in Figure 3.6.3) are also thought as channels.
- When combining all channels illustrated in yellow and red colour lines, the final channel network can be constructed.

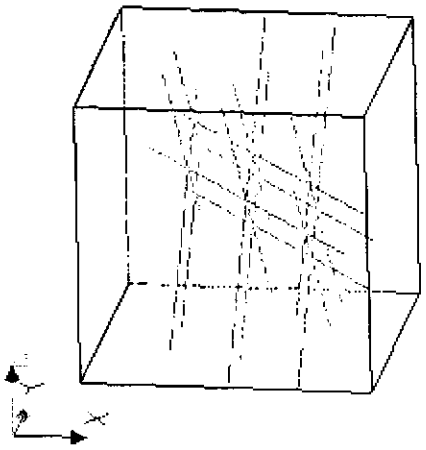

Figure 3.6.3 Model of a channel network.. Combination of regular network (yellow colour) on every fracture and intersection line (red colour).

3.6.3 Process of Channel Network Modeling

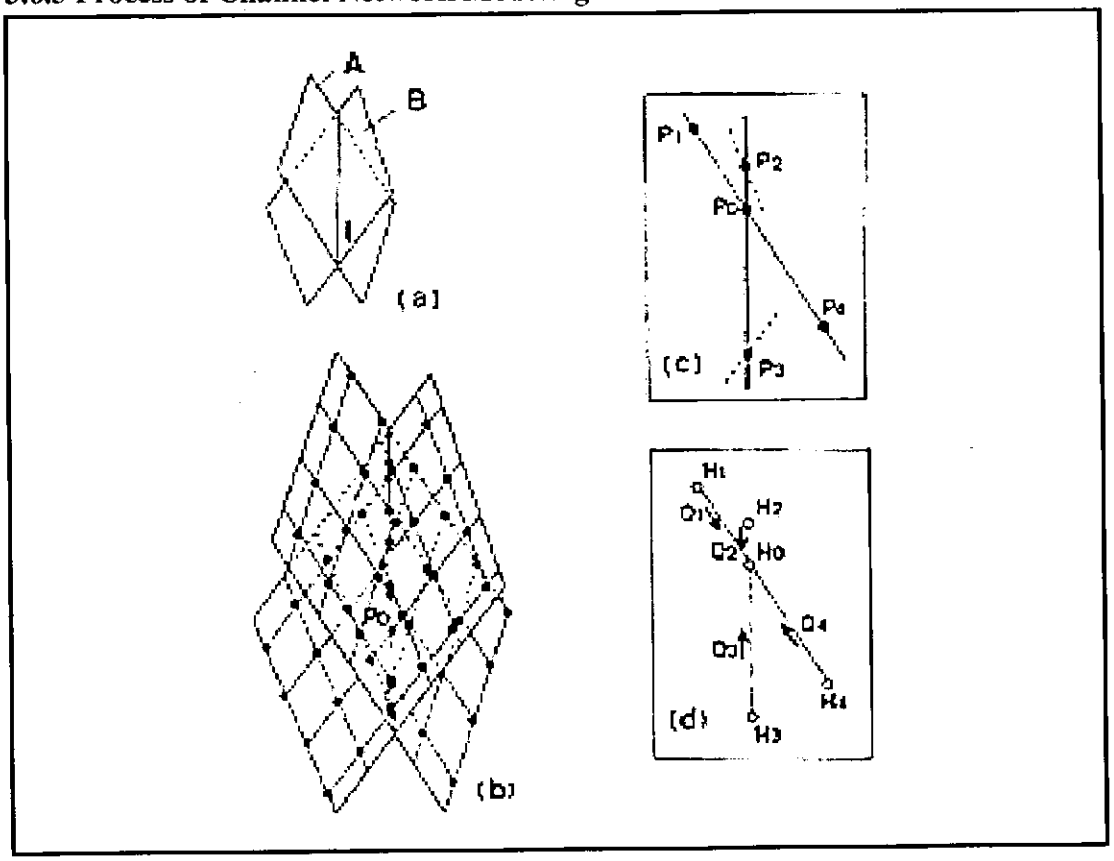

Figure 3.6.4 Schematic illustration of an example of a channel network constructed on fractures A and B shown in (a). Illustration of the network of channels (b). Illustration of the connecting channels and water flow around P0 point (c). The flow conditions in the channels where H0, H1, H2, H3 and H4 are the piezometric heads on points P0, P1, P2, P3 and P4 respectively (d). The letters Q1, Q2, Q3 and Q4 indicate the discharge of groundwater flow. Solid circles are the crossing points between channels.

- Figure (b) illustrates an example of the channel network constructed around an intersection line between two fractures A and B in Figure (a).
- This network is composed of one intersection line and the channels assumed on each fracture. Solid circle indicate the crossing points between these channels.
- Figure (c) represents the connection between a crossing point Po, shown in Figure (b), and surrounding points P1, P2, P3 and P4. These points are connected by channels. The broken lines indicate channels on fracture B.
- Figure (d) illustrates the flow conditions in these channels. H0, H1, H2, H3 and H4 are the piezometric heads on points P0, P1, P2, P3 and P4, respectively. Notation of Q1, Q2, Q3 and Q4 represent the discharge of groundwater flowing into point P0 from P1, P2, P3 and P4, respectively.
- Under steady-state conditions, the sum of Q1,Q2,Q3 and Q4 must be zero. That is:

$$\boxed{Q1 + Q2 + Q3 + Q4 = 0} \qquad (3.6.1)$$

- The discharge for a given point Qi (i= 1 to 4) can be written as :

$$\boxed{Qi = Ti \times (Hi - H0) / Li} \qquad (3.6.2)$$

where, Li is the distance between P0 and Pi (i = 1 to 4) and Ti is the transmissivity of the channel connecting P0 and Pi.

- Transmissivity Estimation :

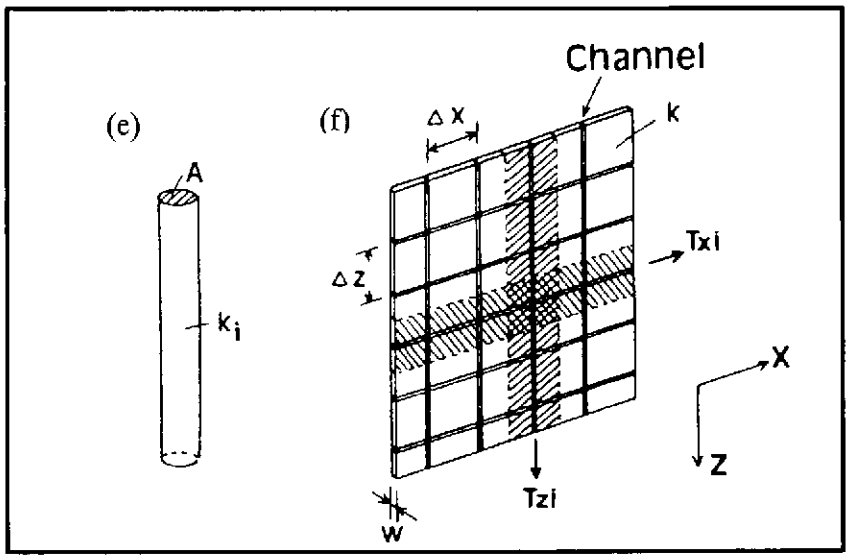

Figure 3.6.5 Schematic illustration for the estimation of transmissivity T. Typical channel along an intersection line, step structure or an end point of a fracture (e). Here, ki is the hydraulic conductivity of the channel and A the area of the channel. Assumed channels on a fracture, oriented in the x and z directions , having the respective transmissivities Txi and Tzi. The x and z spacings of the channels are given by Δx and Δz , respectively (f). w is the width of the fracture and k is the hydraulic conductivity.

- The estimation of the transmissivity Ti of every channel is also important. Figures above schematically illustrate a method to estimate the transmissivity.
- For a channel presenting an intersection line or a step structure, Ti can be simply estimated by the following equation as shown in Figure (e) :

$$\mathbf{Ti = A \times ki} \qquad \textbf{(3.6.3)}$$

where, ki is the hydraulic conductivity of the channel and A is the cross-sectional area of the channel.

- For the assumed channel on a fracture, the transmissivity Ti can estimated as :

$$\mathbf{Txi = w \times \Delta z \times k}$$
$$\mathbf{Tzi = w \times \Delta x \times k} \qquad \textbf{(3.6.4)}$$

where,Δx andΔz are the spacings of the channels in the x and z directions as shown in Figure (f), w is the fracture width and k the hydraulic conductivity of the fracture.

- Transmissivities Txi and Tzi are for the channels that are assumed in the x and z directions, respectively.

- Similar equations can be constructed for every crossing point in the similar manner.
- By solving all equations under given boundary conditions and set channel property, the piezometric head distribution can be calculated.

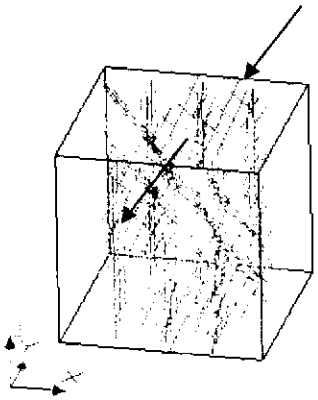

Figure 3.6.6 Example of piezometric head distribution

3.6.4 Extension of the Old Version Don-Chan Model

In the old version of Don-Chan Model, the calculation of groundwater is only applicable for fractured rock mass. In order to enhance capability of Don Chan Model to be applicable in many countries, which have different type of rock, the Don-Chan Model was modified. The new version of Don-Chan Model is also applicable for sedimentary rock condition. In this new Don Chan Program, regular fracture network is assumed for presenting groundwater flow in sedimentary rock and the intersections between these assumed fractures are thought to be the highly permeable channels for groundwater flow. By using the new version of Don-Chan Model, groundwater flow can be calculated, not only at the fractured rock mass, but also at the sedimentary rock condition or at the combined fractured and sedimentary rock condition (composite media).

The main difference for the new version of Don-Chan Model is that the transmissivity calculation for sedimentary rock is added. In this case, channel area and permeability of sedimentary rock are different with the ones in fractured rock. In sedimentary rock, all area can flow water, while in fractured rock only the fractured part can flow water. Input data for sedimentary rock such as regular mesh interval, sedimentary rock permeability, domain type (sedimentary or fractured rock) is also needed.

Old Version of Don-Chan Model

- applicable for fractured rock mass

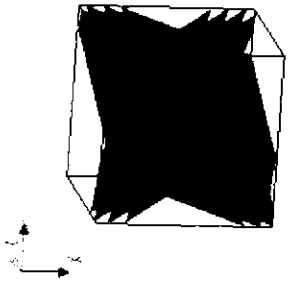

Figure 3.6.7 Model of one domain- fractures

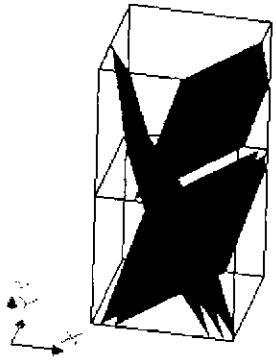

Figure 3.6.8 Model of two domain- fractures

New Version of Don-Chan Model

- applicable for fractured rock mass, sedimentary rock or combination of them

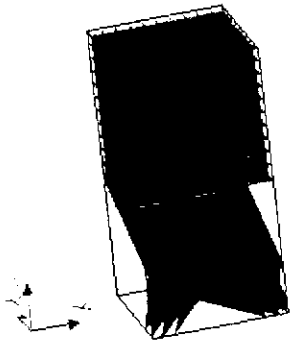

Figure 3.6.9 Composite model of two domain- sedimentary and fractured rock mass

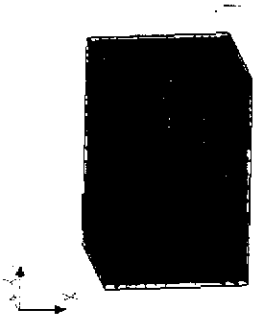

Figure 3.6.10 Composite model of three domain- sedimentary and fractured rock mass

3.7 Groundwater Flow Calculation by Using Don Chan Model

A. Prepared Data

Input data :

1. Model Data
   - Total Domain Number
   - Total Boundary Plane Number
   - Domain Type (Fractured or Sedimentary Rock Mass)
   - Regular Mesh Interval
   - Boundary Plane Coordinate
2. Fracture Data
   - Total Number of Fractures Data
   - Fracture Type
   - Strike, Dip
   - Fracture Generate Interval
   - Total Number of Fracture Domain

Property Setting :

- Total number of regular mesh domain
- Regular mesh (sedimentary rock) permeability
- Total number of fractures groups and fractures domains
- Fractures permeability
- Fractures zone width
-

Boundary Condition Data

- Total number of plane in which boundary conditions are given
- Plane number where boundary conditions are given
- Boundary condition values

B. Calculation

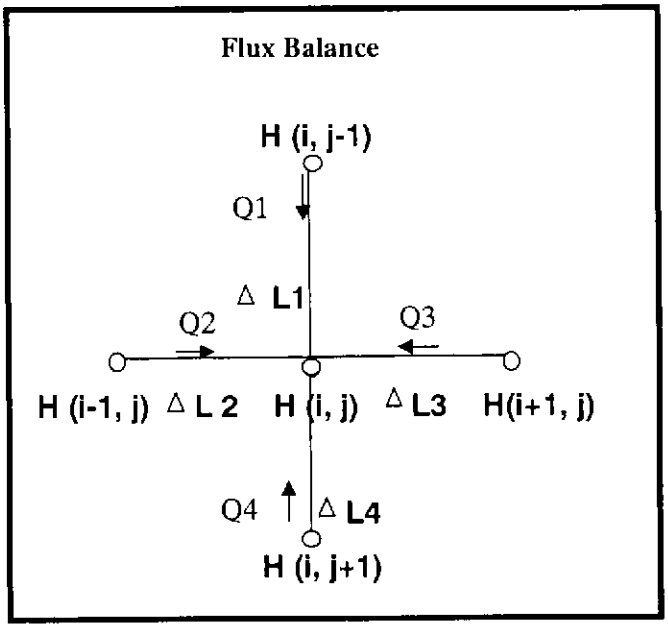

$$Q1 = -k \frac{H(i,j) - H(i,j-1)}{\Delta L1} * A$$

$$Q2 = -k \frac{H(i,j) - H(i-1,j)}{\Delta L2} * A$$

$$Q3 = -k \frac{H(i+1,j) - H(i,j)}{\Delta L3} * A$$

$$Q4 = -k \frac{H(i,j+1) - H(i,j)}{\Delta L4} * A \qquad (3.7.1)$$

CHAPTER 4

MODELING OF FRACTURES IN TONO AREA

4.1 Targeted Area

Japan Nuclear Cycle Development Institute (JNC) has drilled four 1000m-deep boreholes at the Mizunami Underground (MIU) site in Akeyo-cho, Mizunami City, Gifu Prefecture. In the surface-based investigations, specifically three 1000m-deep boreholes, MIU-1, MIU-2 and MIU-3, have been drilled. Investigations in these boreholes have characterised mainly the geological structure and hydrogeological features of the deep geological environment. The MIU-2 borehole investigations aim mainly at characterising the Tsukiyoshi fault that intersects the crystalline basement in the site. In Tono Area, granite is widely distributed as a basement and is overlain unconformably by sedimentary rocks called the Mizunami Group.

Fractures orientation data of four 1000 m boreholes (AN1, MIU1, MIU2 and MIU3), located in the MIU site and obtained by Japan Nuclear Cycle Development Institute (JNC), were used for constructing fracture model. Based on the stereographic projections of fractures orientation data read by Borehole Television (BTV) figures, fractures patterns were analysed and interpreted. The connection of fractures among observed boreholes were also analysed by using 3-D visualization technique developed in this study. Selected fractures patterns were checked by comparing with fractures in bore cores. As the results, six fractures patterns were selected and major fractures directions were defined.

Although the locations of observed boreholes are concentrated in small MIU area, fractures model was applied to the wider calculated area including this MIU area. Calculated area is a real field site, a 4 km x 6 km x 3 km thick fractured granite rock mass overlain by sedimentary layers surrounding the MIU site. Fracture modeling was executed by applying statistical method, calculating average distance (spacing) between fractures of each pattern. Groundwater flows of composite model (fractures model, combined with sedimentary rock) were calculated.

The location of MIU site in Tono area, observed boreholes MIU 1, MIU 2, MIU 3 and AN 1 at the MIU site and calculated area, including the MIU site are shown by the following figure 4.1.1, figure 4.1.2., and figure 4.1.3.

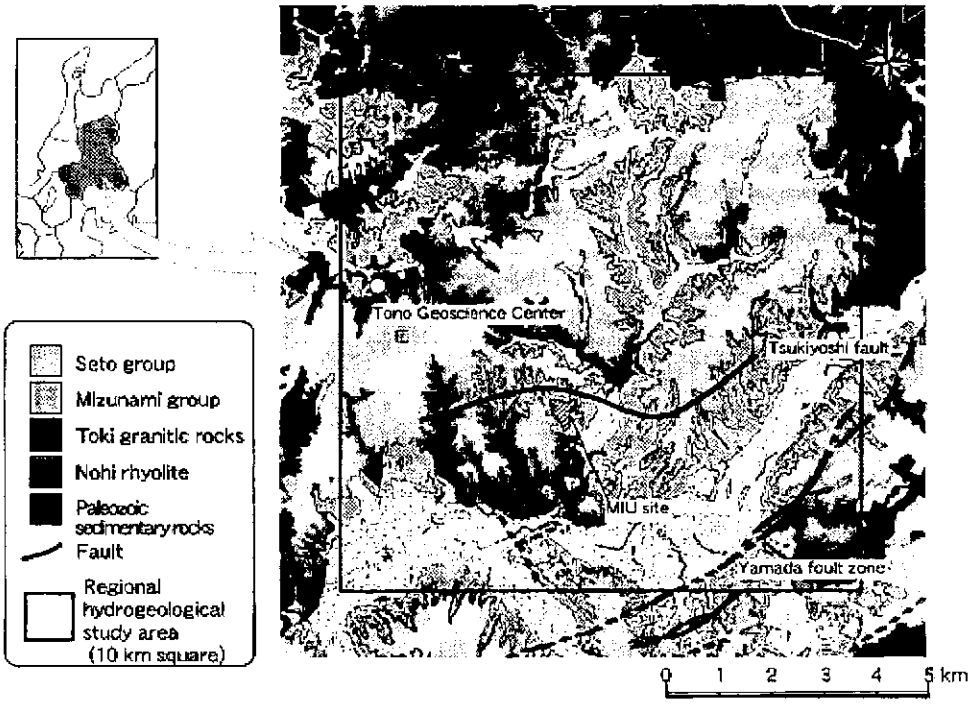

Figure 4.1.1 Location of MIU site and geological settings in Tono Area

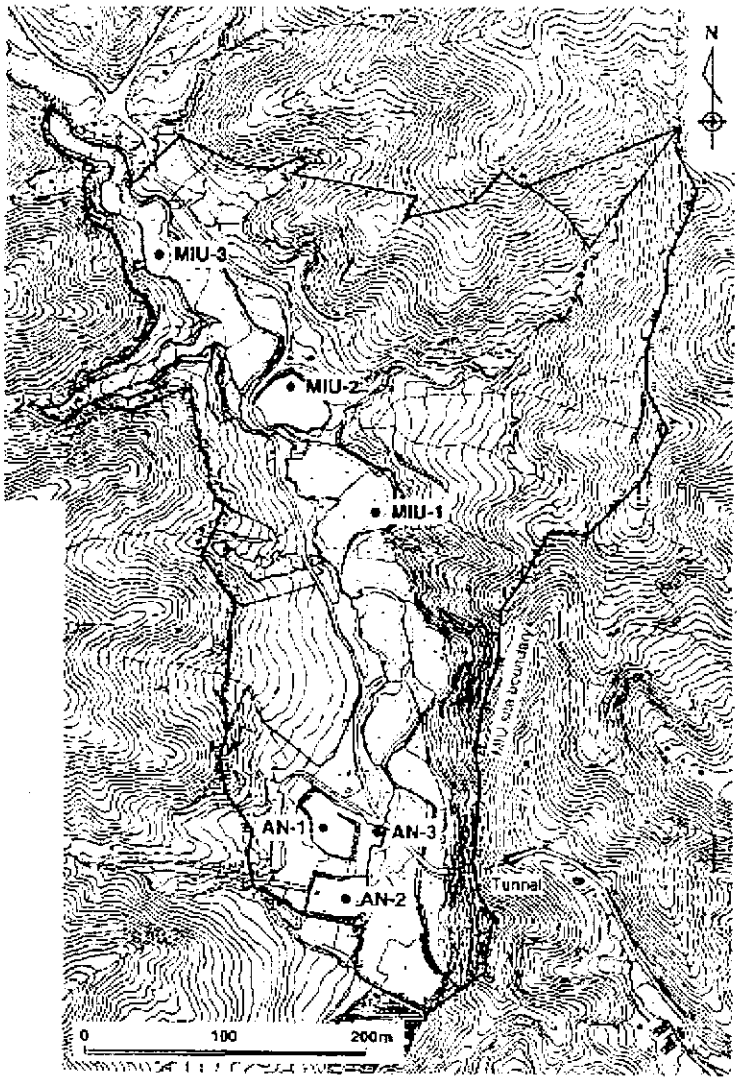

Figure 4.1.2 Location of boreholes in MIU site

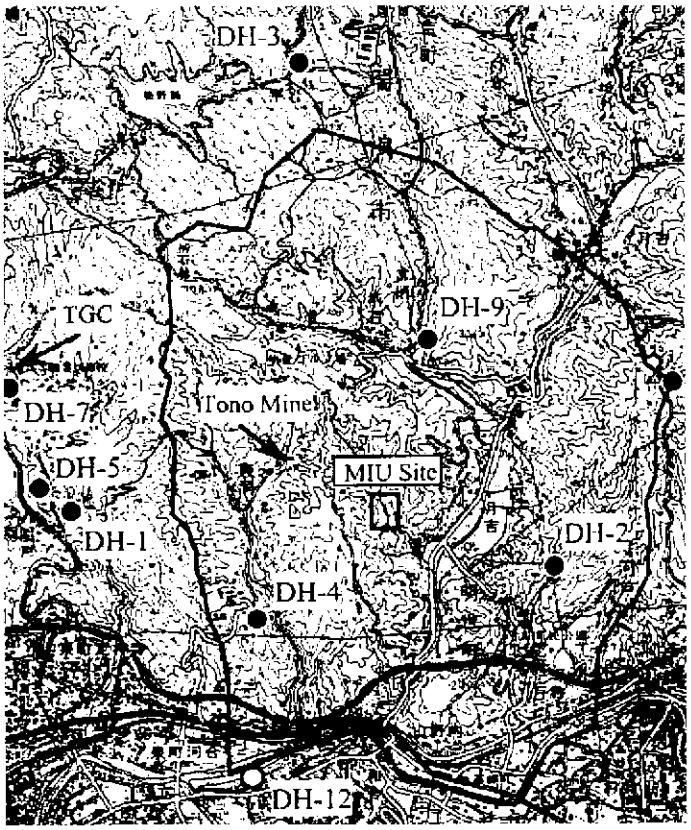

Figure 4.1.3 Calculated area (4 km x 6 km x 3 km)
including MIU site in Tono Area

4.2 Boreholes

Each borehole location coordinate in Tono Area is as follow:

- MIU 1 = (X = 5488.826 ; Y = -68629.358 ; Z = 220,074)
- MIU 2 = (X = 5433.295 ; Y = -68552.402 ; Z = 223,755)
- MIU 3 = (X = 5488.826 ; Y = -68629.358 ; Z = 220,074)
- AN 1 = (X = 5454.72 ; Y = -68877.34 ; Z = 216,38)

Geological cross section of the MIU site, shows locations of AN1, MIU1, MIU2 and MIU3 boreholes is shown by the following figure.

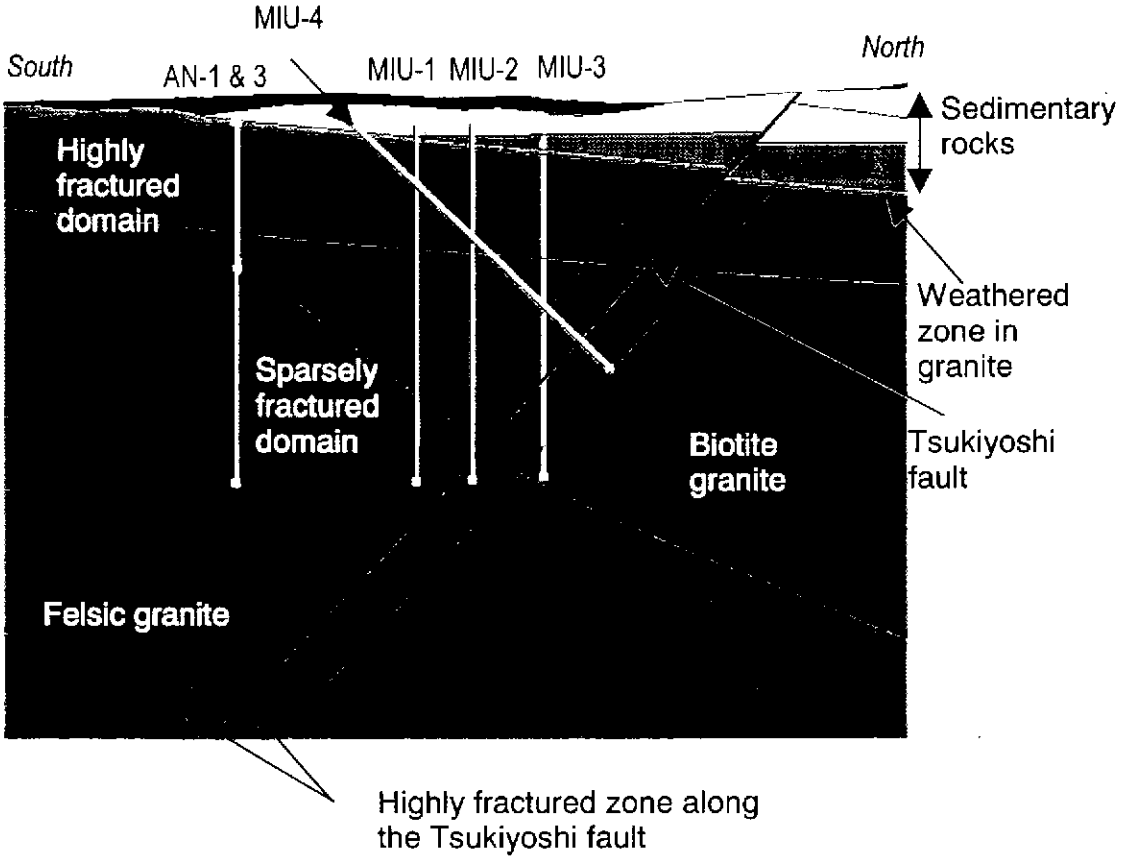

Figure 4.1.4 The geological cross section of the MIU site

Two vertical 1000m-deep boreholes, MIU 1 and MIU 2 have been extensively investigated. These boreholes investigations allow geological, hydrogeological and geomechanical characterisation of the crystalline basement, thereby advancing the

understanding of the geological environment at MIU site. An overview of the current status of knowledge gained from the previous borehole investigations can be presented as follow:

Geology

- Tertiary sedimentary rocks (Mizunami Group) unconformably overlie the eroded cretaceous crystalline basement (Toki granite) with a basal conglomerate. An unconformity and weathering surface occur horizontally between the two boreholes.
- The Mizunami Group is stratigraphically divided into the Toki lignite-bearing and Akeyo Formations in ascending order.
- The Toki granite can be divided lithologically into two main facies: biotite granite and felsic granite (Figure 4.2.1). They are subdivided into three types (coarse, medium and fined grained) based upon the size of quartz phenocrysts. The felsic granite is highly fractured with fracture density over 1000 fractures per 100 m.
- Major water-conducting features were identified. These features are:
  - Strongly weathered, permeable zones in the vicinity of the unconformity
  - Open fractures (201 mbgl in the MIU 1 borehole and 223mbgl in the MIU 2 borehole)
  - Steeply dipping fractures in the felsic granite
- A reverse fault, the Tsukiyoshi fault, intersects the MIU site and is encountered in the MIU 2 borehole at a depth of 890.0 to 915.2 mbgl. The fault is oriented E-W with a dip of 70° to 80° S.

Rock Name

- Assign rocks (unconsolidated materials) recovered to one of the following units: the Seto Group, the Mizunami Group, the Toki Granite, the Mesozoic sedimentary rocks of the Mino Belt and dykes. Sedimentary rocks are divided into sandstone, mudstone, tuff and conglomerate. Granitic rocks are classified into 3 groups in terms of an average diameter of quartz phenocrysts; fine-grained ($\varnothing \leq$ 1mm), medium grained (1mm $\leq \varnothing \leq$ 5mm) and coarse-grained (5 mm $\leq \varnothing$)

The geological model of the MIU site is shown at the following figure:

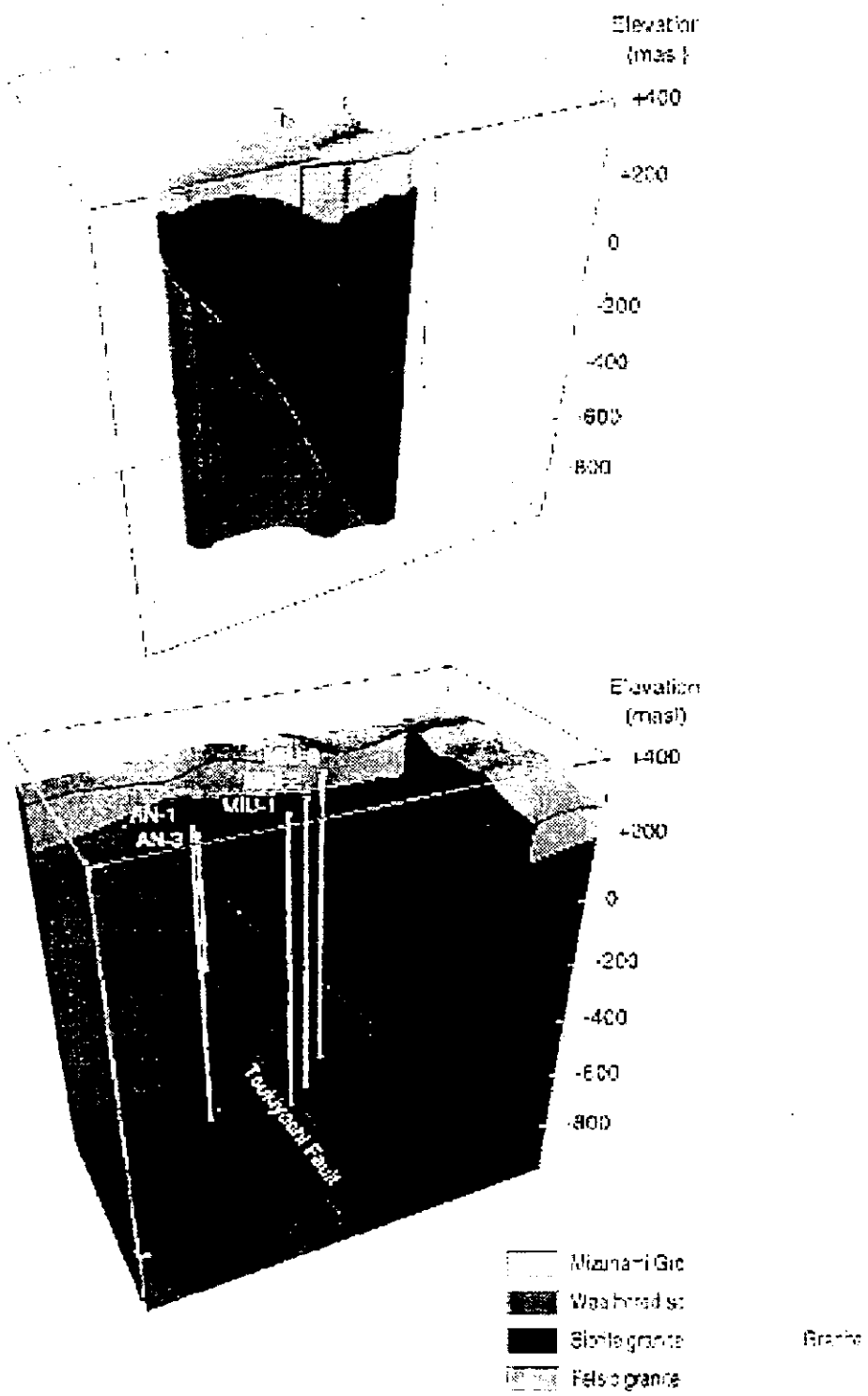

Figure 4.2.1 3D conceptual geological model of the MIU site

Hydrogeology

- The mean hydraulic conductivity of the Toki granite is in the order of 10^{-7} m/s. The felsic granite close to the Tsukiyoshi fault is designated as a higher permeability domain ($K \geq 10^{-6}$ m/s). A lower permeability domain ($K \leq 10^{-9}$ m/s) is also identified in the interval of 400.7 to 503.0 mbgl in the MIU 1 borehole on the basis of pumping tests, which correlates with a silica rich facies ($SiO_2 \geq 75$ wt %) in the biotite granite.
- The mean hydraulic conductivity of the major water-conducting features identified is in the order of 10^{-6} m/s ($T \approx 10^{-5}$ m^2/s).
- The hydraulic conductivity of the Tsukiyoshi Fault is relatively low.

Rock mechanics

- The Toki granite can be divided into three zones in terms of mechanical properties and in situ stress state, especially in the hanging wall of the Tsukiyoshi fault : 0-300mbgl, 300-700mbgl and 700-1000mbgl
- The direction of the maximum principal stress in a horizontal plane also changes at about 300mbgl from N-S (0-300mbgl) to NW-SE (300-1000mbgl)

4.3 Fracture Data

Fractures orientation data read by Borehole Television (BTV) include:

- Depth (m)
- Strike (deg)
- Dip (deg)
- Status (hair crack, crack, open crack)
- Aperture (mm)
- Style

Criteria for acquiring data of borehole television

All discontinuity data for analysis of fractures and directions using pictures was sorted out as follows:

1. **Depth**

depth along the borehole axis

a. Measuring depth: the mean value between top and bottom of fracture.

b. Unit: meter. The accuracy shows centimeter unit.

c. Measuring depth was calibrated by geological references (core observation).

2. **Strike and Dip**

a. Foliations were measured if they continue more than 70% along circumference

b. Strikes and dips were taken the average of the coordinates more than three points.

3. **Foliations** were classified 9 groups as follows:

a. Crack

Fissures and joints, especially shapes and continuities were extremely obvious.

b. Open crack

Cracks, especially which were verified the opening conditions.

c. Hair crack

Fissures and joints, especially shapes and continuities were not obvious.

d. Hanging wall of crush zone

Hanging side of shear side or crush zone.

e. Footwall of crush zone

Footwall of shear side or crush zone.

f. Mineral vein

Structures of mineral vein, for example calcite or quartz.

g. Flow structure

Primary structures of granite.

h. Bedding plane

Primary structures of sedimentary rocks.

i. boundary

Lithofacies boundary or boundary between intrusions and host rocks.

4. Opening Width

a. Opening widths were measured as a maximum width.

b. Scale plate was used as a measurement tool.

c. Width shows 0.1 mm unit except for DH-2, 3, 4 (DH-2: 1 mm unit, DH-3, 4: 0.5 mm unit).

5. Style/Type of Fracture

Classify fractures according to the following definitions:

- ❖ P planar type
- ❖ I irregular type
- ❖ C curved type
- ❖ S stepped type

Furthermore shapes are subdivided as derivations:

- n : discontinuity along circumference
- h : accompanying minor fractures
- j : crossing the other cracks
- n/h :discontinuity along circumference and accompanying minor fractures
- n/j :discontinuity along circumference, besides crossing the other cracks
- h/j :bringing accompanying fractures, besides crossing the other cracks
- n/h/j:discontinuity along circumference and accompanying minor fractures besides crossing the other cracks

(Example: P-n, I-n/h, S-h, etc.)

The orientation of a fracture is usually expressed by its strike and dip. The strike is the trace of the intersection of the fracture with a horizontal plane. Its direction can be specified by its azimuth, counted in degrees clockwise from the North. The dip (inclination or plunge) is the magnitude of the angle between the fracture and a horizontal plane expressed in degrees.

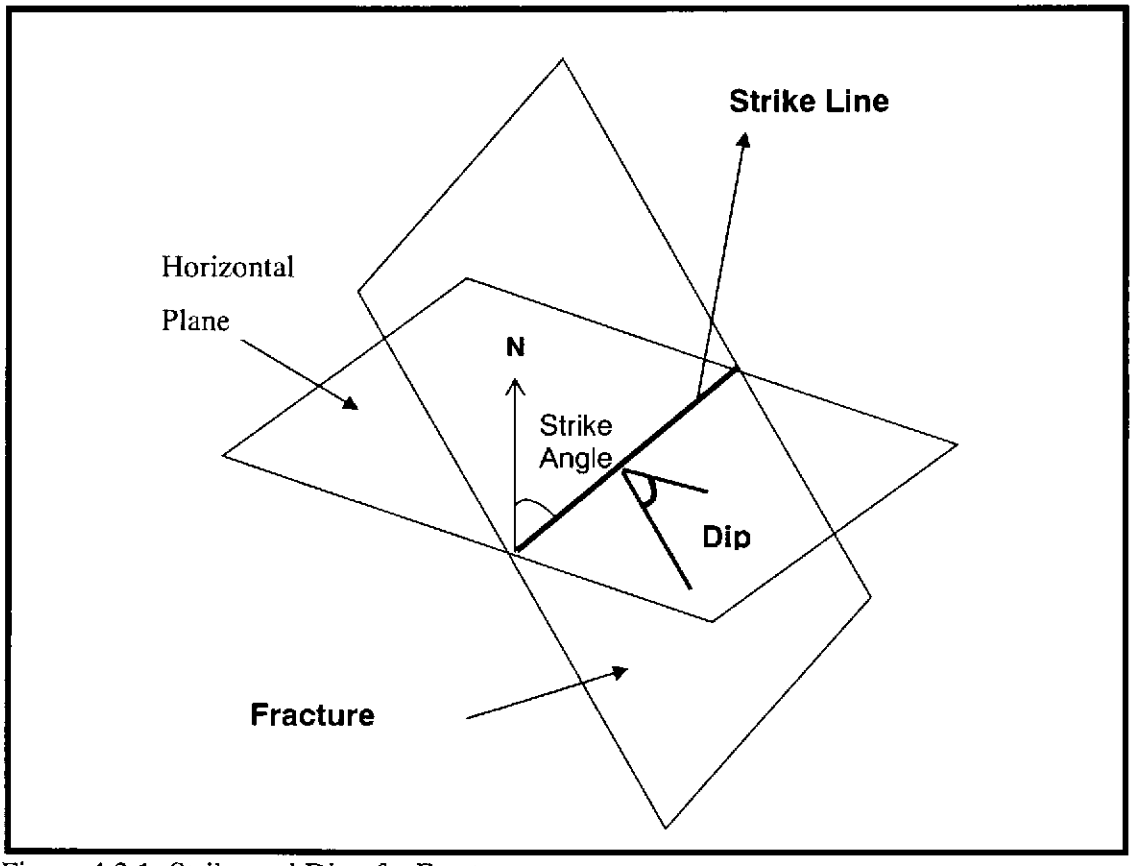

Figure 4.3.1. Strike and Dip of a Fracture

Strike Line

- Cross line between fracture plane and horizontal plane

Strike Angle

- Angle created between North direction and fracture direction (strike line)

Dip Angle

- Angle created between fracture plane and horizontal plane (between 0° and 90°)

Fractures data shown in the overview of each borehole investigation include :

Fracture Density

- Number of fractures per unit length. Unit of fracture density stated in fracture/m shows the number of fractures per unit meter core

Borehole

- A hole, usually vertical, bored to determine ground conditions, for extraction of water or measurement of groundwater level.

Casing

- tubular retaining structure, which is installed in a drilled borehole or excavated well, to maintain the borehole opening. Plain casing prevents the entry of water.

Hydraulic Conductivity

- volume of water at the existing kinematic viscosity that will move in unit time under a unit hydraulic gradient through a unit area measured perpendicular to the direction of flow.

Lithology

- physical character and mineralogical composition that gives rise to the appearance and properties of a rock

4.4 Borehole Data Interpretation and Fractures Selection

DATA

Analysis fractures orientation data of four 1000 m boreholes located at MIU site (AN1, MIU1, MIU2 and MIU3) read by Borehole Television (BTV)

DATA INTERPRETATION

1. Stereographic – every 5m range

- Make stereographic projections (projection of a fracture at the lower or upper hemisphere) of every 5-meter range borehole depth to have rough interpretation about the fractures patterns. Example of fracture interpretations, based on the 5-meter range stereographic projections, are shown at the following figures:

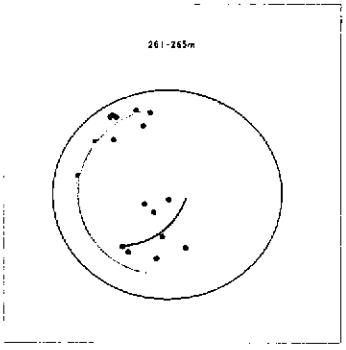

261-265 m

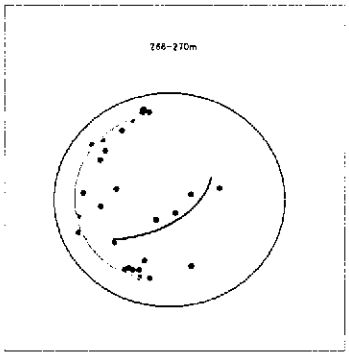

266-270 m

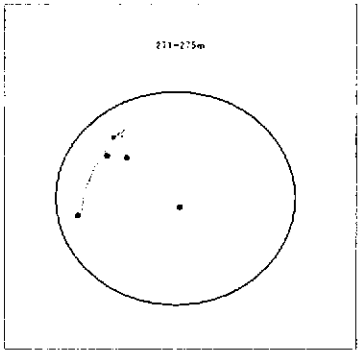

271-275 m

2. Stereographic – every 5m range sliding 1 m

- Stereographic projections in every 5 meter borehole depth with sliding 1 meter were drawn for making clear the gradual change of fracture pattern around every major fracture. This step is also to check relation between fracture pattern and hydraulic conductivity.
- Stereographic projections examples of every 5m range with sliding 1m and the interpretations are shown by the following figures:

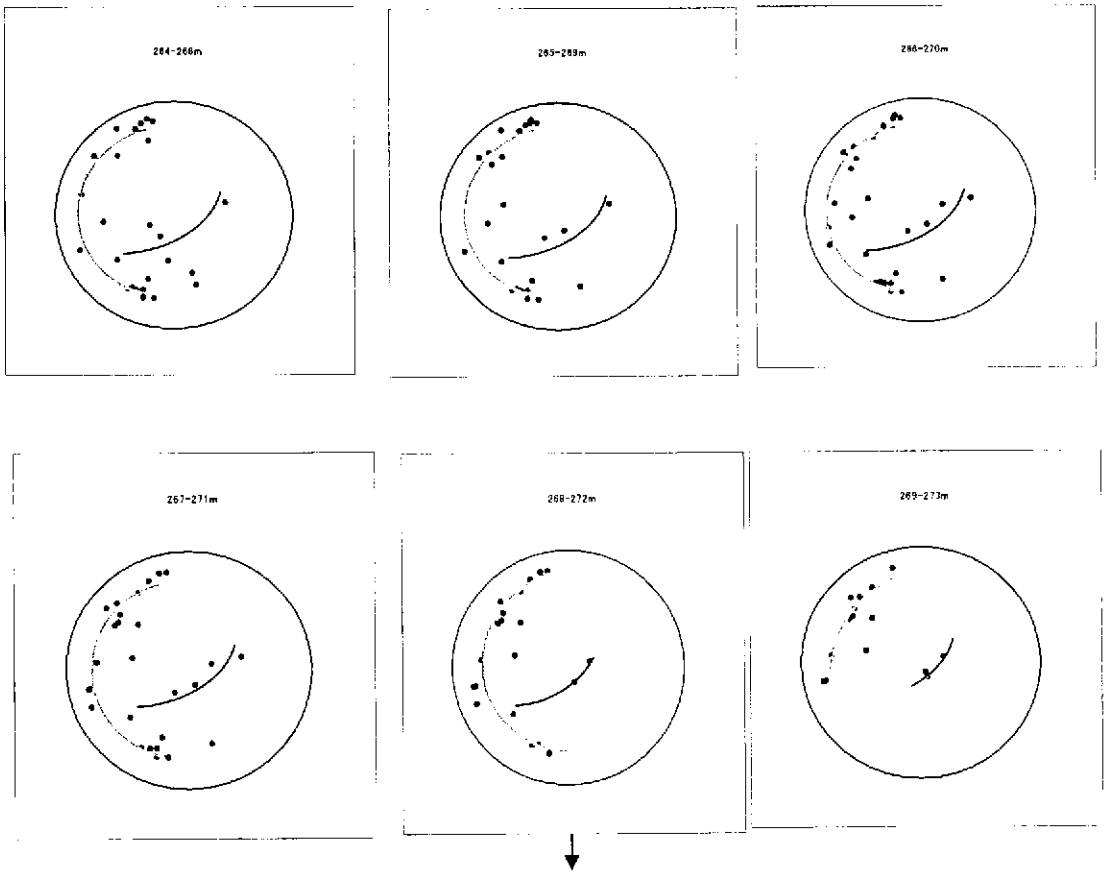

3. Stereographic – every 1 m range

- Making stereographic projections of fractures in every 1-meter range borehole depth to check fractures patterns in detail (scale/width of major fracture). In this step, the numbers of fractures fewer than or equal to 3 fractures are not considered because the fracture pattern is difficult to be defined.
- Stereographic projections examples of fractures in every 1-meter range borehole depth within 265-270 meter and fractures patterns interpretations are shown by the following figures:

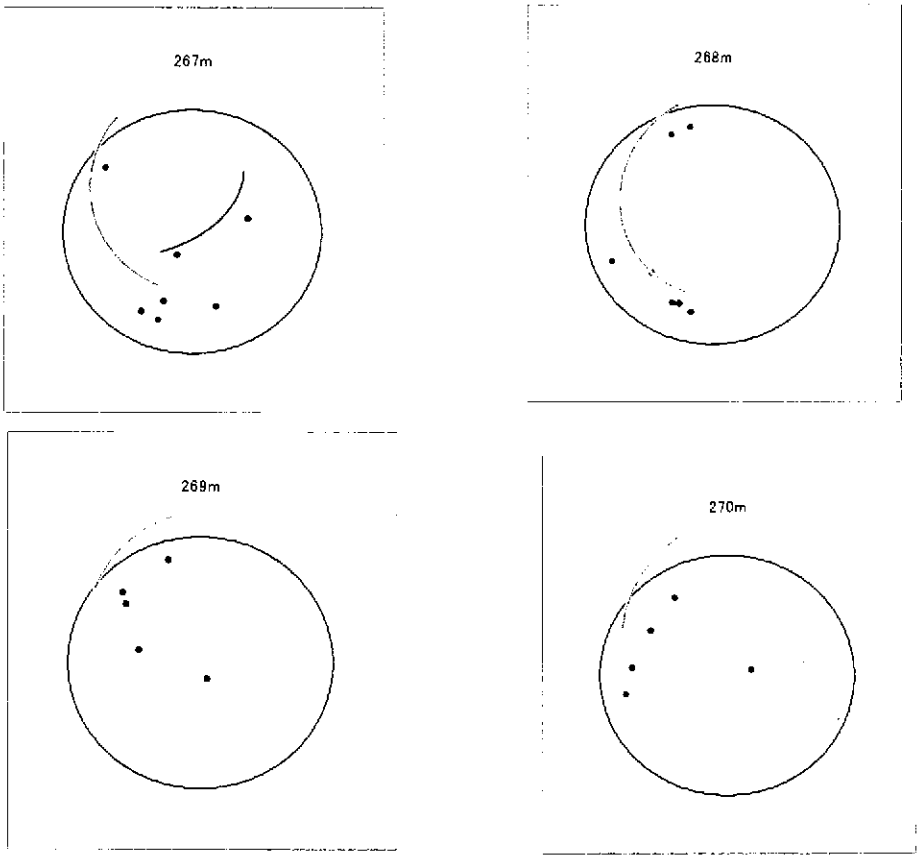

It is not simple to select fracture pattern. Complicated pattern sometimes found in stereographic projection. As the examples, composite models/patterns were found in the depth 266 m-270 m of AN 1 borehole and in the depth of 882 m of MIU 2 borehole.

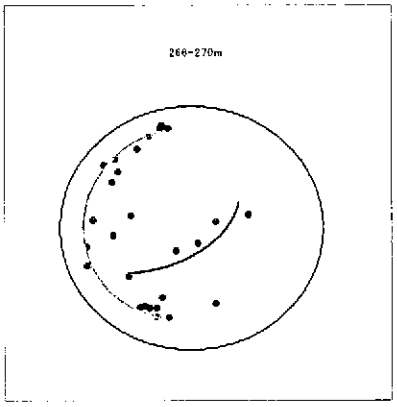

266 m - 270 m (AN 1)

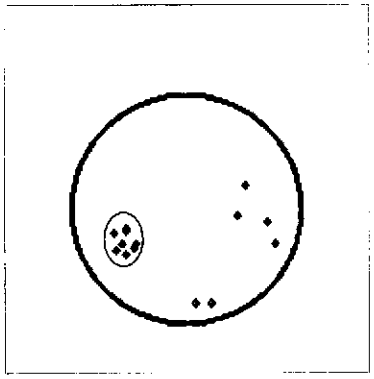

882 m (MIU 2)

It may be due to stress condition change or intersection of fractures. Figures 4.4.1 and 4.4.2 show both possibilities. Figures 4.4.1 show composite model in AN 1 (266m-270 m). In the case of stress condition change, first fracture pattern was created by the first stress condition and was followed by the creation of second fracture pattern due to stress condition change. By using stereographic projection, it could not be observed which fracture pattern created first. Then, similar clearer fracture pattern could be observed in other parts of stereographic projections, at depth 157 m -162 m in MIU 1 (Pattern 1) and at depth 455 m – 460 m in AN 1 (Pattern 3). Both fractures patterns were selected .

As a second example, a composite model observed in MIU 2 (882 m) is shown by Figure 4.4.2, with the same possibilities as the first example. Then, similar clearer fracture pattern could be observed in another part of stereographic projection, at depth 541 m in AN 1 (Pattern 2). This fracture pattern was selected. Another fracture pattern created in this composite model was not selected because it showed unclear fracture pattern. Similar unclear fracture pattern was also observed at depth 957 m in MIU 2

There was also a possibility that the composite models were created due to intersection of fractures.

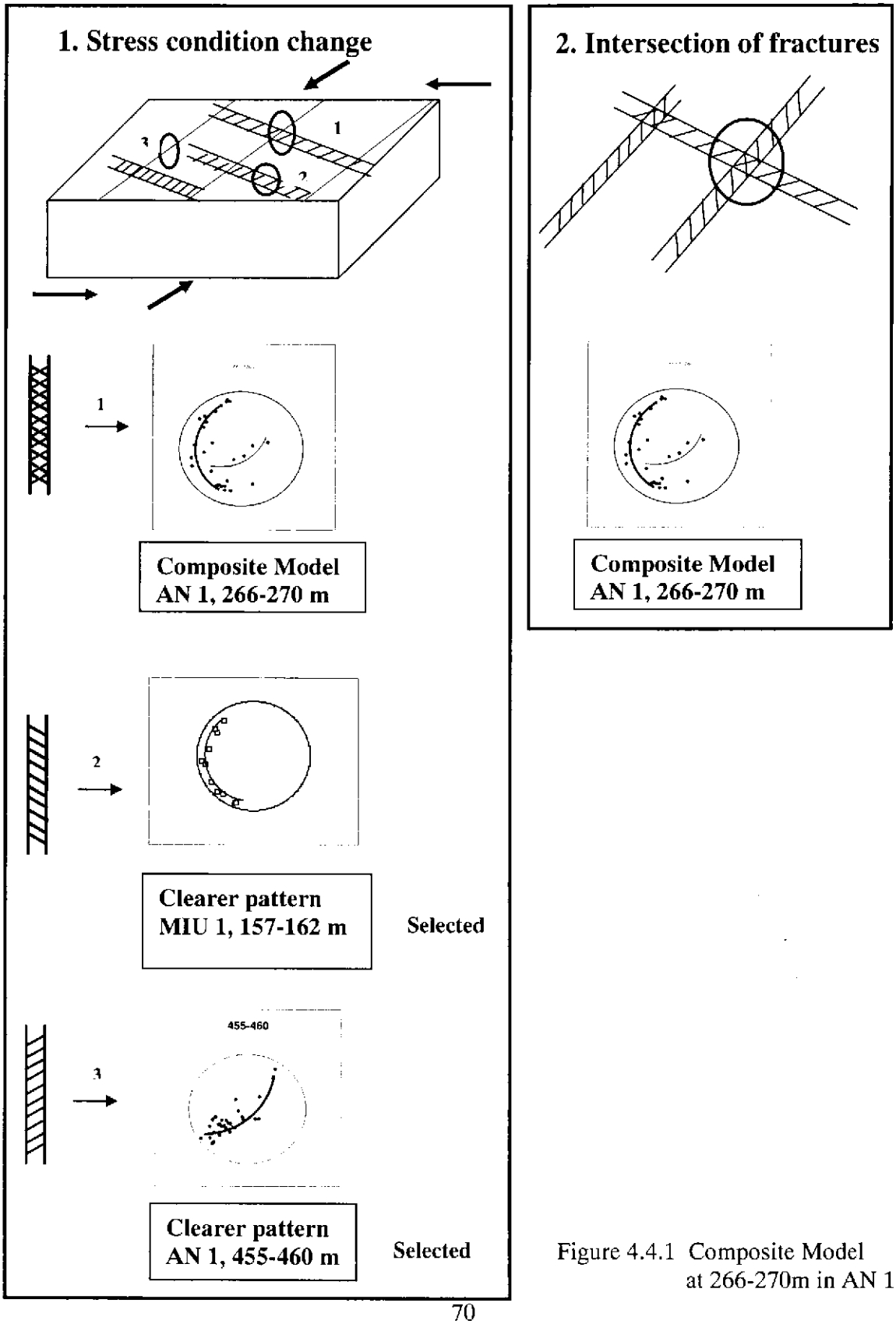

Figure 4.4.1 Composite Model at 266-270m in AN 1

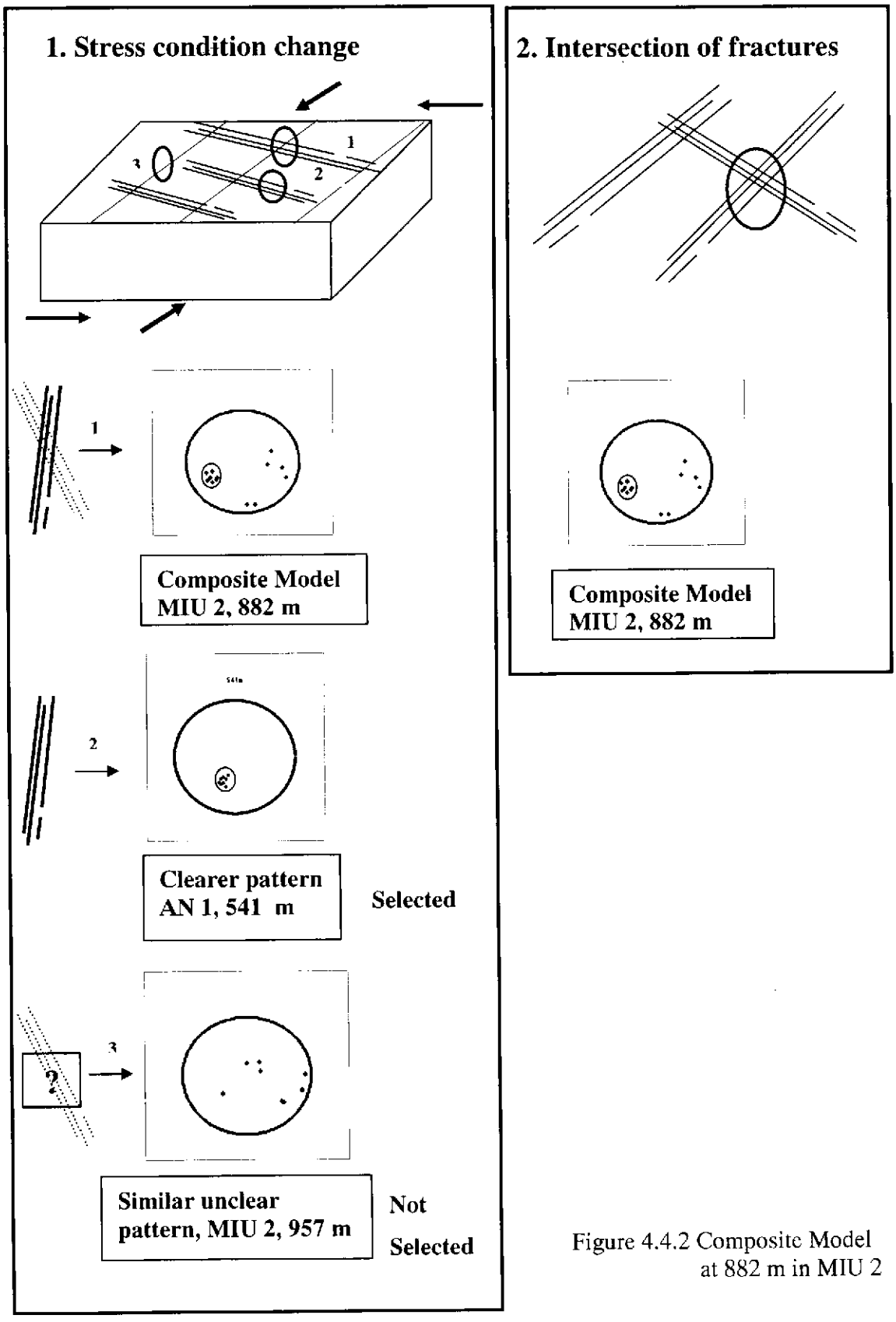

Figure 4.4.2 Composite Model at 882 m in MIU 2

Based on the stereographic projections interpretations, some fractures patterns were observed. Examples of some selected fractures patterns observed at certain depths are as follows:

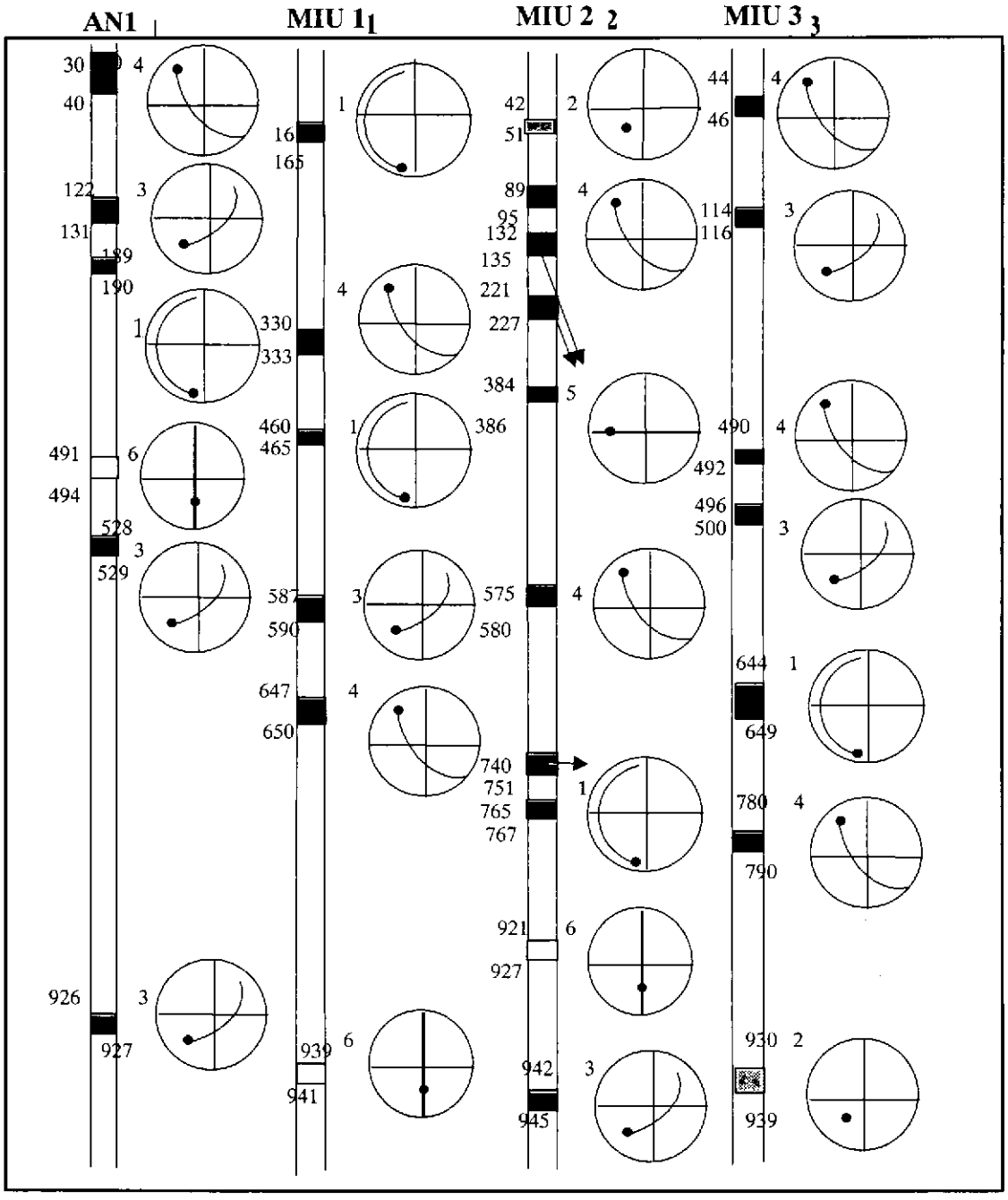

Figure 4.4.3 Selected Major Fractures
(Assumption: fracture directions are plotted at great circle)

Six Fractures Patterns

- Referring to the fractures patterns interpretations results using stereographic projections, the results show that there are mostly six different types of fractures patterns observed.

Major Fracture Selection

- Each pattern type shows concentrated points/patterns, which were assumed as major fractures. The directions of major fractures can be estimated.

Connection of Fractures among Observed Boreholes

- By using estimated major fractures directions, figures of each pattern in four boreholes were made by using 3-D visualization technique and each pattern of four boreholes was connected to each other.

Bore cores Observation

- Interpretation results based on stereographic projections were compared with the fractures in bore cores
- The estimated major fractures were checked whether the fractures had major fracture features such as shear movement or there were many small fractures terminated by major fracture.
- Major fractures directions were defined

Selected Major Fractures

- Six fractures patterns and major fractures directions are as follows:

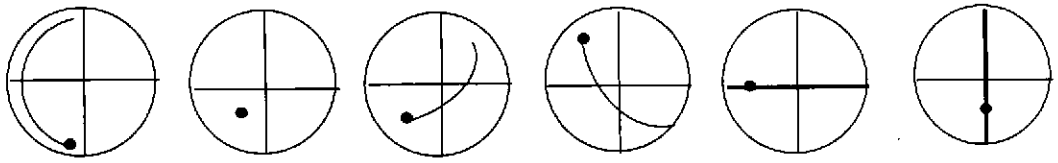

1 2 3 4 5 6

1. **PATTERN 1 : N 70 W 80 N**
2. **PATTERN 2 : N 45 W 20 N**
3. **PATTERN 3 : N 40 W 60 N**
4. **PATTERN 4 :N 40 E 75 S**
5. **PATTERN 5 : NS 60 E**
6. **PATTERN 6 : EW 40 N**

- The selected major fractures were checked by comparing with lineament data of Tono Area taken by remote sensing system. The selected major fractures are in accordance with the lineament data.

4.5 Three-Dimensional Treatment of Major Fractures

The following figures show the fractures original data read by Borehole Television (BTV) and the selected major fractures in AN1 borehole.

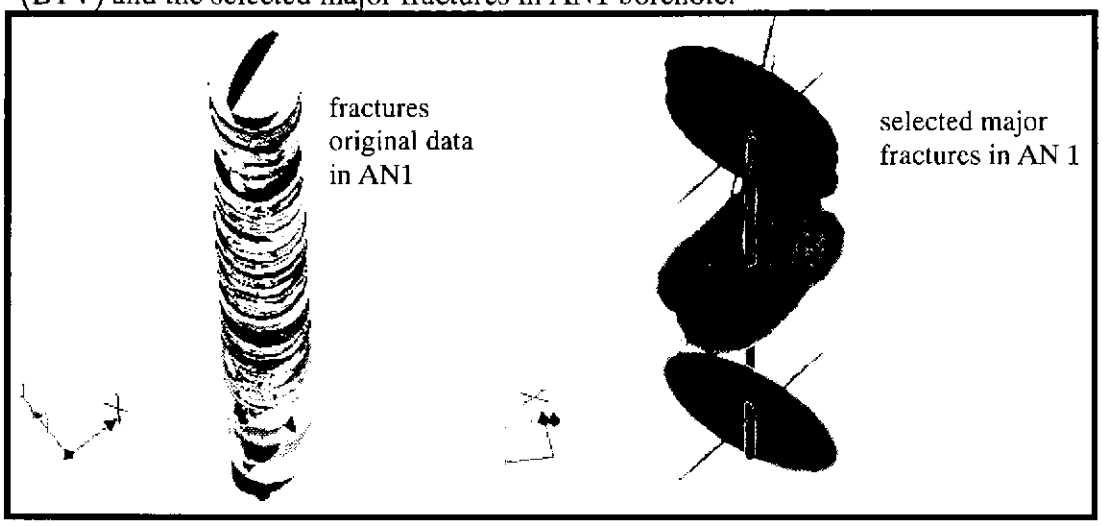

Figure 4.5.1 Fractures original data read by BTV and the selected major fractures in AN1 borehole

Based on interpretations results of stereograph projections, figures of each selected fractures patterns in four boreholes were made by using 3-D visualization technique. The selected major fractures in MIU 1, MIU 2, MIU 3 and AN 1 boreholes are shown by the following figures:

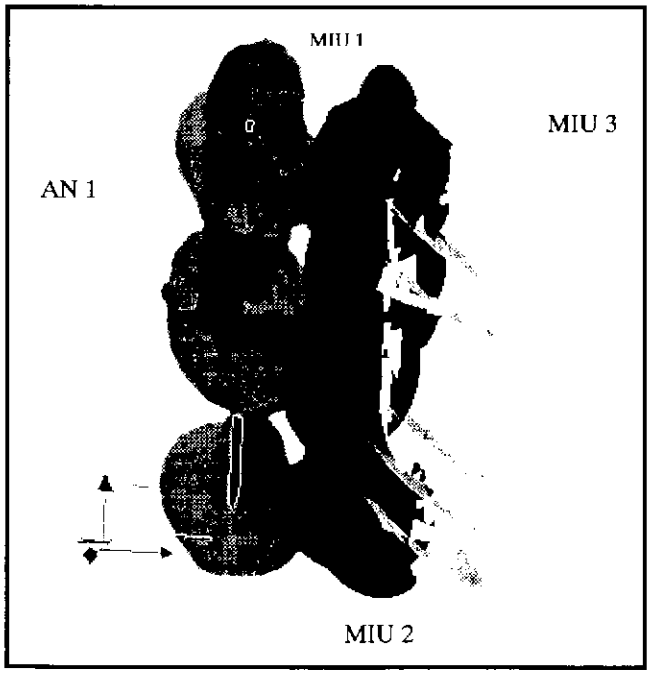

Figure 4.5.2 Selected major fractures in observed boreholes (6 patterns)

By using 3-D visualization technique, each pattern of four boreholes was connected to each other. The connections of fractures among observed boreholes were analysed and compared with the fractures in bore cores.

1. PATTERN 1

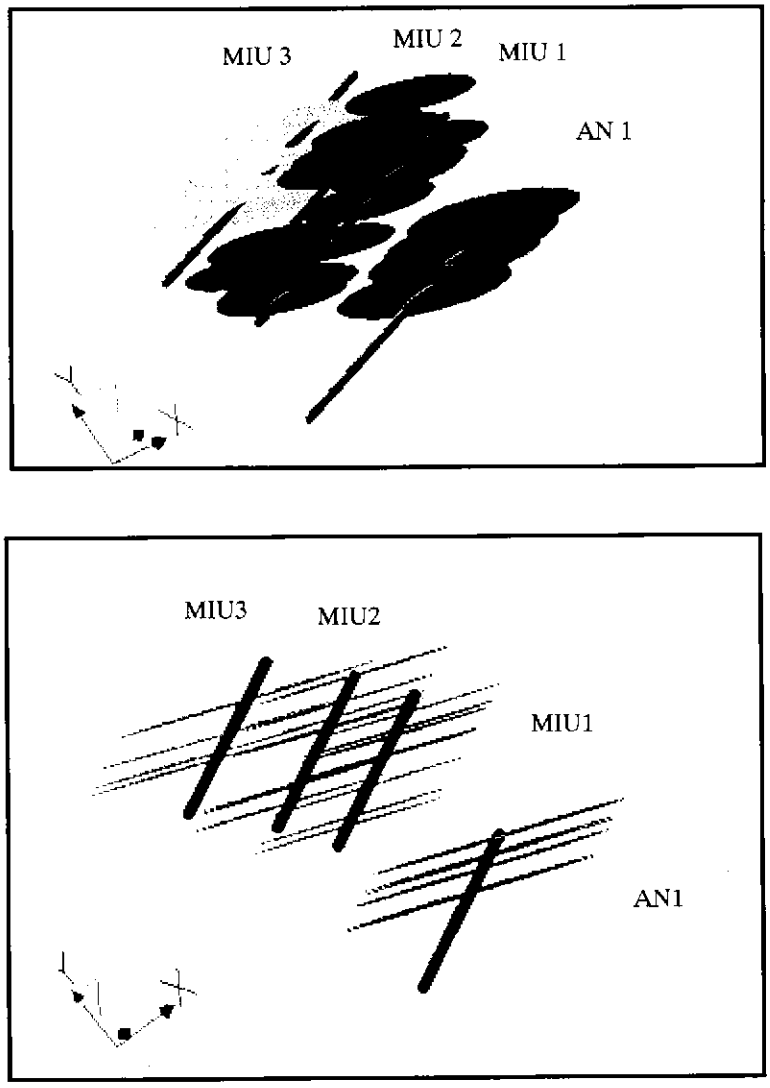

Figure 4.5.3. a. Selected major fractures in observed boreholes (pattern 1)

2. PATTERN 2

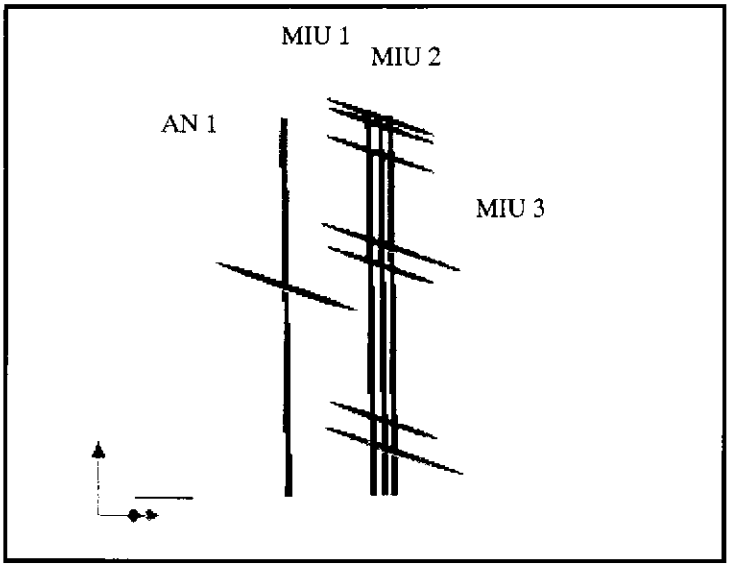

Figure 4.5.3 b. Selected major fractures in observed boreholes (pattern 2)

3. PATTERN 3

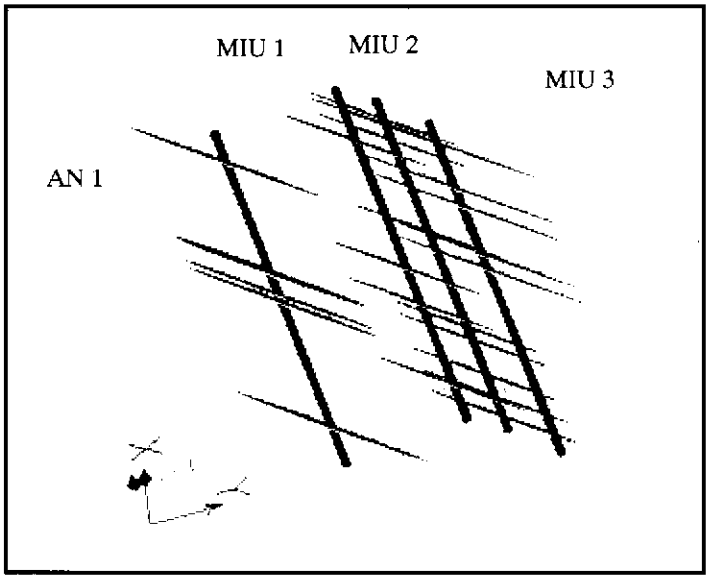

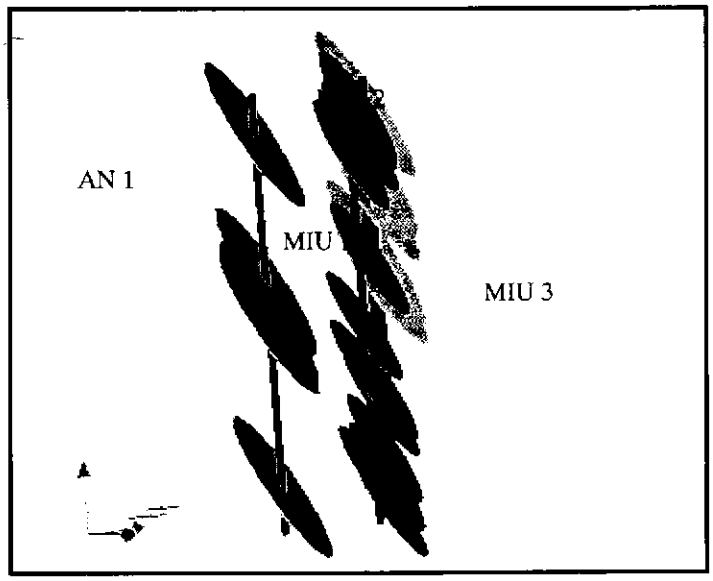

Figure 4.5.3. c. Selected major fractures in observed boreholes (pattern 3)

4. PATTERN 4

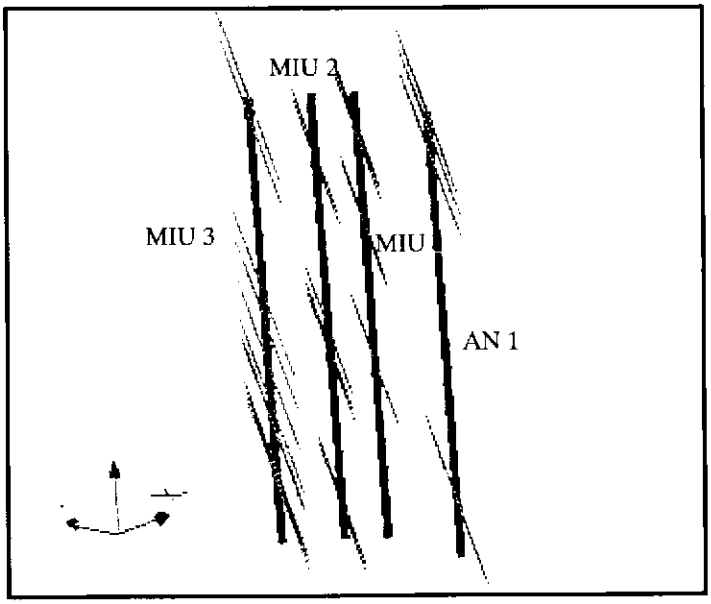

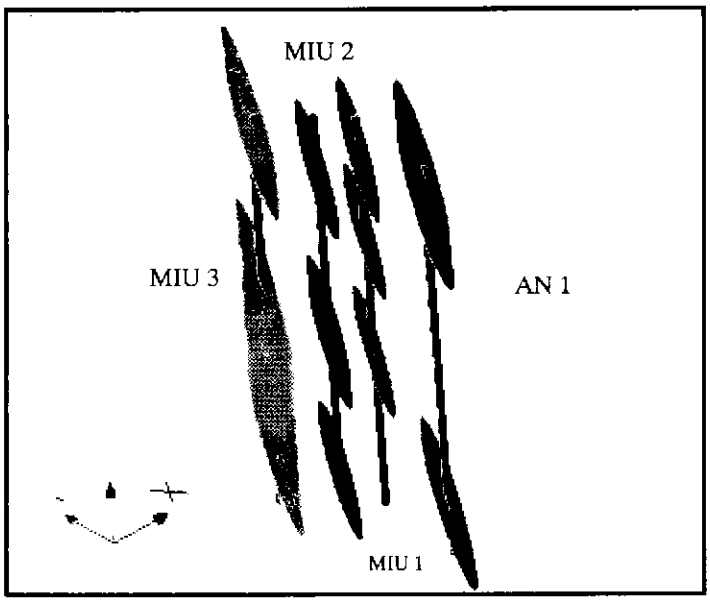

Figure 4.5.3.d. Selected major fractures in observed boreholes (pattern 4)

5. PATTERN 5

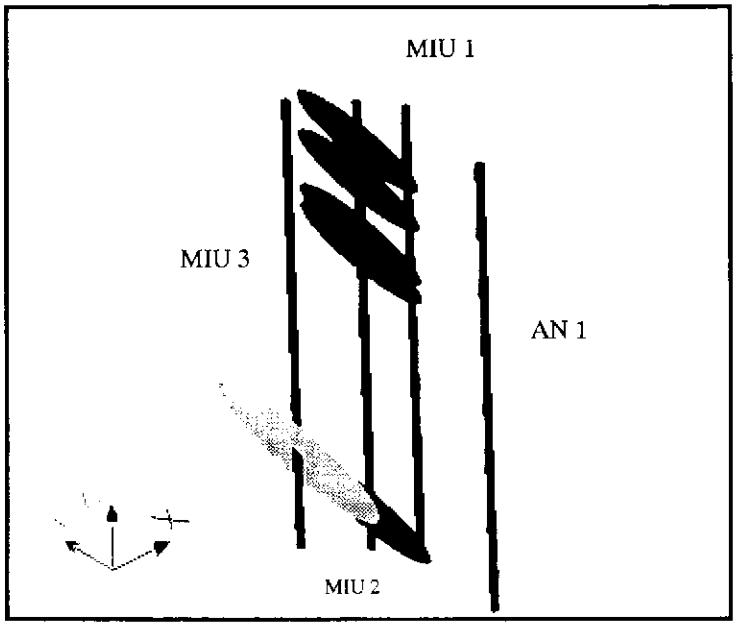

Figure 4.5.3. e. Selected major fractures in observed boreholes (pattern 5)

6. PATTERN 6

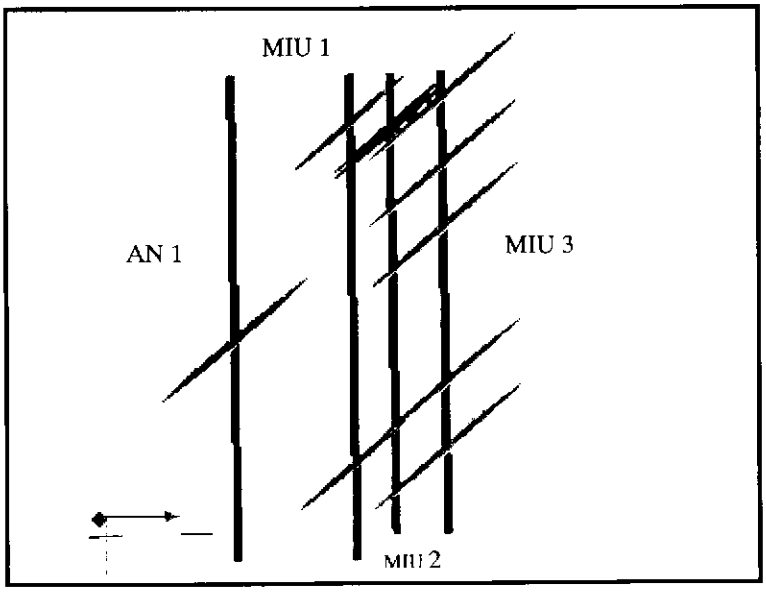

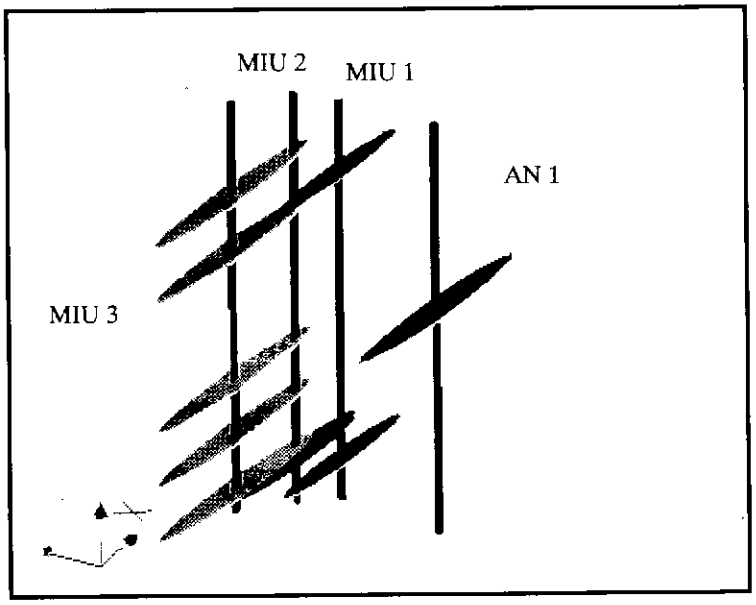

Figure 4.5.3.f. Selected major fractures in observed boreholes (pattern 6)

Considering continuity of fractures, uncertainty problems of fractures connections rise. Some fractures in a borehole are not in good positions to have connection with other fractures in other boreholes. Therefore, in this study, fracture modeling was executed by

applying statistical method, calculating average distance (spacing) between fractures of each pattern.

4.6 Bore cores Observations

By comparing with fractures in bore cores, stereographic interpretations of six patterns, connection of each pattern among 4 boreholes and assumed major fractures, were checked. The major fractures features such as shear movement, hydrothermal altered fractures (green colour) or many small fractures having the same pattern terminated by major fractures were also checked. Some of the fractures patterns, major fractures features, Tsukiyoshi Fault observed at bore cores are shown by the following figures:

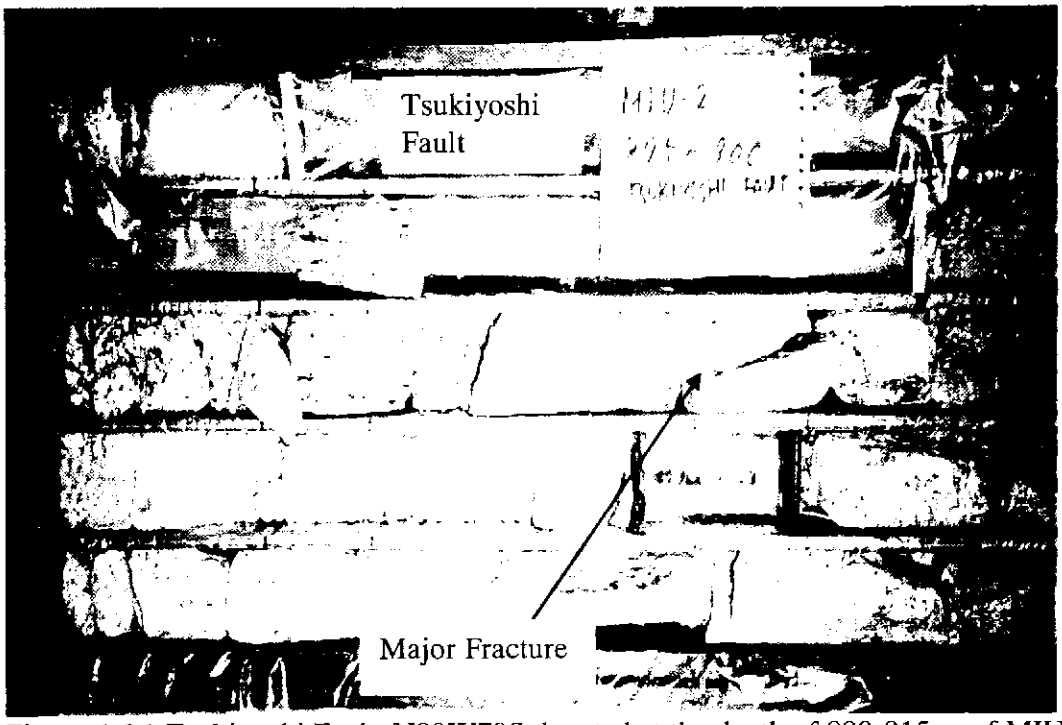

Figure 4.6.1 Tsukiyoshi Fault, N80W70S, located at the depth of 890-915 m of MIU2

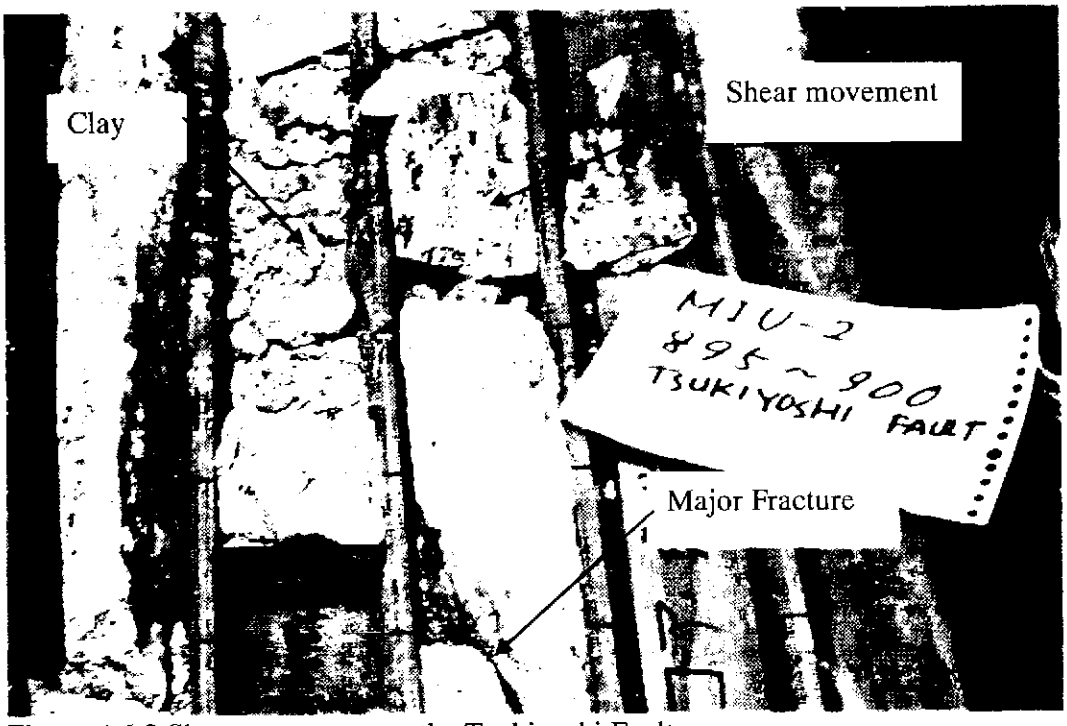

Figure 4.6.2 Shear movement at the Tsukiyoshi Fault

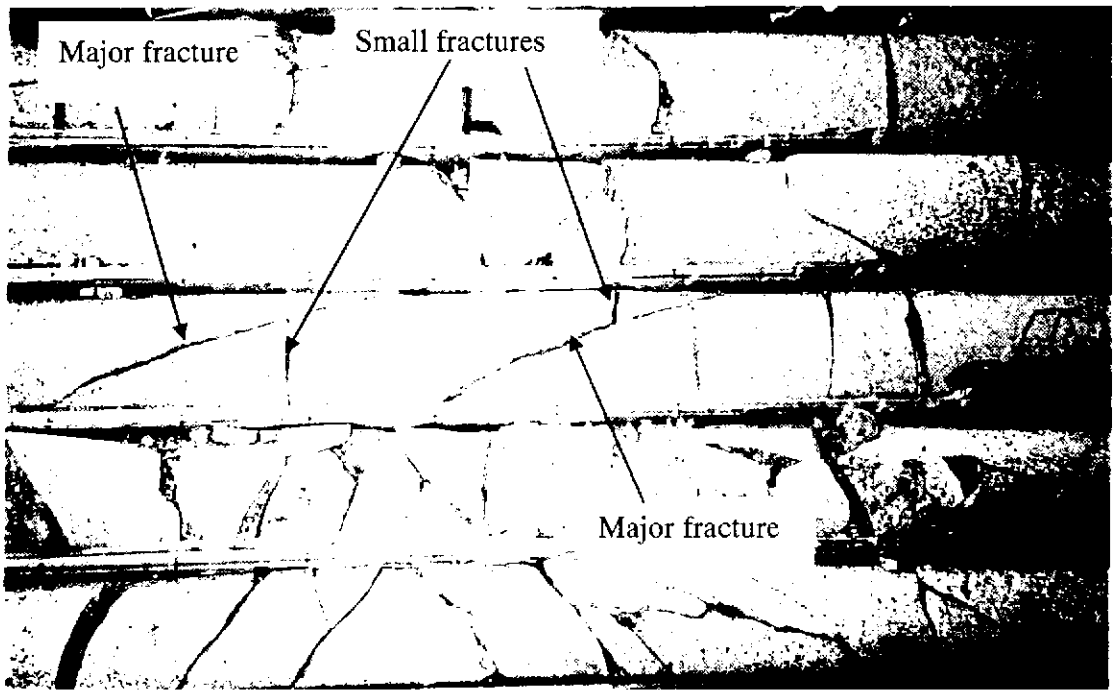

Figure 4.6.3 Small fractures terminated by major fracture in MIU2 borehole

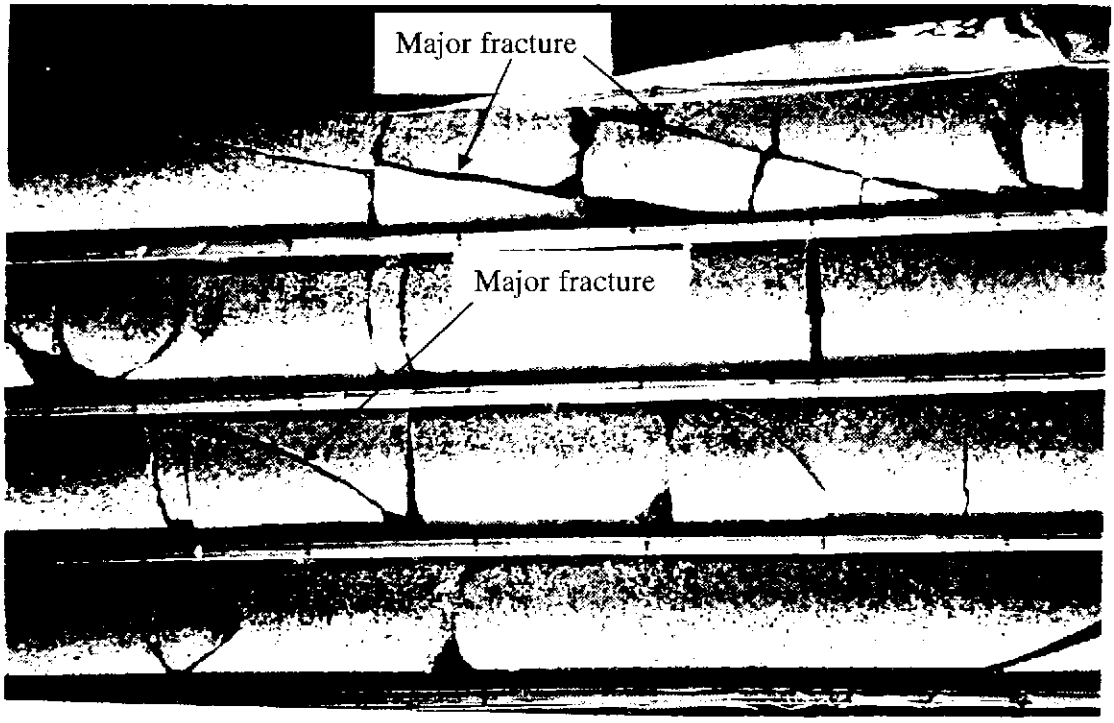

Figure 4.6.4 Small fractures terminated by major fracture in MIU2 borehole

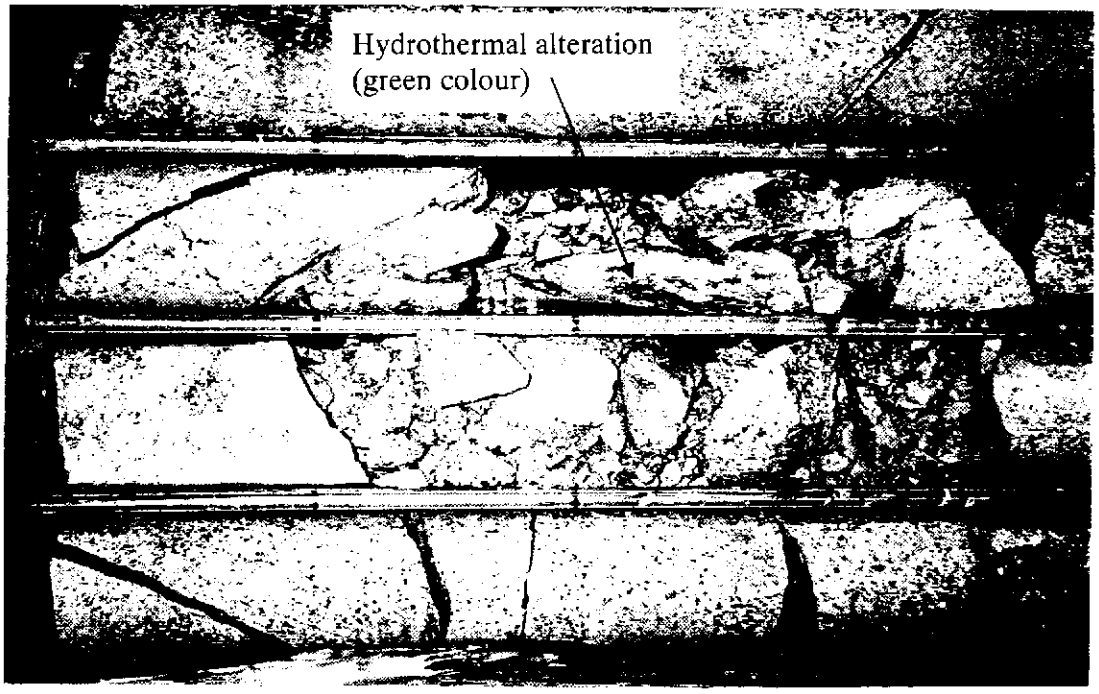

Figure 4.6.5 Hydrothermal altered feature (green colour)

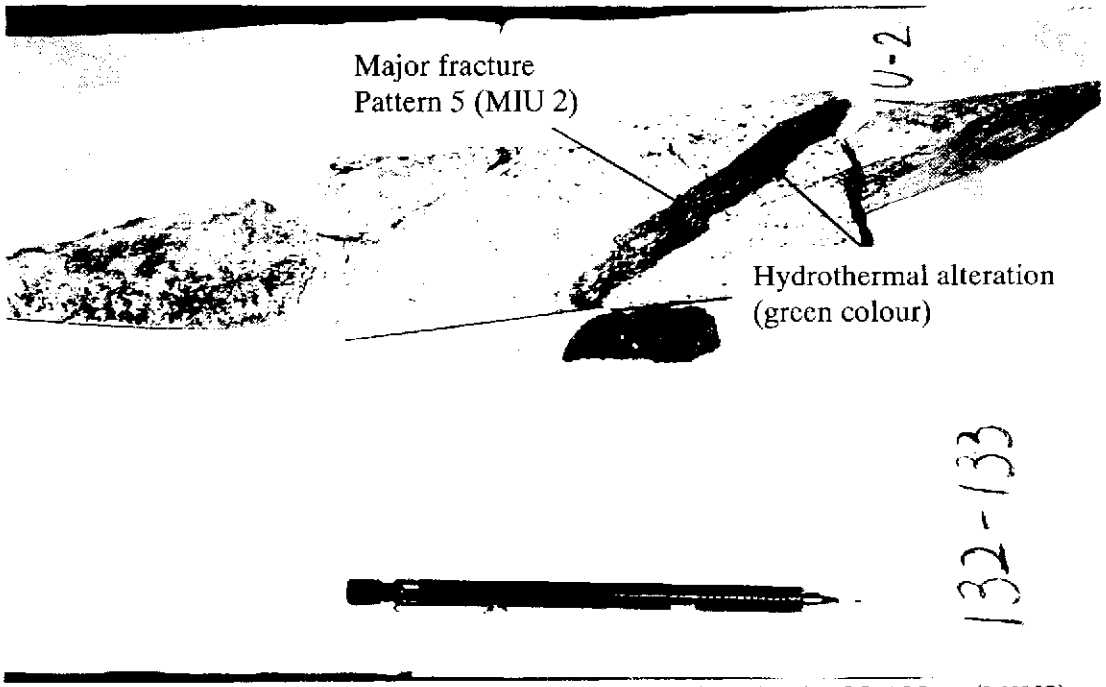

Figure 4.6.6 Hydrothermal altered feature (green colour) at depth 132-133 m (MIU2)

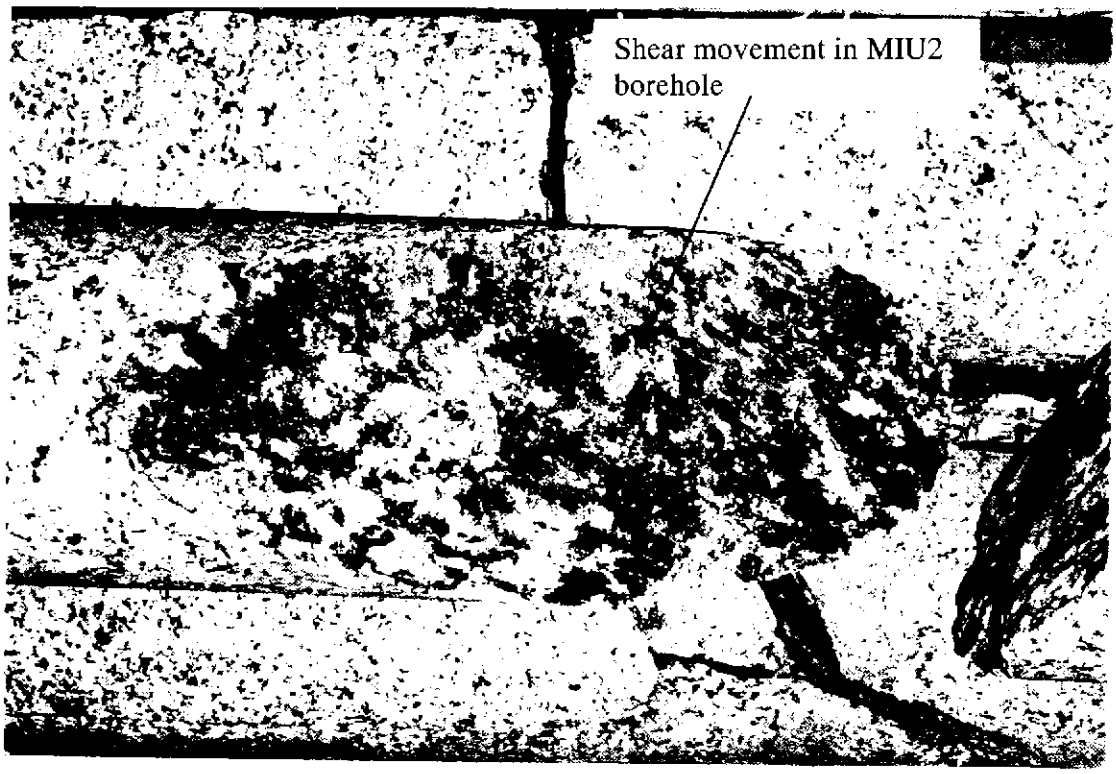

Figure 4.6.7 Shear movement feature

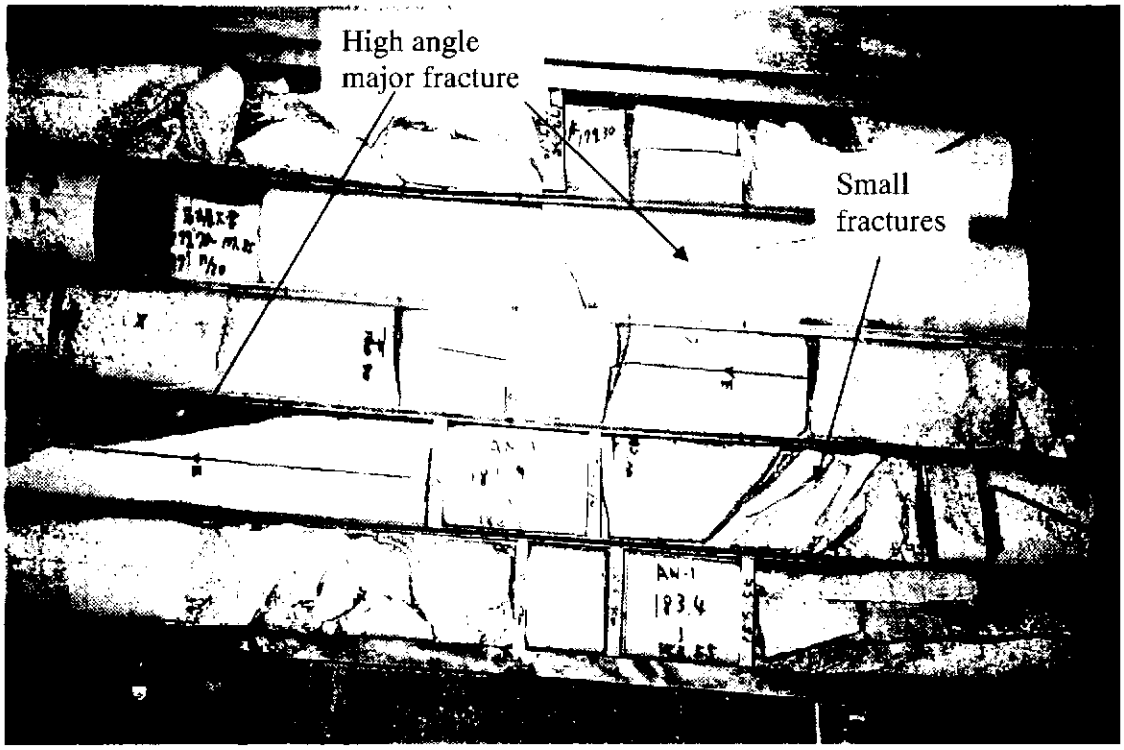

Figure 4.6.8 High angle major fracture (pattern 1) at depth 189-190 m in AN1

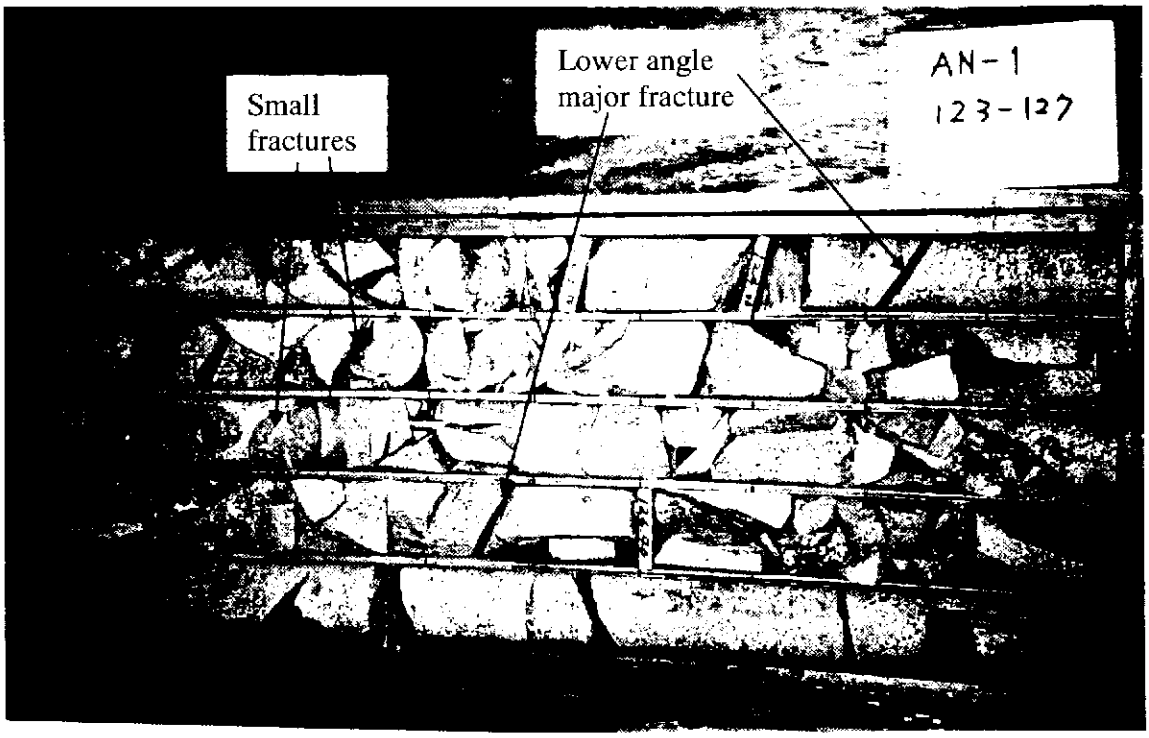

Figure 4.6.9 Lower angle major fracture (pattern 3) at depth 123-127 m in AN1

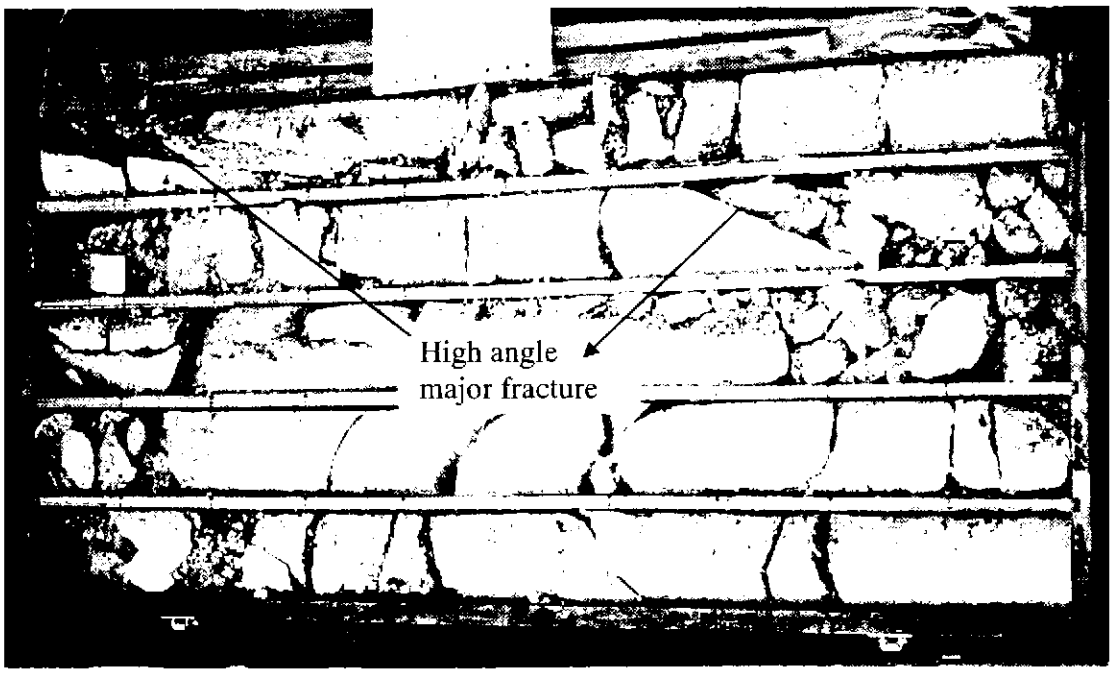

Figure 4.6.10 High angle major fracture (pattern 4) at depth 91-95 m in MIU 2

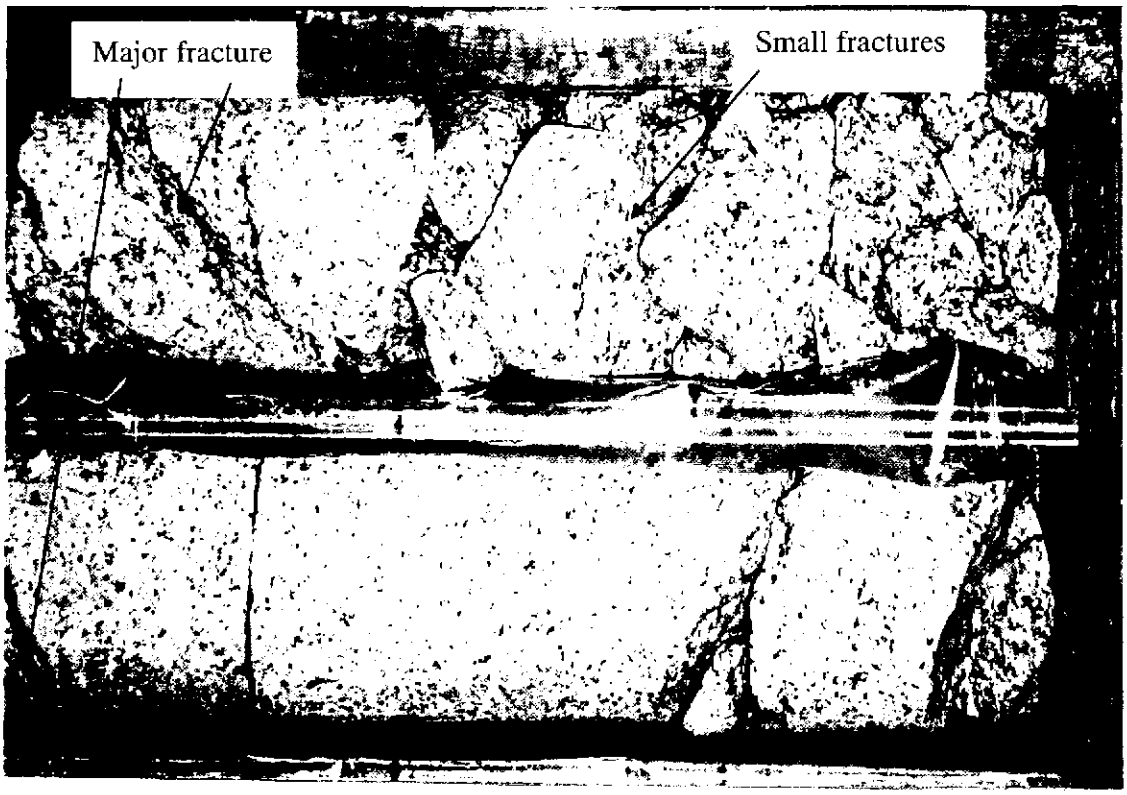

Figure 4.6.11 Lower angle major fracture (pattern 5) at depth 221-227 m MIU2

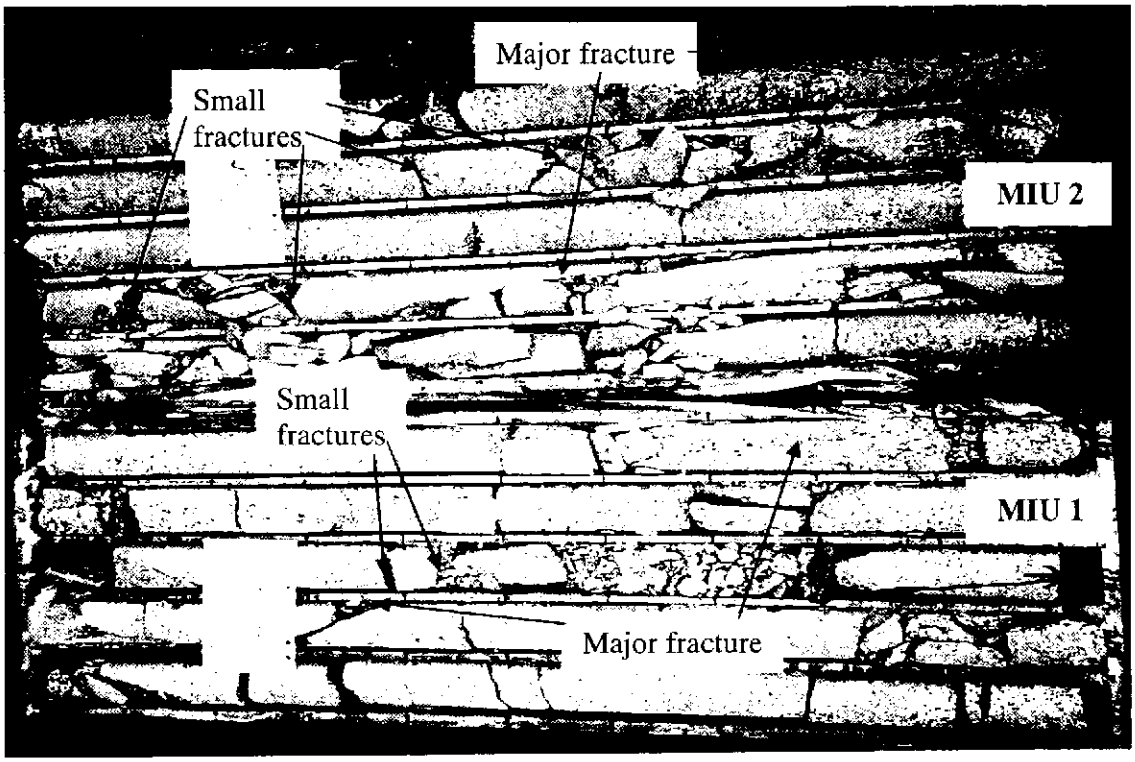

Figure 4.6.12 Connection between major fracture (pattern 1) at depth 460-465 m in MIU1 and at depth 740-745 m in MIU 2

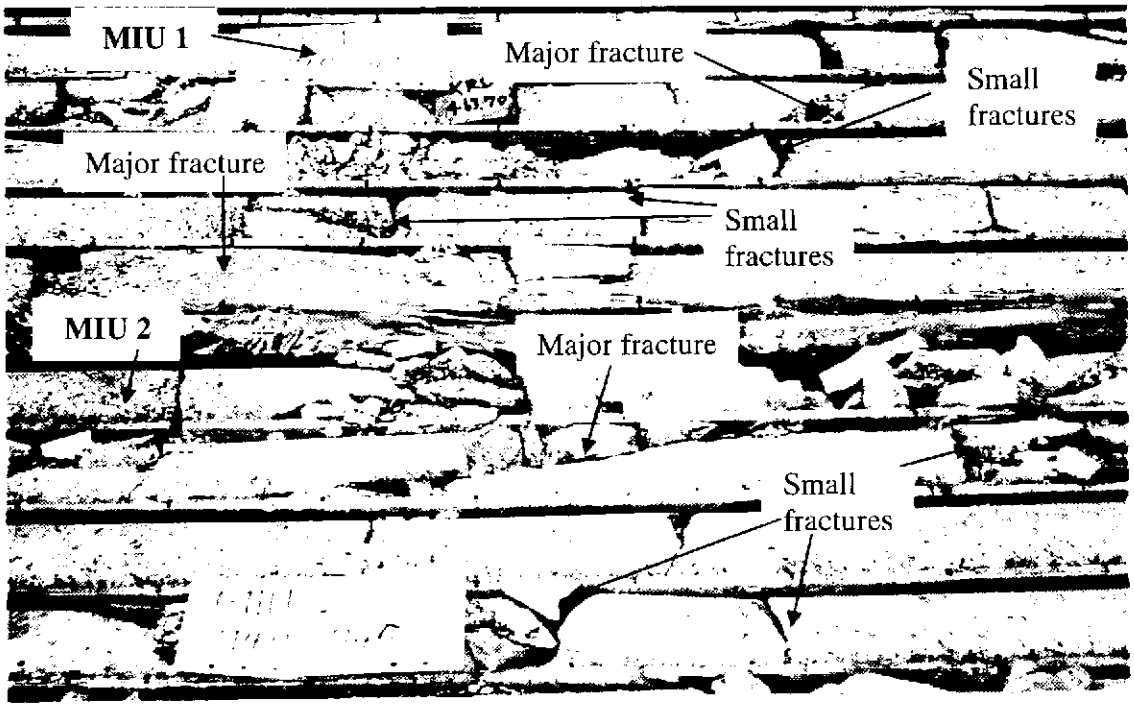

Figure 4.6.13 Connection between major fracture (pattern 1) at depth 460-465 m in MIU1 and at depth 740-745 m in MIU 2

CHAPTER 5

GROUNDWATER FLOW IN A COMPOSITE MEDIA

5.1 Example of Don-Chan Model

In the Donnen-Saitama Channeling (Don-Chan) Program, regular fracture network is assumed for presenting groundwater flow in sedimentary rock and the intersections between these assumed fractures are thought to be the highly permeable channels for groundwater flow. At the fractured rock mass, fractures intersection lines are thought to be indications of highly permeable regions and act as conduits (channels) for groundwater flow. A Don-Chan Model is shown by the following example.

5.1.1 Prepared Data

Input Data of Region

- Total number of boundary planes = 11
- Total number of geological domain = 1
- Geological domain code = 20
- Total number of domain = 2
- Domain 1
  - type = sedimentary rock (code = 10)
  - total number of boundary planes = 6
  - regular mesh interval = 100 m
  - planes numbers = 1, 2, 3, 4, 5, 6
- Domain 2
  - type = fractured rock (code = 11)
  - total number of boundary planes = 6
  - planes numbers = 6, 7, 8, 9, 10, 11
  - boundary planes types:
    - ❖ 1 = top side plane
    - ❖ 12 = side planes
    - ❖ 20 = geological domain planes
    - ❖ 13 = bottom side plane
- Total number of plane component points = 4 (rectangular)
- Plane component points coordinates (x, y, z)

Input Data of Fractures

- Total number of fractures = 52
- Fracture type = regular fracture (not water barrier fracture)
- Fracture direction = **N 30 W 75 N** and **N 30 E 75 N**
- Total number of considered domains for fractures location = 1 domain
- Considered domain number for fractures location = domain number 2
- Channel generate angle = 90° and 0°
- Distance between channel (channel interval) = 50 m

5.1.2 Calculation Steps

1. Domain Generator

- Input : Region data, Fractures data
- Output : Fracture model figures and data

Domain 1 (for sedimentary rock)

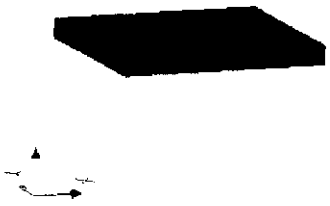

Figure 5.1.1 Domain of sedimentary rock

Domain 2 (for fractured rock)

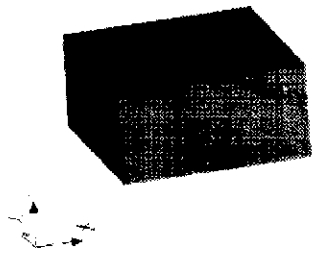

Figure 5.1.2 Domain of fractured rock

2. Fracture Generator

a. Sedimentary rock

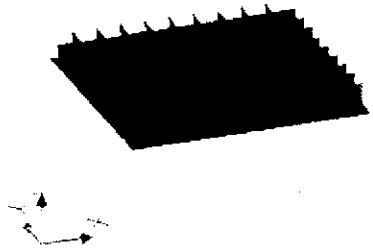

Figure 5.1.3 Model of sedimentary rock

b. Fractured rock

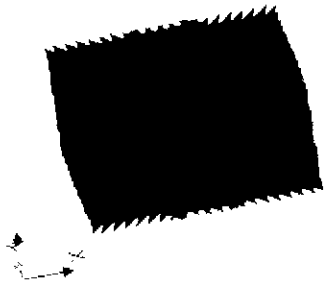

Figure 5.1.4 Model of fractured rock

c. Model of sedimentary and fractured rock

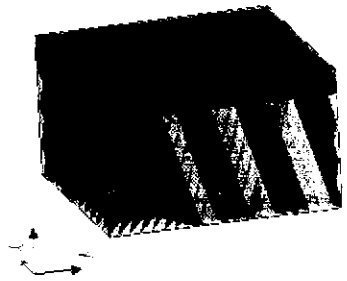

Figure 5.1.5 Composite model of sedimentary and fractured rock

3. Channel Network Generator

- Input : Fracture model data
- Output : - Property setting data 1
  - Channel network data and figure

Channel network

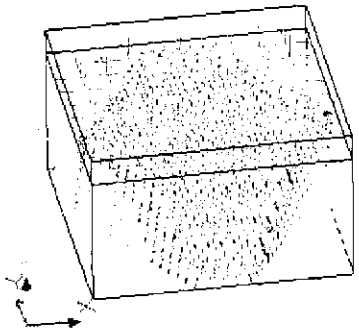

Figure 5.1.6 Channel network of sedimentary and fractured rock

4. Property and Boundary Condition Setting

Input :

- ❖ Channel network data
- ❖ Property setting data1 (permeability of sedimentary rock and fractures)
- ❖ Property setting data 2 (permeability of intersection channels)
- ❖ Boundary condition setting data
  - Boundary condition type = constant head (type number: 12)
  - Total number of boundary planes in which constant head are given = 4 boundary planes
  - Plane numbers in which constant head are given:
    - Plane numbers 4 and 2 (sedimentary rock)
    - Plane numbers 9 and 7 (fractured rock)
  - Constant head values given:
    - Plane numbers 4 and 9 = 210 m
    - Plane numbers 2 and 7 = 130 m

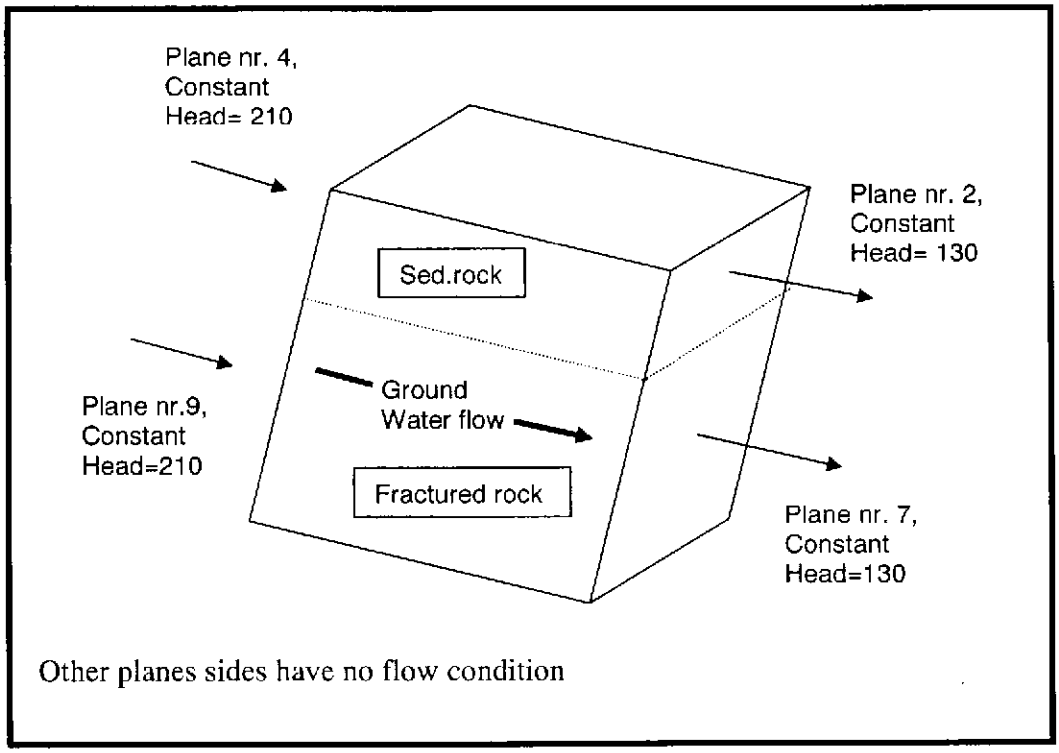

Figure 5.1.7 Boundary condition model of sedimentary and fractured rock

- Output: Groundwater flow analysis data

5.1.3 Groundwater Flow Calculation Result

- Input : Groundwater flow analysis data
- Output : Groundwater flow calculation result

Piezometric head distribution

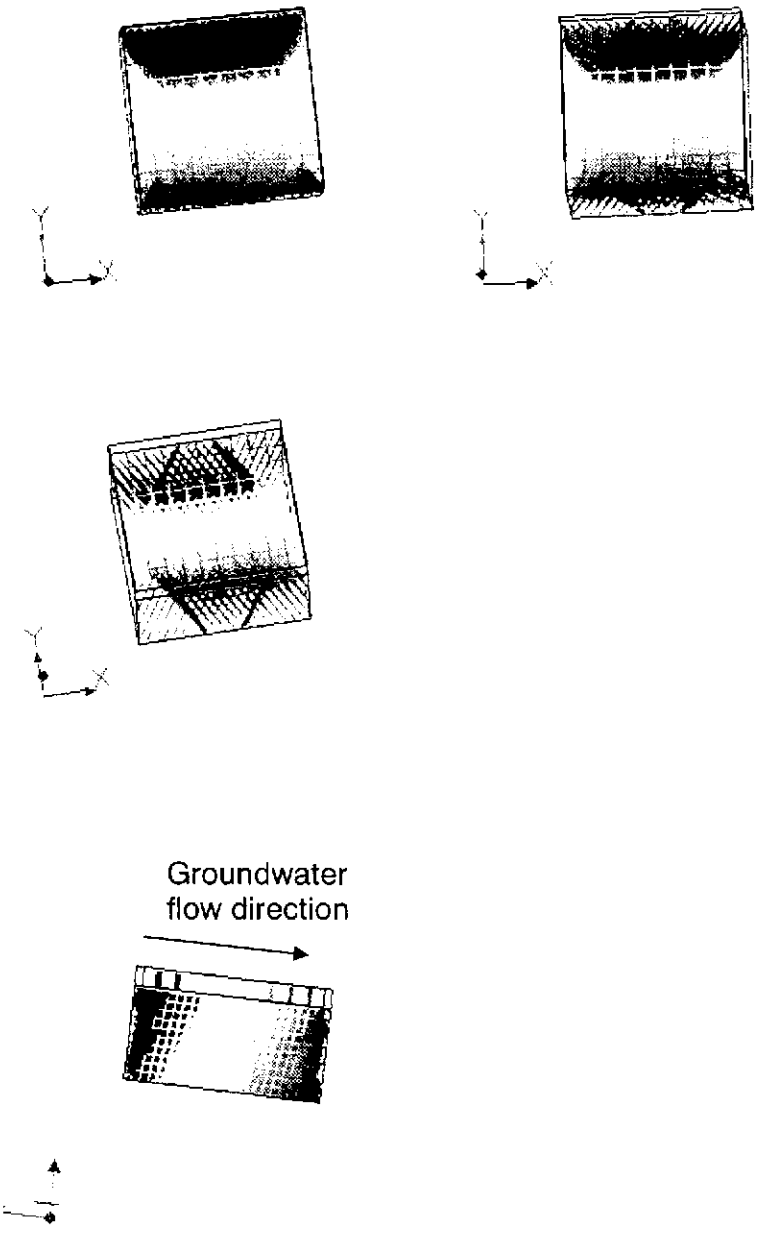

Figure 5.1.8 Piezometric head distribution in sedimentary and fractured rock

5.2 Groundwater Flow Analysis in Tono Area

Calculated area is a real field site, a 4 km x 6 km x 3 km thick fractured granite rock mass overlain by sedimentary layers approximately 100 m thick, including the MIU site, in the Tono Area of Gifu, Japan. Regular mesh was created to calculate groundwater flow in sedimentary rock and highly weathered area.

In this study, fracture modeling was executed by applying statistical method, calculating average distance/spacing between fractures (Fracture Generate Interval) of each pattern. Hydraulic conductivity values given for every major fracture are estimated from the hydraulic test results data obtained by JNC.

Table 5.2.1 Fractures Data

	Pattern 1	**Pattern 2**	**Pattern 3**	**Pattern 4**	**Pattern 5**	**Pattern 6**
Dip Strike	N70W80N	N45W20N	N40W60N	N40E75S	NS60E	EW40N
Fracture Generate Interval (m)	880	470	270	550	600	490
Fracture Zone Width of one Fracture (m)	1	9	2	1	2	4
Hydraulic Conductivity (m/s)	4.82E-07	5.11E-08	9.68E-07	9.08E-07	1.33E-06	5.35E-07

5.2.1 Prepared Data

Input Data of Domain
Total number of boundary planes = 2097

- Total number of geological domain = 1, Geological domain code = 20
- Total number of domain = 2
- Domain 1
  - type = sedimentary rock (code = 10)
  - total number of boundary planes = 2005
  - regular mesh interval = 50 m
  - planes numbers = 1, ..., 2005
- Domain 2
  - type = fractured rock (code = 11)
  - total number of boundary planes = 1049
  - planes numbers = 957, ..., 2097

- boundary planes types:
  - ❖ 1 = top side plane
  - ❖ 12 = side planes
  - ❖ 20 = geological domain planes
  - ❖ 13 = bottom side plane
- Total number of plane component points = 4 (rectangular) and 3 (triangle)
- Plane component points coordinates (x, y, z)

Input Data of Fractures

- Total numbers of fractures groups = 7 groups
  - group 1 : Big fault (Tsukiyoshi Fault)
  - group 2 : Fractures of Pattern 1
  - group 3 : Fractures of Pattern 2
  - group 4 : Fractures of Pattern 3
  - group 5 : Fractures of Pattern 4
  - group 6 : Fractures of Pattern 5
  - group 7 : Fractures of Pattern 6
- Fracture type (group 2-group7) = regular fracture (type 3)
- Fracture type (group 1) = water barrier fracture (type 12)
- Total number of considered domains for fractures location = 1 domain
- Considered domain number for fractures location = domain number 2
- Fracture direction =

1. **Tsukiyoshi Fault : N80W 70S**
2. **PATTERN 1 : N 70 W 80 N** (Fracture Generate Interval = 880 m)
3. **PATTERN 2 : N 45 W 20 N** (Fracture Generate Interval = 470 m)
4. **PATTERN 3 : N 40 W 60 N** (Fracture Generate Interval = 270 m)
5. **PATTERN 4 :N 40 E 75 S** (Fracture Generate Interval = 550 m)
6. **PATTERN 5 : NS 60 E** (Fracture Generate Interval = 600 m)
7. **PATTERN 6 : EW 40 N** (Fracture Generate Interval = 490 m)

Property Setting

- hydraulic conductivity of sedimentary rock = 1.80E-07
- total number of fractures group = 7
- total number of domain = 2
- hydraulic conductivity of fractures (based on JNC hydraulic test results data)
  - Tsukiyoshi Fault = 1.0E-10 m/s
  - Fractures Pattern 1= 4.82E-07
  - Fractures Pattern 2= 5.11E-08
  - Fractures Pattern 3= 9.68E-07
  - Fractures Pattern 4= 9.08E-07
  - Fractures Pattern 5= 1.33E-06
  - Fractures Pattern 6= 5.35E-07

- fracture zone width of :
  - Tsukiyoshi Fault = 9 m
  - Fractures Pattern 1= 6 m
  - Fractures Pattern 2= 9 m
  - Fractures Pattern 3= 4 m
  - Fractures Pattern 4= 3 m
  - Fractures Pattern 5= 4 m
  - Fractures Pattern 6= 4 m

Boundary condition

- Boundary condition type:
  - constant head (type number: 12)
  - no flow (type number: 11)
- Boundary condition data:

Table 5.2.2 Boundary Condition Setting

No	Top boundary condition	Side boundary condition
1	(Z-5m)	constant head (Z-5m)
2	(Z-10%)	constant head (Z-10%)
3	(Z-5m)	no flow
4	(Z-10%)	no flow
5	(Z-20%)	no flow

Remark:

(Z-5m) : 5 meter below surface

(Z-10%) : 10% (of each top point elevation-minimum elevation) below surface

Z : top/ground surface elevation (m)

constant head : for all side except southern side has no flow boundary condition

5.2.2 Calculation Steps

1. Domain Generator

Domain 1 (for sedimentary rock)

Figure 5.2.1 Domain of sedimentary rock

Domain 2 (for fractured rock)

Figure 5.2.2 Domain of fractured rock

Combined Domain 1 and Domain 2 (for sedimentary and fractured rock)

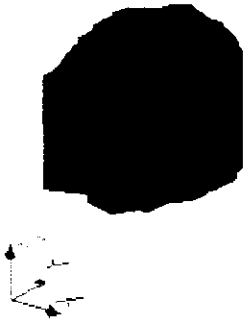

Figure 5.2.3 Domain of sedimentary and fractured rock

2. Fracture Generator
a. Sedimentary rock

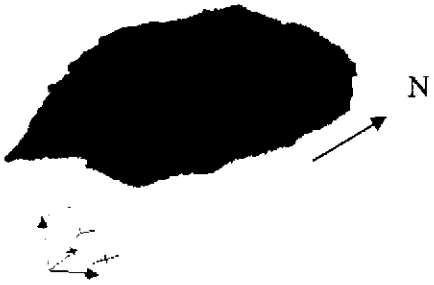

(eastern side)

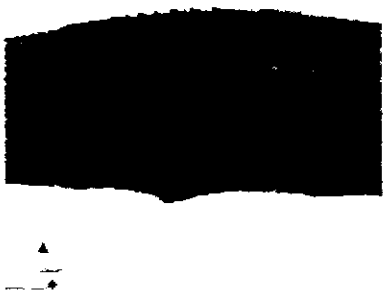

(western side)

Figure 5.2.4 Model of sedimentary rock

b. Fractured rock

Group 1 (PATTERN 1) : N 70 W 80 N

Figure 5.2.5a Model of fractured rock
(Pattern 1)

Group 2 (PATTERN 2) : N 45 W 20 N

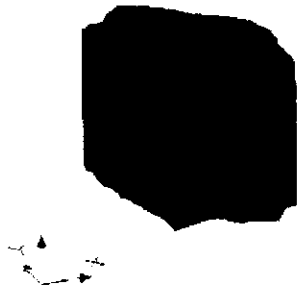

Figure 5.2.5 b. Model of fractured rock
(Pattern 2)

Group 3 (PATTERN 3) : N 40 W 60 N

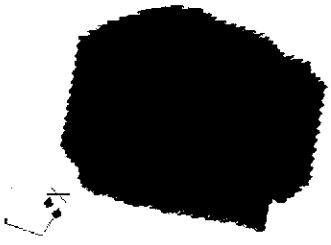

Figure 5.2.5 c. Model of fractured rock
(Pattern 3)

Group 4 (PATTERN 4): N 40 E 75 S

Figure 5.2.5 d. Model of fractured rock
(Pattern 4)

Group 5 (PATTERN 5) : NS 60 E

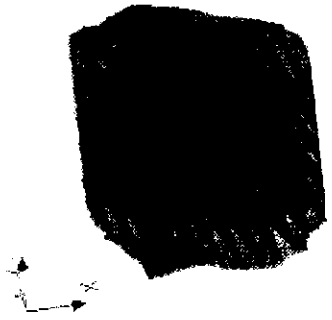

Figure 5.2.5 e. Model of fractured rock (Pattern 5)

Group 6 (PATTERN 6) : EW 40 N

Figure 5.2.5f Model of fractured rock (Pattern 6)

c. Combined Fractures Group 1 to Group 6 and Tsukiyoshi Fault

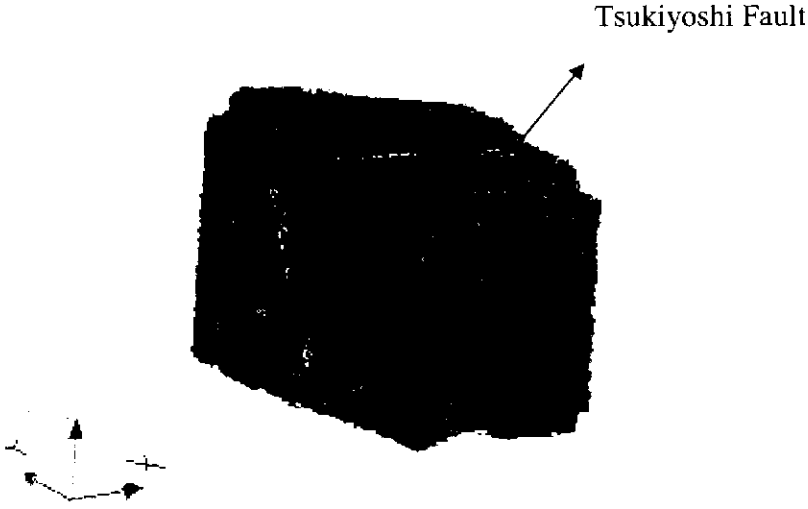

Figure 5.2.6 Model of fractured rock (group 1 to group 6) and Tsukiyoshi Fault

d. Composite Model of sedimentary and fractured rock

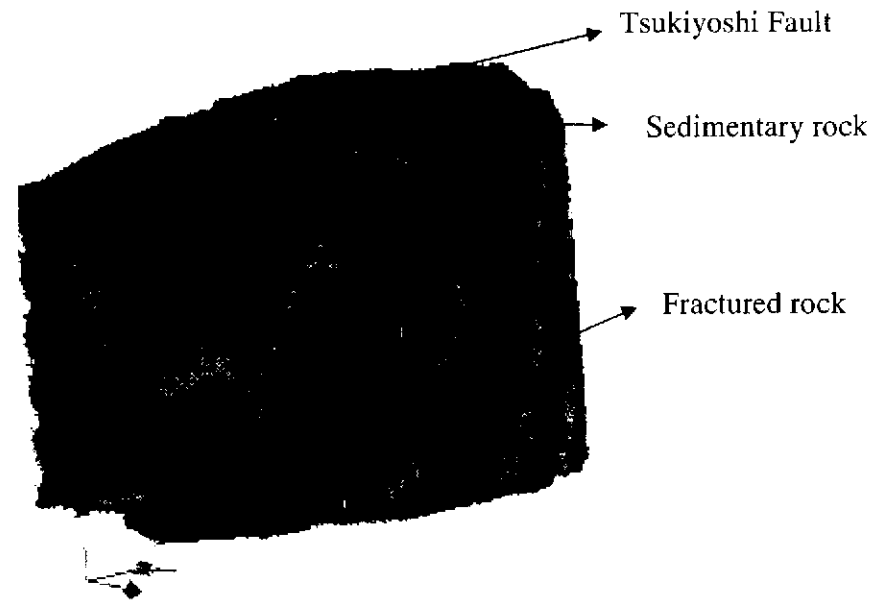

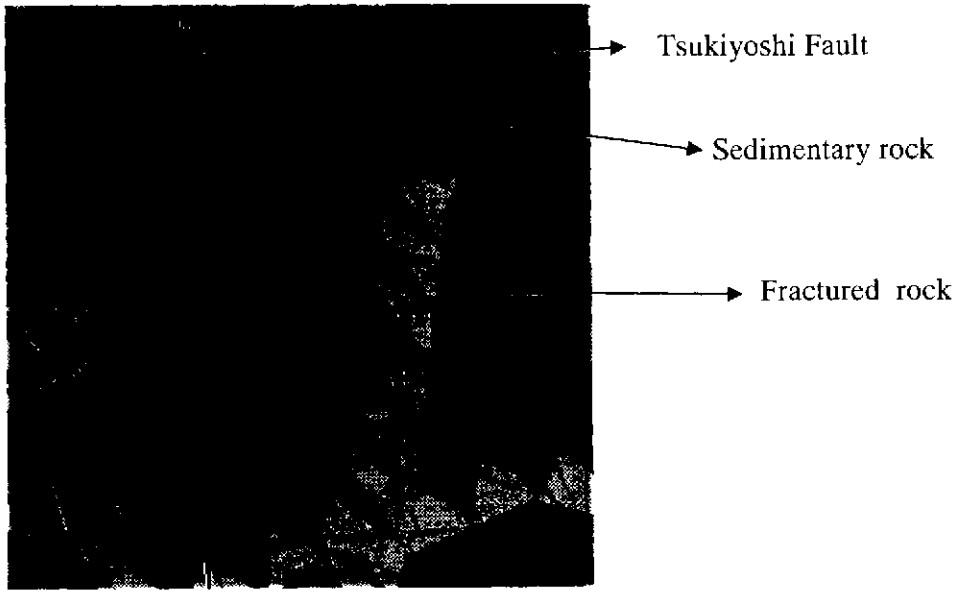

Figure 5.2.7 Composite model of sedimentary and fractured rock

3. Channel Network Generator

Channel network

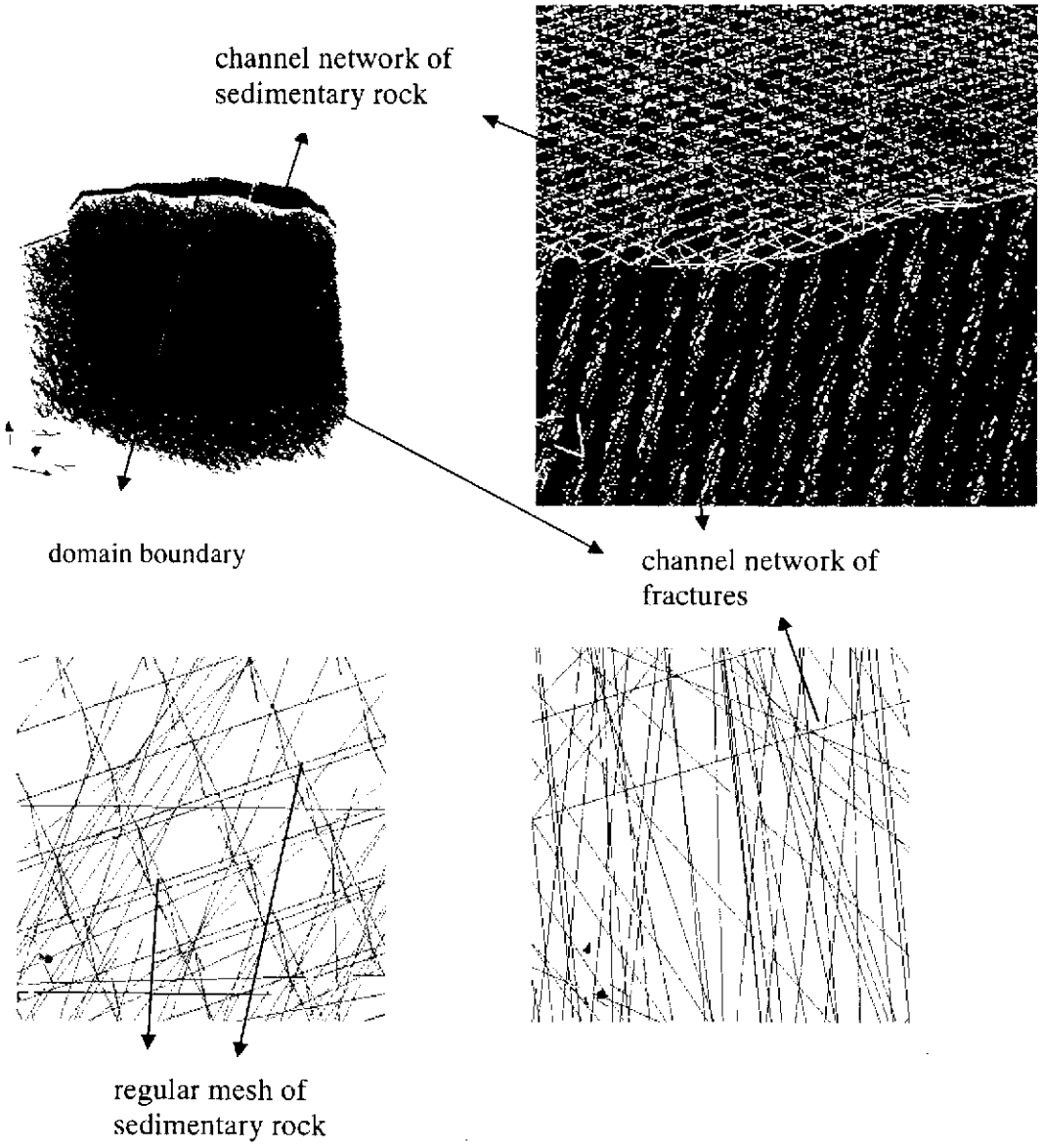

Figure 5.2.8 Channel network of sedimentary and fractured rock

5.2.3 Groundwater Flow Calculation Result

Piezometric head

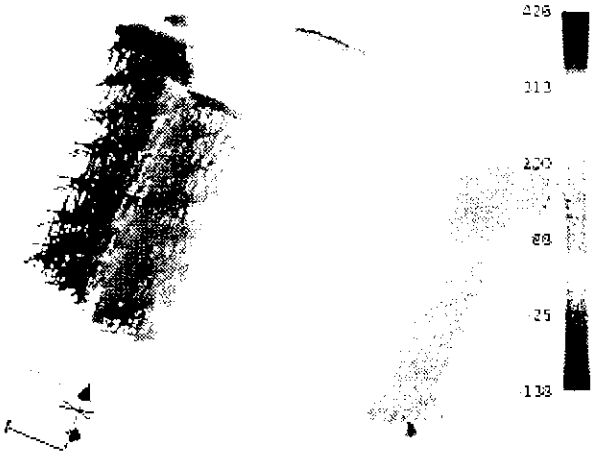

Figure 5.2.9 Figure of piezometric head distribution case 1
(top b.c.=(Z-5m) , side b.c.=constant head (Z-5m))

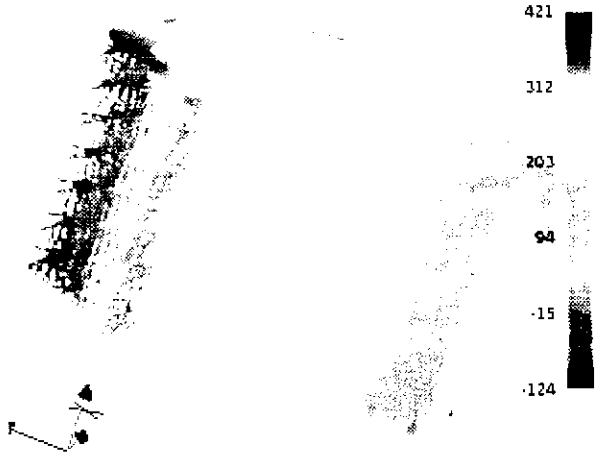

Figure 5.2.10 Figure of piezometric head distribution case 2
(top b.c.=(Z-10%) , side b.c.=constant head (Z-10%))

Figure 5.2.11 Figure of piezometric head distribution case 3
(top b.c.=(Z-5m) , side b.c.= no flow)

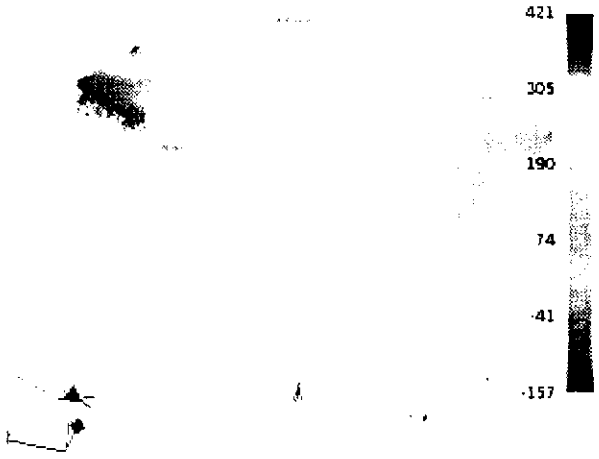

Figure 5.2.12 Figure of piezometric head distribution case 4
(top b.c.=(Z-10%) , side b.c.= no flow)

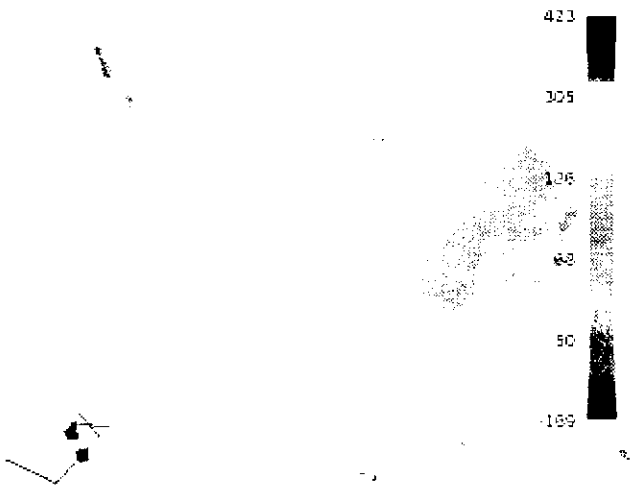

Figure 5.2.13 Figure of piezometric head distribution case 5
(top b.c.=(Z-20%) , side b.c.= no flow)

5.3 Results and Discussions

All piezometric head distributions results showed that groundwater mainly flow from north direction to the south direction in the analysed area. To validate the model, calculation results of the piezometric head along MIU 2, were compared with the measured values in MIU 2 borehole obtained by JNC (Table 5.3.1). All calculation results presented and discussed in this part are relating to the head values in MIU 2 borehole. Calculated results with 4 different boundary conditions are summarized in Table 5.3.2.

Table 5.3.1 PiezometricHead Measurement along MIU2 borehole obtained by JNC

Probe No	Packer Reference Depth (m)	Measurement Port Depth (m)	Measurement Port Elevation (m)	Total Head (m)	Average (m)
1	979.5	981	-757.245	245.7	Below part
2	970.3	971.8	-748.045	245.4	
3	959.5	961	-737.245	244.9	
4	930.8	932.3	-708.545	240.4	
5	918.4	920	-696.245	246.1	
6	886.6	888.2	-664.445	245.8	
7	867.4	868.9	-645.145	237.1	243.6
8	255.1	256.6	-32.845	214.9	Above part
9	187.5	189	34.755	214.5	
10	120.1	121.6	102.155	214.4	214.6

Table 5.3.2 Piezometric Head Calculation Results along MIU 2 borehole using Don Chan Program

	top b.c. = (Z-5m)	
	above part	below part
side b.c. = constant head (Z-5m)	**244**	**275**
	top b.c. = (Z-10%)	
	above part	below part
side b.c. = constant head (Z-10%)	**243**	**265**
	top b.c. = (Z-5m)	
	above part	below part
side b.c. = no flow	**244**	**262**
	top b.c. = (Z-10%)	
	above part	below part
side b.c. = no flow	**243**	**254**

	top b.c. = (Z-20%)	
	above part	below part
side b.c. = no flow	**226**	**242.6**

Remark:
(Z-5m) : 5 meter below surface
(Z-10%) : 10% (of each top point elevation-minimum elevation) below surface
Z : top/ground surface elevation (m)
constant head : for all side except south side has no flow boundary condition
above part : elevation 200m to -200m
below part : elevation -600m to -1000m

First, in the calculation, groundwater table was set 5 meter below ground surface for top and side boundary condition except for southern side having no flow boundary condition. Piezometric head distribution along the MIU 2 borehole were checked. Calculated and measured values are plotted in Figure 5.3.1. Comparing with the measured values, the calculated head values were parallel shifted that may be due to top boundary condition or side boundary condition.

The head difference between below part and above part (275m-246m = 29 m), which show the head jump below and above Tsukiyoshi Fault, well agreed with the head difference shown by JNC field measurement (243.6m-214.6m = 29m). Tsukiyoshi Fault is a water barrier fracture that has low hydraulic conductivity. The groundwater flow was interrupted by such fault. Therefore, head jump existed and piezometric head values at position below Tsukiyoshi Fault were higher than the ones above Tsukiyoshi Fault.

For making clear the reason of parallel shift of piezometric head distribution, boundary condition effect was checked, by changing the assumed groundwater table into 10% (of each ground surface elevation-minimum elevation) below ground surface, for top and side boundary condition. The above part showed nearly same head calculation result and below part gave head changes from 275 meter to 265 meter as shown by Figure 5.3.1. Assumption of groundwater table 10% below ground surface gave smaller head calculation result than groundwater table 5 meter below ground surface so that the head jump below and above Tsukiyoshi fault is also smaller.

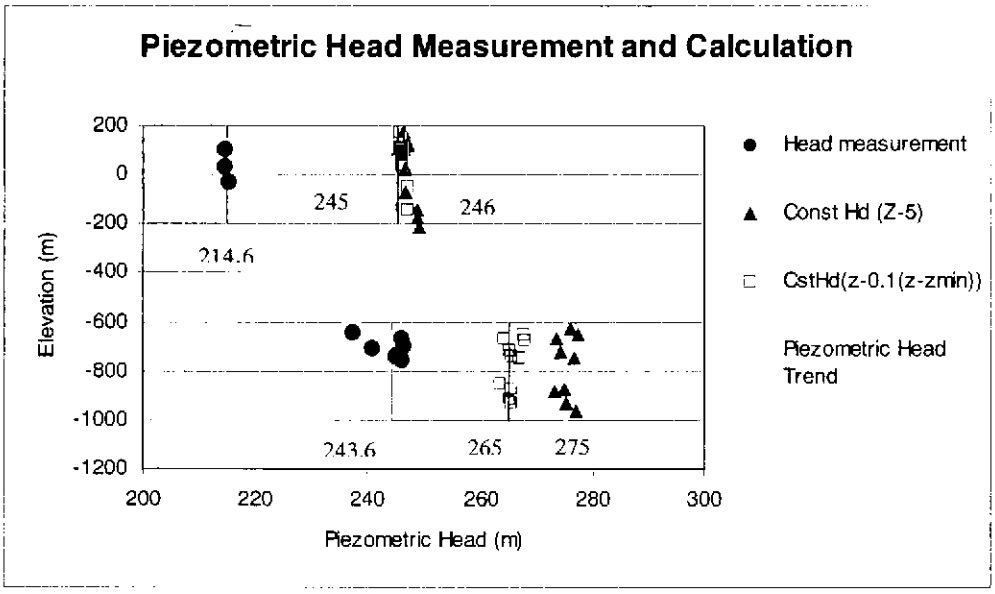

Figure 5.3.1 Measured and Calculated Piezometric Head Profile at Constant Head Side Boundary Condition

Next, side boundary condition effect was checked, by changing the constant head side boundary condition into no flow side boundary condition. As first step, top boundary condition was set at the groundwater table 5 meter below ground surface. At above part, head values showed the same results between side boundary condition constant head (Z-5m) at top boundary condition (Z-5m) and no flow side boundary condition. As second step, top boundary condition was set at the groundwater table 10% (of each ground surface elevation-minimum elevation) below ground surface. The same phenomena, as obtained by former boundary condition, were observed. At above part, head values showed the same results between side boundary condition constant head (Z-10%) at top boundary condition (Z-10%) and no flow side boundary condition.

At the above part, the changes of side boundary condition gave the same head results for the same top boundary condition. The piezometric head values when top boundary conditions were set as (Z-5m) showed the same results between constant head and no flow side boundary conditions. The same piezometric head values were also observed when top boundary conditions were set as (Z-10%) between constant head and no flow side boundary conditions. Piezometric head calculation results were influenced by the

top boundary condition given. From these results, it can be found that the side boundary condition gave no significant influences to the above part head values. On the other hand, above part head values were influenced by top boundary condition.

However, the head values at below part showed the significant differences between constant head and no flow side boundary conditions, from 275 m to 262 m when top boundary conditions were set as (Z-5m) and from 265 m to 254 m when top boundary conditions were set as (Z-10%) as shown by Figure 5.3.2.

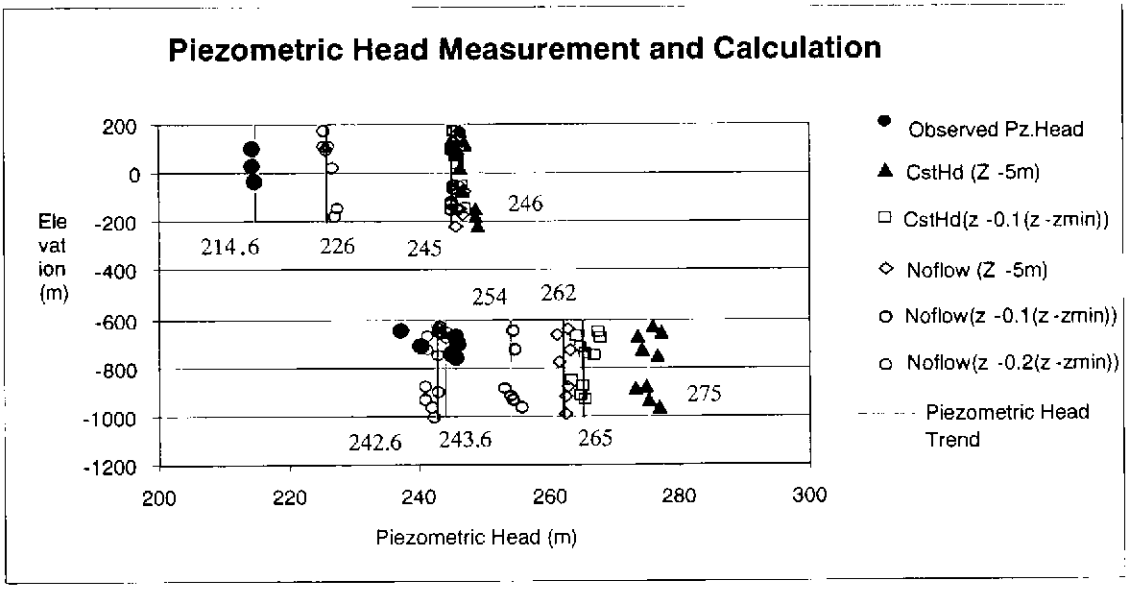

Figure 5.3.2 Measured and Calculated Piezometric Head Profile at Constant Head and No Flow Side Boundary Condition

The above results show that below part head values were much influenced by side boundary condition. The significant differences of head values exist between constant head and no flow side boundary condition at the top boundary condition (Z-5m) and top boundary condition (Z-10 %). At the below part, constant head side boundary condition gave higher head values than no flow side boundary condition.

To check the top boundary condition effect, we can analyse the head calculation results at the same no flow side boundary condition, for different top boundary condition (Z-5m)

and (Z-10%). At below part, head values gave significant differences from 262 m to 254 m, for top boundary condition (Z-5m) and (Z-10%). This result showed that below part head values were also influenced by top boundary condition.

At above part, change of top boundary condition showed the change of head values from 246 m to 245 m. The same phenomena were also observed at this different top boundary condition (Z-5m) and (Z-10%) for constant head side boundary condition. The head values changes are from 246 m to 245 m. Top boundary condition gave influence to above part head values. This top boundary condition checking also showed that by giving the same no flow side boundary condition or different constant head (Z-5) and (Z-10%) side boundary condition, the changes of head values at above part were same, from 246 m for top boundary condition (Z-5) to 245 m for top boundary condition (Z-10%). These emphasize the previous analysis that above part head values were influenced by top boundary condition while side boundary condition did not give significant influences to this part.

As the final step of calculation, top boundary condition was set at the groundwater table 20 % below ground surface. The result showed that top boundary condition influence the profiles below and above fault. Piezometric head profile below fault was almost fit with the observed piezometric head profile obtained by JNC.

At the no flow side boundary condition, flow is influenced only by infiltration. At the constant head side boundary condition, besides infiltration, flow in the analysed area is also influenced by the flows that pass through the side boundary condition.

There will be much water at the northern part (upstream part) of the water barrier feature. This fault gave significant influences to the groundwater flow, which was observed along MIU 2 borehole. The head jump below and above Tsukiyoshi Fault created by constant head side boundary condition is higher than no flow side boundary condition.
Based on the above analysis, we can conclude that below part head values were much influenced by top and side boundary condition, while above part head values were

influenced by top boundary condition. Since the calculated head values have not fitted with the measured head values obtained by JNC, while above and below part head values were influenced by top and side boundary condition, more considerations of top and side boundary condition are needed, in order to have good agreement of above and below part head values, with the JNC measurement results.

CHAPTER 6

CONCLUSIONS AND FURTHER IMPROVEMENT

6.1 Conclusions

Fractures data of four 1000 m boreholes (AN1, MIU1, MIU2 and MIU3), located in the MIU site and obtained by Japan Nuclear Cycle Depvelopment Institute (JNC), were used for constructing fracture model. Based on the stereographic projections of fractures orientation data read by Borehole Television (BTV) figures, fractures patterns were analysed and interpreted.. Stereographic projections were made in every 5-m range borehole depth, every 5-m range borehole depth with sliding 1 meter and every 1-m range borehole depth. The connection of fractures among observed boreholes were also analysed by using 3-D visualization technique developed in this study. Selected fractures patterns were checked by comparing with fractures in bore cores.

The obtained results are as follows:

- Six fractures patterns were selected and major fractures directions were defined by stereographic projection and bore cores observation.
- The selected major fractures are in accordance with lineament data of Tono Area taken by remote sensing system.
- Technique of groundwater flow calculation on the basis of the borehole information can be proposed.
- The changes of boundary conditions were given for making clear the effect of boundary conditions on calculated piezometric head. The calculated piezometric head results along MIU2 borehole, where the Tsukiyoshi Fault exists, were checked and compared with the measured piezometric head values along MIU2 borehole obtained by JNC. Phenomena of piezometric head distributions were simulated. Groundwater mainly flow from north direction to the south direction in the analysed area.
- In the MIU2 borehole, Tsukiyoshi Fault, a water barrier fracture that has low hydraulic conductivity, was observed. This fault gave significant influences to

the piezometric head values along MIU 2 borehole. Groundwater flows were interrupted by this fault so that the significant head differences (head jumps) exist below and above the fault. Piezometric head values below the fault were higher than the ones above it.

- Based on the analysis, we can conclude that along MIU 2 borehole, below part head values were much influenced by top and side boundary condition, while above part head values were influenced by top boundary condition.

6.2 Further Improvement

- Since the calculated head values have not fitted with the measured head values obtained by JNC, while above and below part head values were influenced by top and side boundary condition, more considerations of top and side boundary condition are needed, in order to have good agreement of above and below part head values, with the JNC measurement results. More detailed field observation on the top and side boundary conditions are proposed.

REFERENCES

- Kunio Watanabe, Yokito Sugimura, Yutaka Morita, Tatsuya Tanaka,1997, Channel Network Modelling of the Fractured Granite in the Hinachi area, Japan, a paper at the topic of Earthquake Proof Design and Active Faults, Elsevier

- Martin Mazurek, Paul Bossart, Thomas Eliasson, 1996, Classification and Characterization of Water-Conducting Features at ASPO: Results of Investigations on the Outcrop Scale, NAGRA, Switzerland and SKB, Sweden

- Jacob Bear, Chin-Fu Tsang, Ghislain de Marsily, 1993, Flow and Contaminant Transport in Fractured Rock, Academic Press

- Robert Bowen, 1984, Geology in Engineering, Elsevier Applied Science Publishers

- A.C. McLean and C.D. Gribble, 1979, Geology for Civil Engineers, Fakenham Press.

- B.Jamtveit and B.W.D. Yardley, 1997, Fluid Flow and Transport in Rocks, Chapman & Hall

- Jacob Bear and Arnold Verruijt, 1987, Modeling Groundwater Flow and Pollution, D.Reidel Publishing Company

- David R. Maidment, 1992, Handbook of Hydrology, McGraw-Hill, INC
- David Keith Todd, 1980, Groundwater Hydrology, John Wiley & Sons
- Herman Bouwer, 1978, Groundwater Hydrology, McGraw-Hill
- William C. Walton, 1970, Groundwater Resource Evaluation, McGraw-Hill
- Stanley N.Davis and R.J.M. DeWiest, 1996, Hydrogeology, John Wiley & Sons

Part Ⅱ

花崗岩における
水みちの構造的特徴に関する研究

第7章　序論

7.1　研究背景

原子力発電によるエネルギーの生産にともなって発生する放射性廃棄物の処分は、現代社会が避けることのできない課題である。この処分方法として現在もっとも有力視されているのが地層処分であり、日本のみならず世界各国で研究が進められている。

現在、核燃料サイクル開発機構東濃地科学センターでは、花崗岩を対象として、地層処分研究開発の基盤となる深部地質環境の科学的研究を進めている。この研究における重要な課題の一つに、研究対象となる場の3次元的な地下水流動場を把握するためのモデル化・解析技術の構築が挙げられる。

7.2　研究目的

研究対象となる 3 次元的な花崗岩内の地下水流動場を把握するためには、地下水の卓越した流動経路を支配していると考えられる割れ目系を評価する手法を開発することが重要である。したがって、本研究では割れ目系の有する規則性や割れ目系内に発達する水みちの規則性を抽出することを目的とした。

第8章　東濃付近の地質概要

研究実施領域周辺の地質は、主に中生代の基盤岩類とそれらを不整合に覆う新第三紀の堆積岩類からなる。図 8.1 に地形図を，図 8.2 に地質図を，図 8.3 に地質断面図を示す。

中生代の基盤岩類は、美濃帯に属する堆積岩類、これを覆う濃飛流紋岩、これらに貫入する土岐花崗岩からなる。広域的に東濃地域は、美濃―丹波帯と領家帯の境界付近に位置しており、北側から西方に美濃帯の堆積岩類、東側に濃飛流紋岩、南側に白亜紀花崗岩が分布している。美濃帯堆積岩類は、チャート、砂岩、泥岩、礫岩、で構成され、領域の縁辺部に一部が認められる。この美濃帯堆積岩類は土岐花崗岩に貫入されるが、その境界付近では接触変成作用によりホルンフェルス化している。濃飛流紋岩は流紋岩質～デイサイト質の溶結凝灰岩からなり、凝灰岩、角礫岩、溶岩、水底堆積の堆積岩を伴う。本領域では、濃飛流紋岩の南西端部が領域北東部に分布する。土岐花崗岩は、領域に分布する基盤岩類の大部分を占め、東西約 12ｋｍ、南北約 14ｋｍのほぼ円形の岩体として分布する。本花崗岩は、主に細～粗粒の黒雲母花崗岩からなり、岩体中には石英班岩質、アプライト質などの岩脈が NNW 方向にいくつか貫入する。黒雲母花崗岩に含有される石英は、放射線により黒～暗灰色を呈する。土岐花崗岩の年代は、82～68Ma と報告されている。

新第三紀の堆積岩類は中新世の瑞浪層群と鮮新世の瀬戸層群からなり、上位の瀬戸層群は下位の瑞浪層群を不整合に覆う。

瑞浪層群は、海進に伴う非海成～海成の堆積岩からなり、全体的に南方へ緩い傾斜を示す。その分類は下位より土岐夾炭累層、本郷累層、明世累層、生俵累層に区分される。土岐夾炭累層は、炭質泥岩・亜炭を夾在する泥岩・砂岩からなり、基盤岩類を不整合に覆う。基底には礫岩が認められる。本郷累層、土岐夾炭累層を不整合に覆い、凝灰岩質の砂岩・シルト・泥岩の互層で特徴付けられ、基底礫岩を有する。明世累層は、凝灰質砂岩～泥岩からなり、凝灰岩の薄層を挟む。生俵累層は、無層理のシルト岩～細粒凝灰質泥岩であり、基底部には礫岩、中～粗粒砂岩を伴う。明世累層と生俵累層の境界には不整合面が存在する。

瀬戸層群は領域全体に渡って水平に分布し、下位より粘土質の土岐口陶土層、礫質の土岐砂礫層からなる。

領域の地質構造として、領域中央部にほぼ E-W 系の走向を示す月吉断層、領域南東部に NE 系の山田断層帯および屏風山断層が分布する。月吉断層は、東濃鉱山調査孔で走向 N80° W、傾斜 70° S、幅 10～30m、垂直変位 30mを示す南側が衝上する逆断層であり、その活動は鍵層の解析より、生俵累層堆積

後～瀬戸層群堆積前と考えられる。山田断層帯は、NE 系の走向を示し、SE 方向に急傾斜(合計垂直変位：数十 m)する複数の逆断層からなる断層帯と報告されている。また、同様の走向および傾斜を示す屏風山断層も逆断層であり(垂直変位：約 300m)、活断層研究会では活断層とされている。

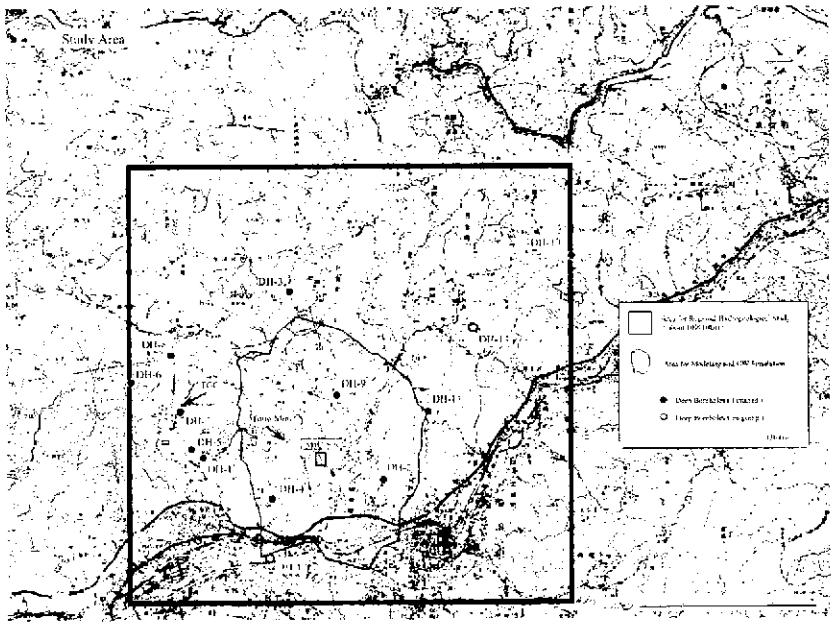

図 8.1　地形図（解析対象領域）

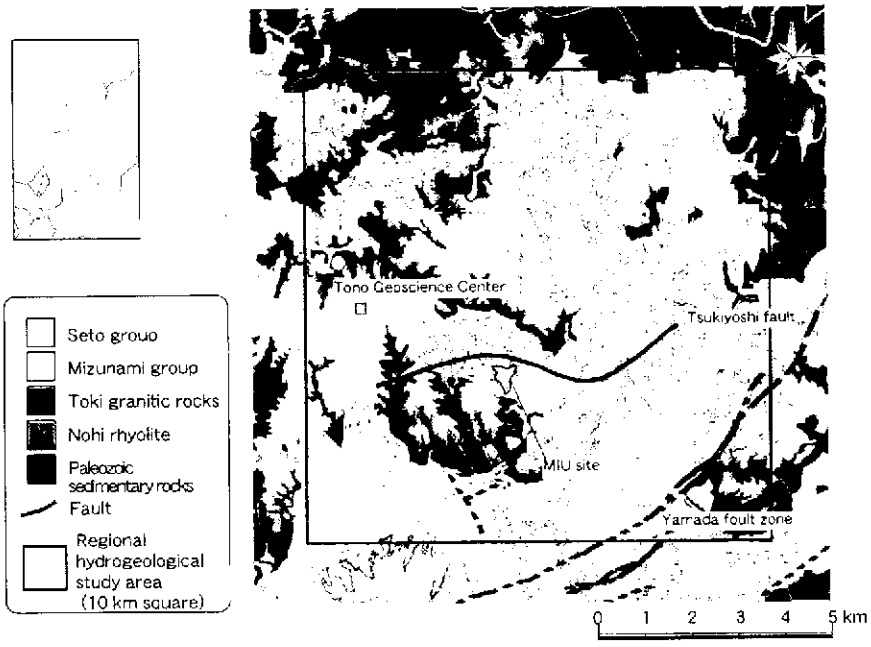

Fig.2 Geological settings of Tono area

図 8.2　地質図

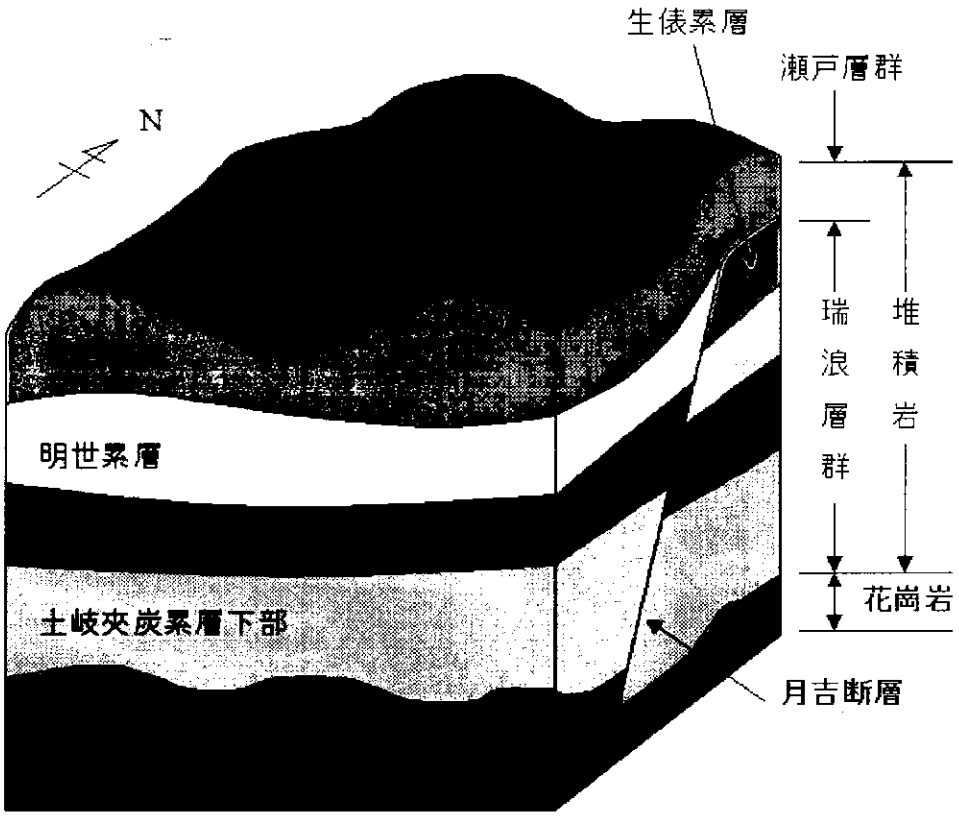

図 8.3　地質断面図

第9章　割れ目分布

本研究では核燃料サイクル開発機構が行ったボアホールテレビ（BTV）調査から、割れ目の傾斜角（dip）と傾斜方位（dip direction）を取りだし、深度や岩相の違いによる比較検討を土岐花崗岩を対象とし行った。比較には月吉断層が通り、他のボーリングと比べ割れ目が発達しているMIU孔を用いた。図9.1にボーリング位置図を示す。また水みちを形成する可能性がある、構造的特徴を持った割れ目割れ目を取りだし、その方向や逸水箇所との比較も行った。

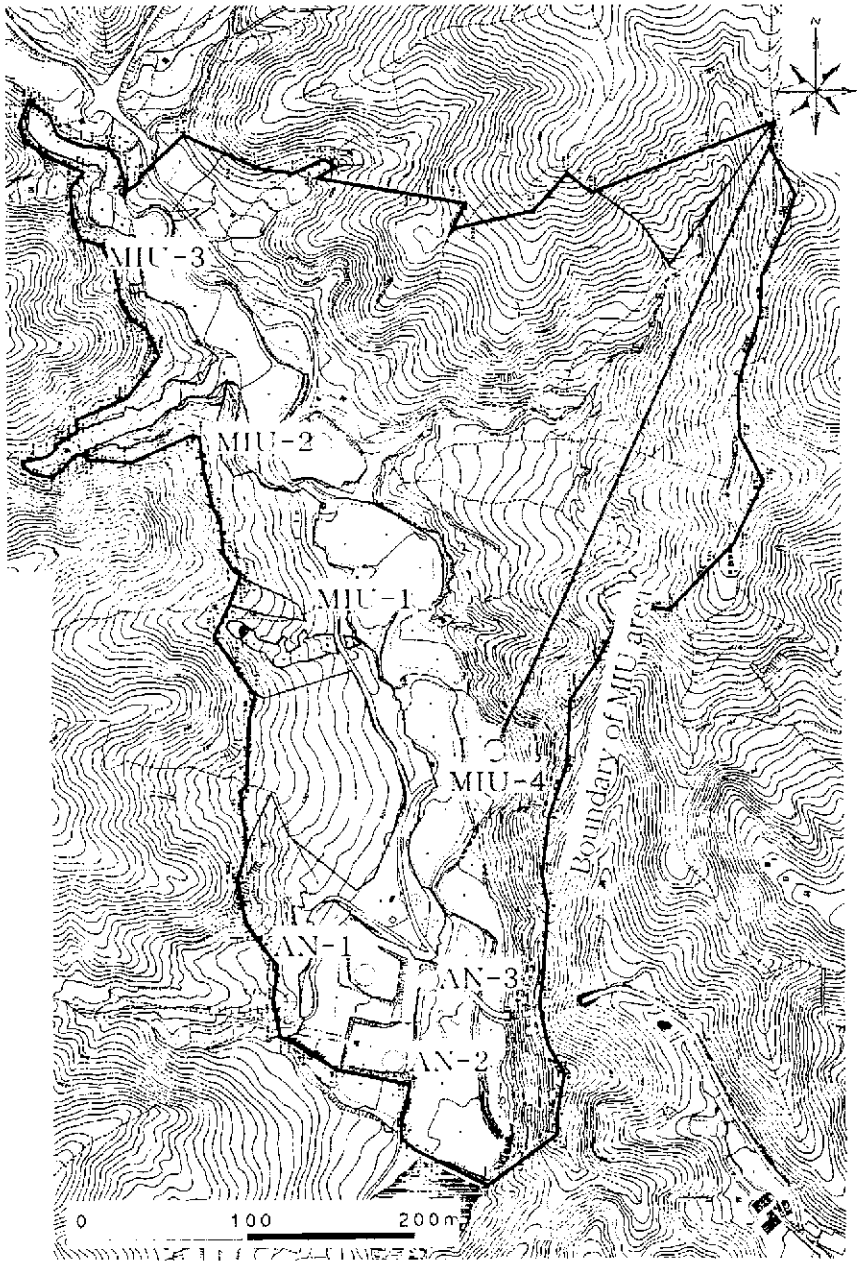

図9.1　ボーリング孔位置図

9.1 深度による違い

深度の違いによる割れ目の方向を比較するために、MIU-1,2,3 孔において花崗岩を対象とし、深度 100～1000mの区間を 20mずつに分け、傾斜角と傾斜方位をステレオ投影した（Lower-hemisphere, Schmidt net）。図 9.1.1、図 9.1.2、図 9.1.3 にその結果を示す。コンターはパーセント表示である。

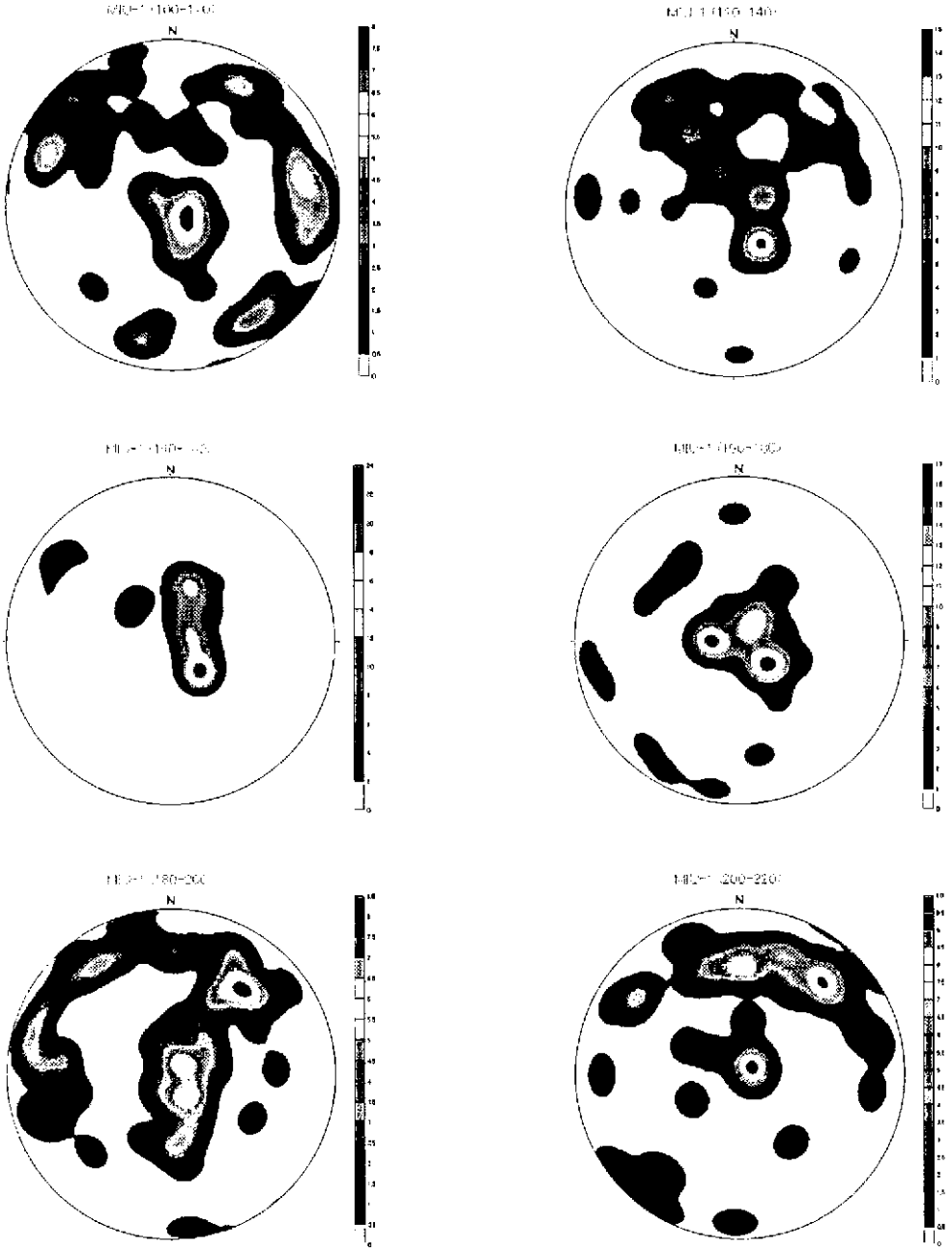

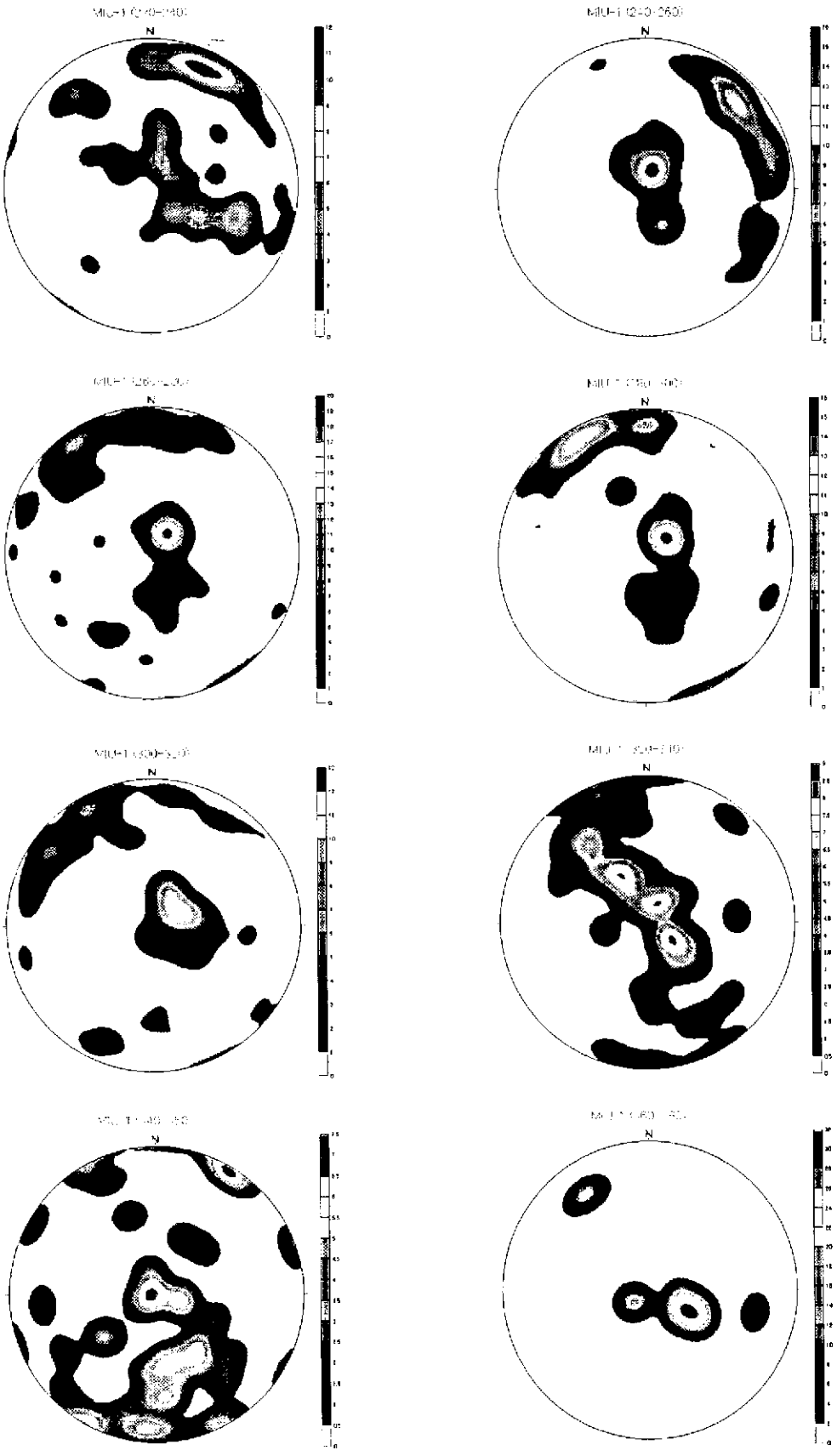

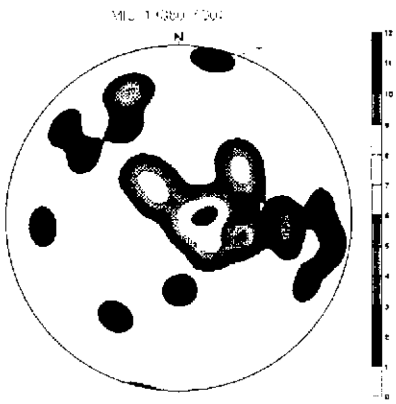
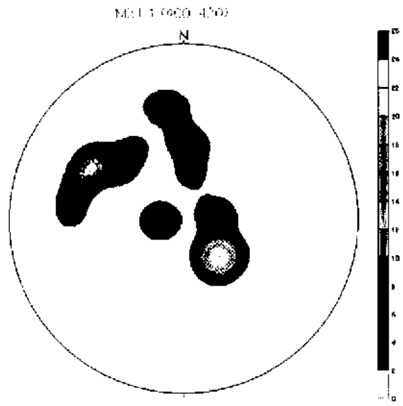
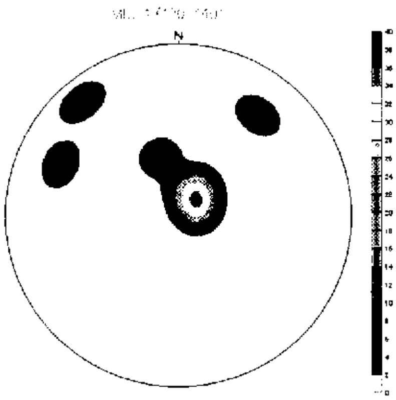
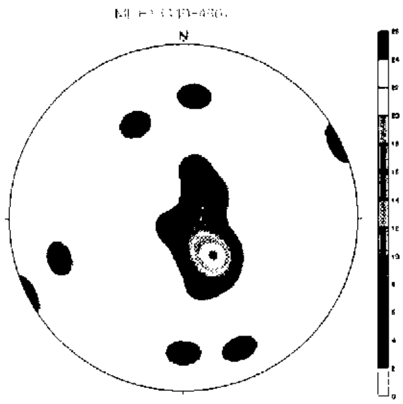
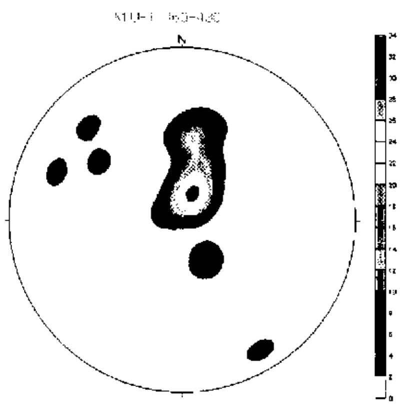
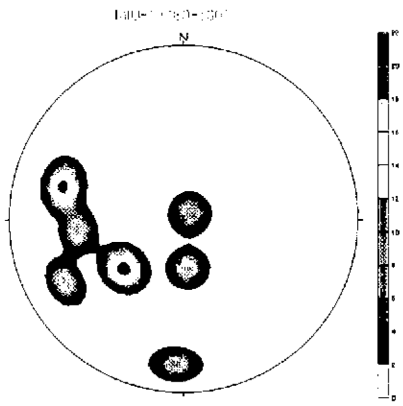
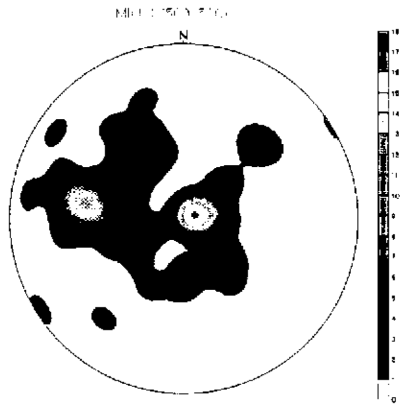
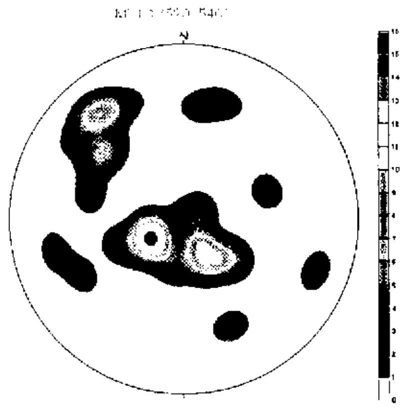

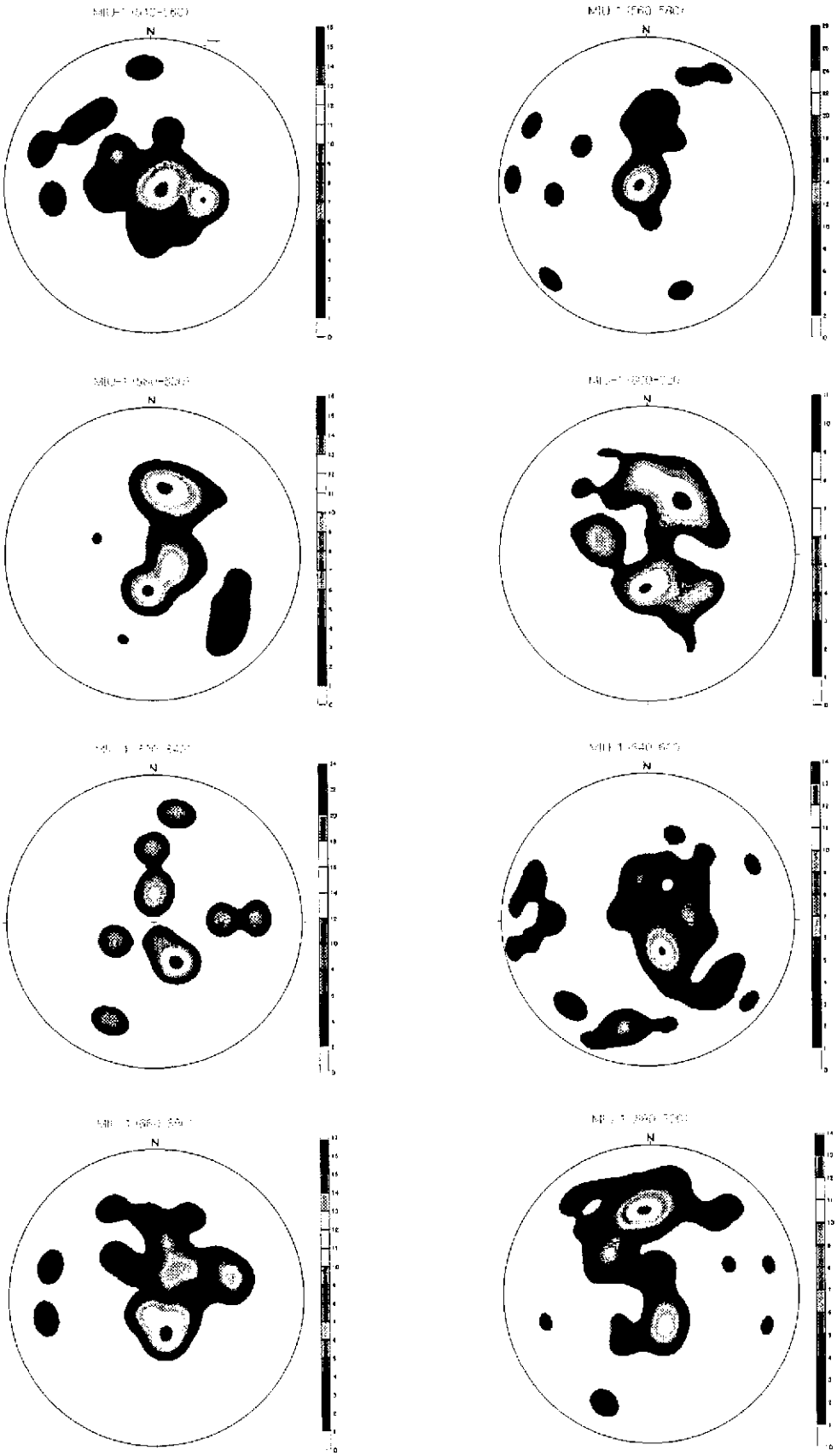

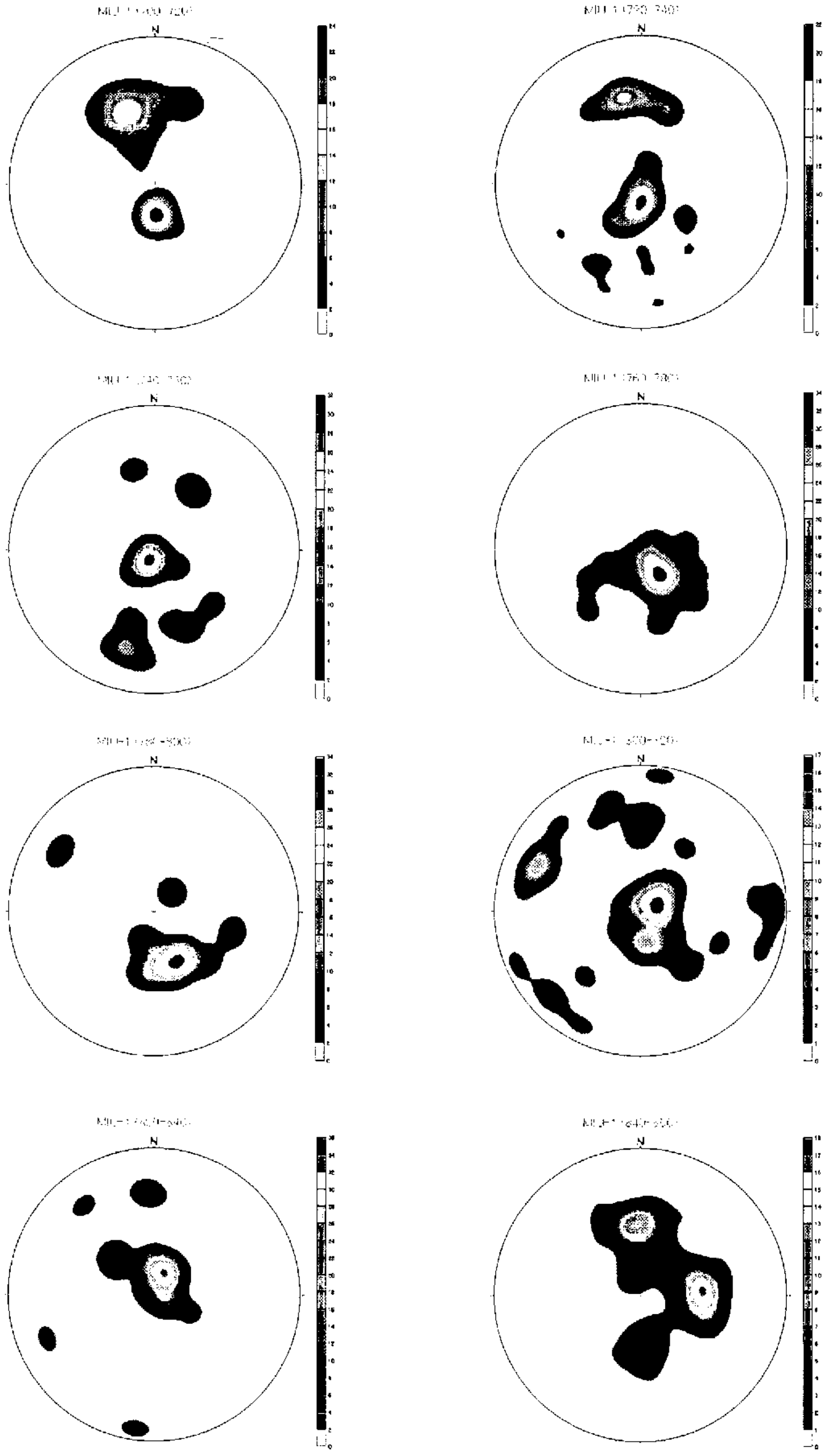

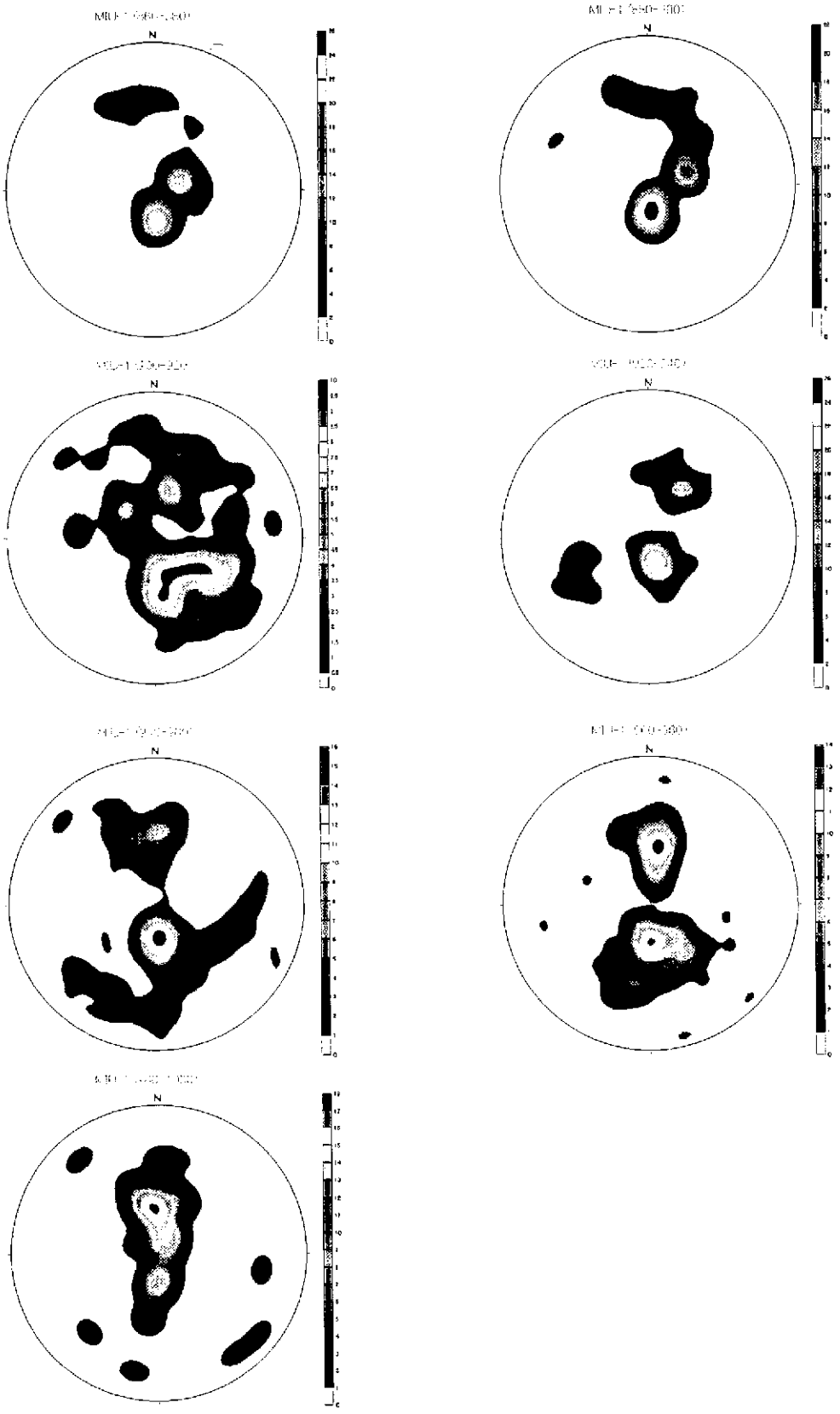

図 9.1.1　MIU-1 孔における割れ目分布（深度別）

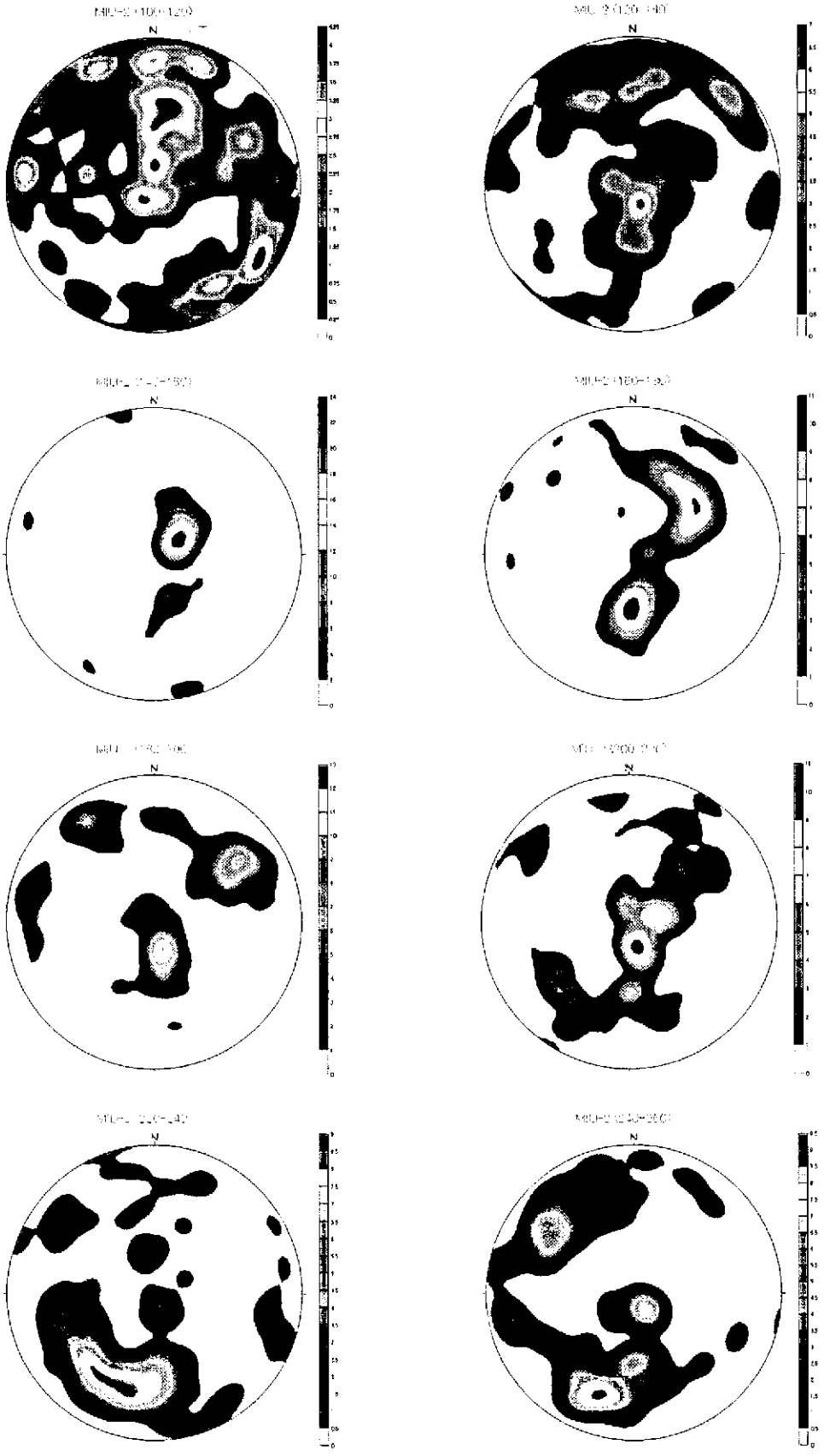
N
N
N
N
N
N
N
N

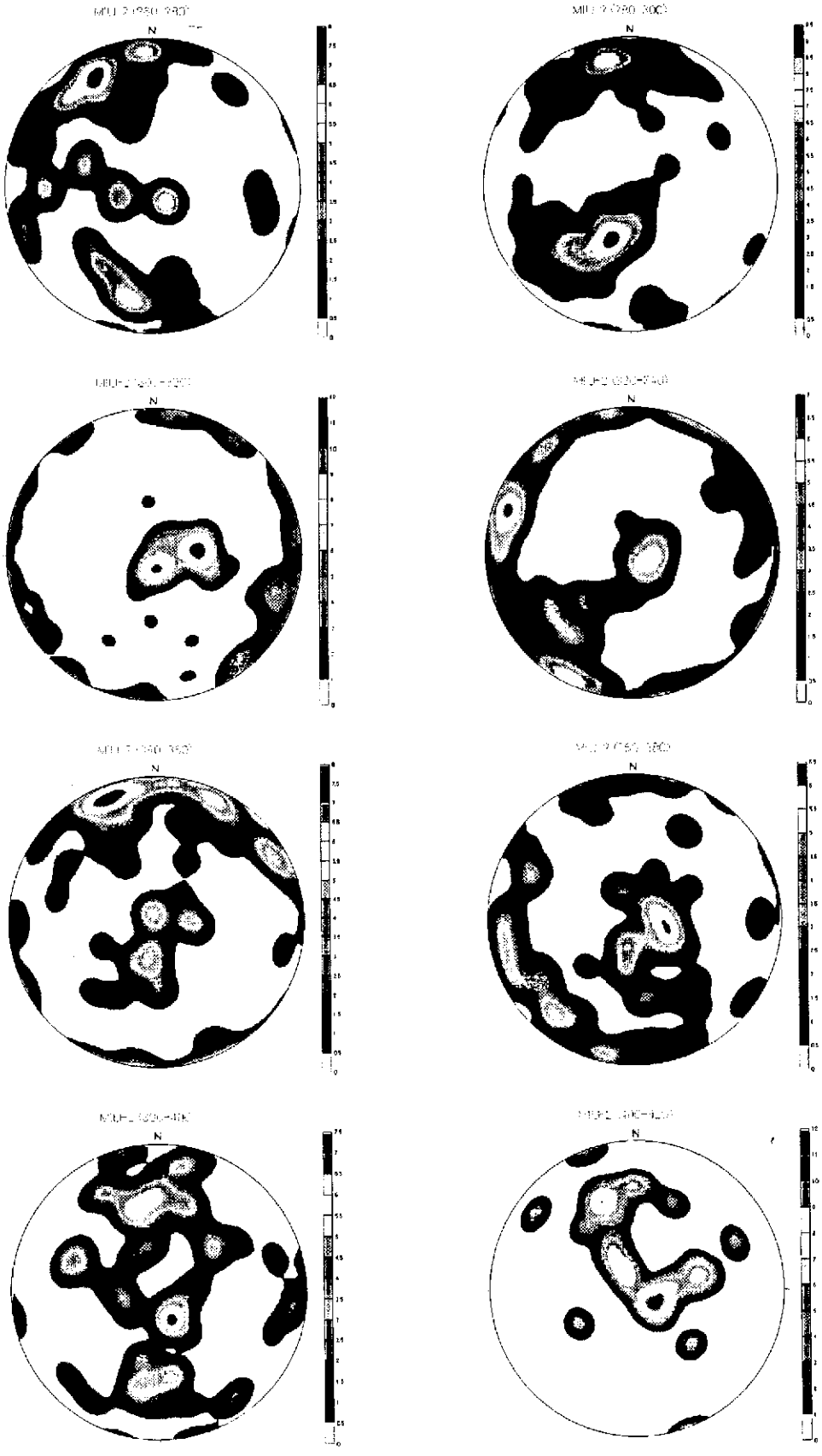
N
N
N
N
N
N
N
N

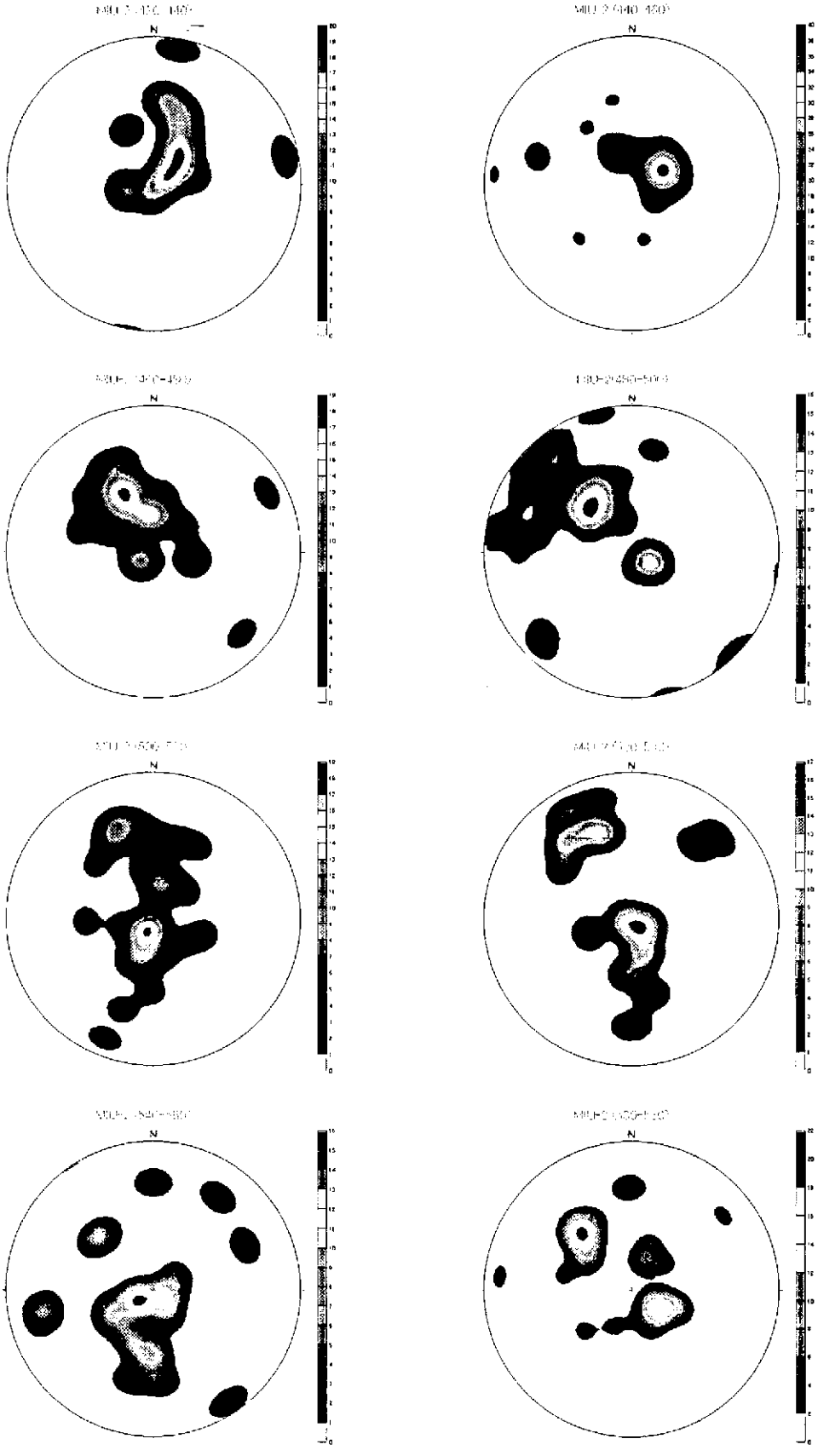

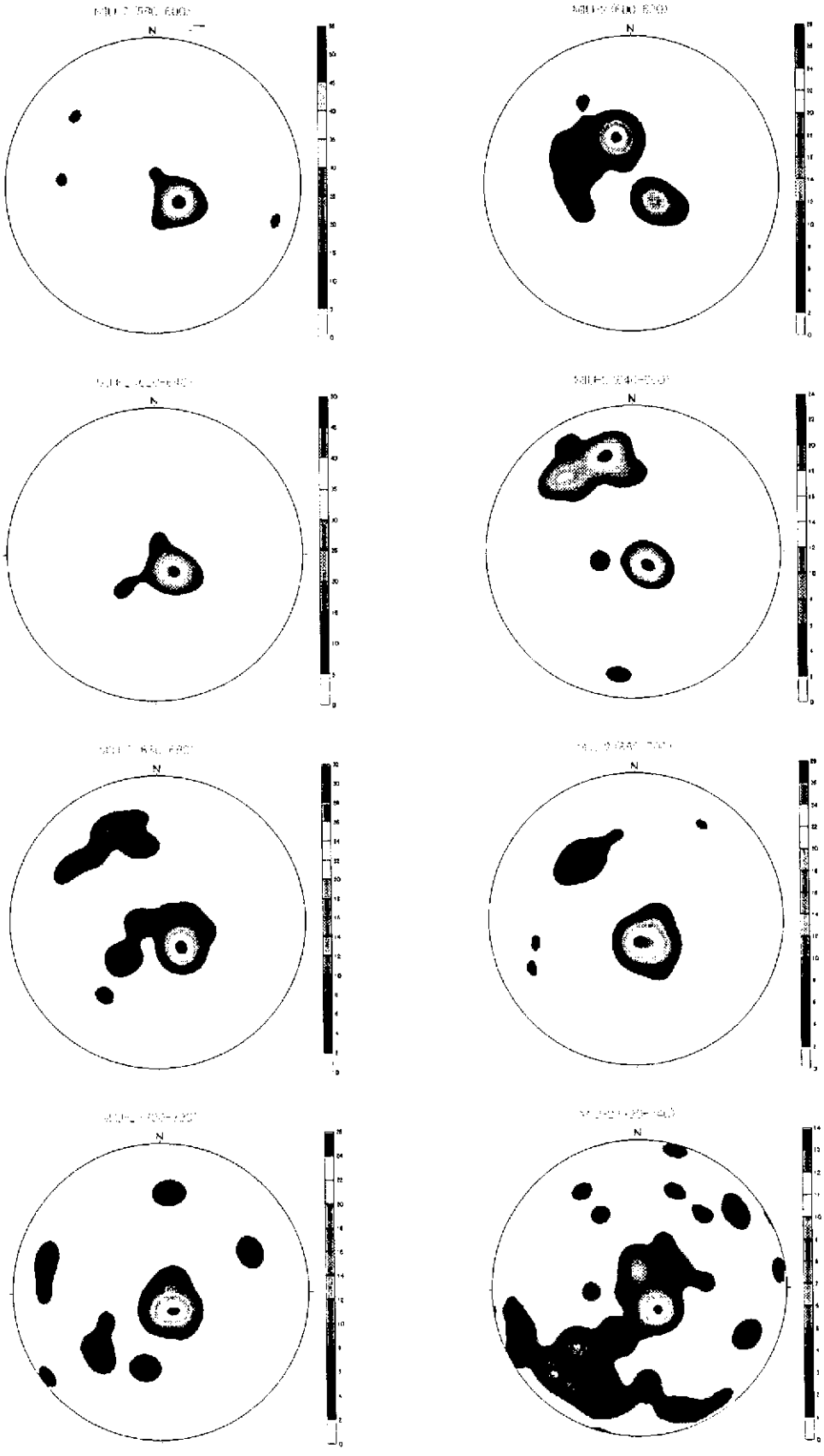

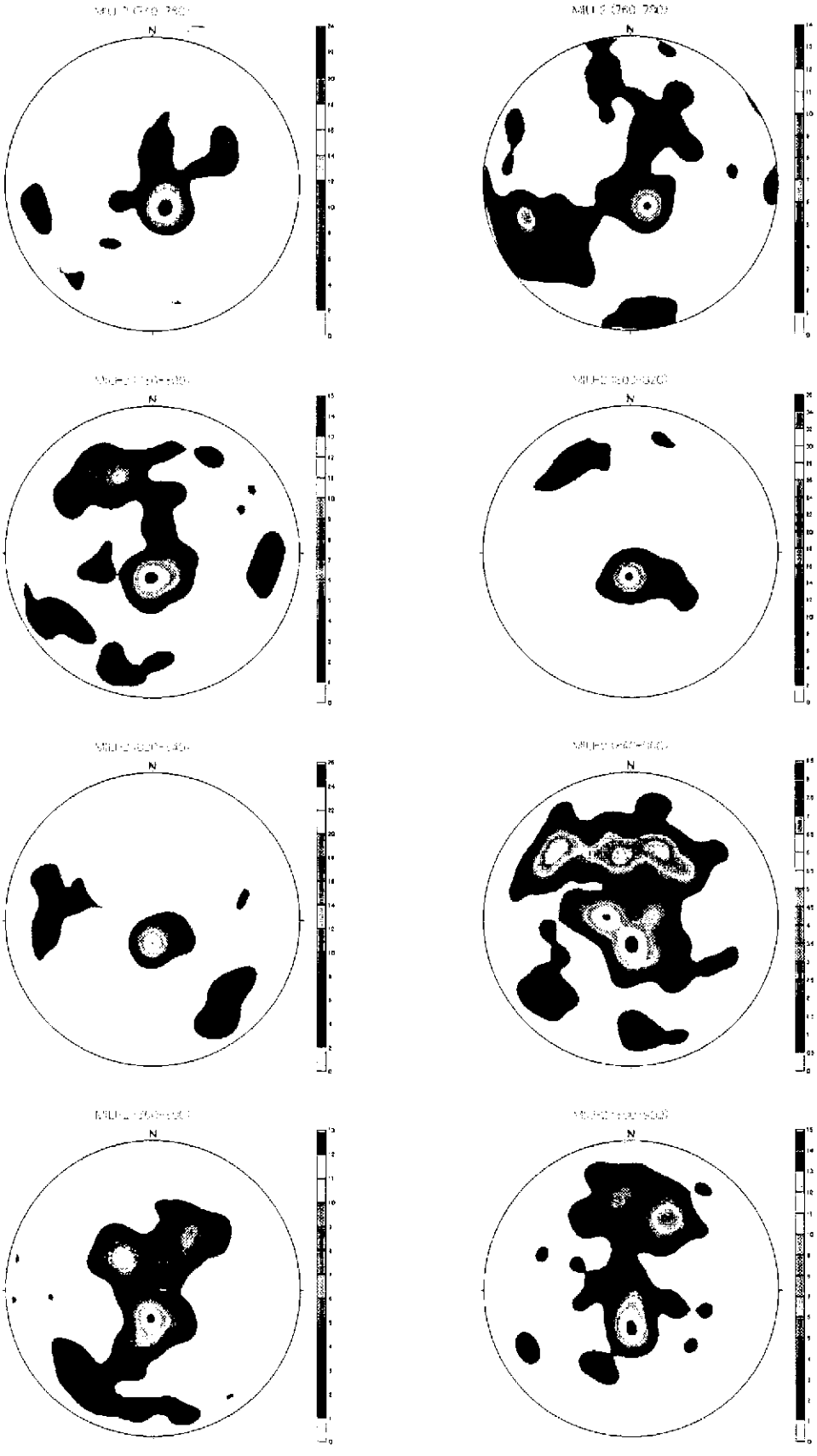

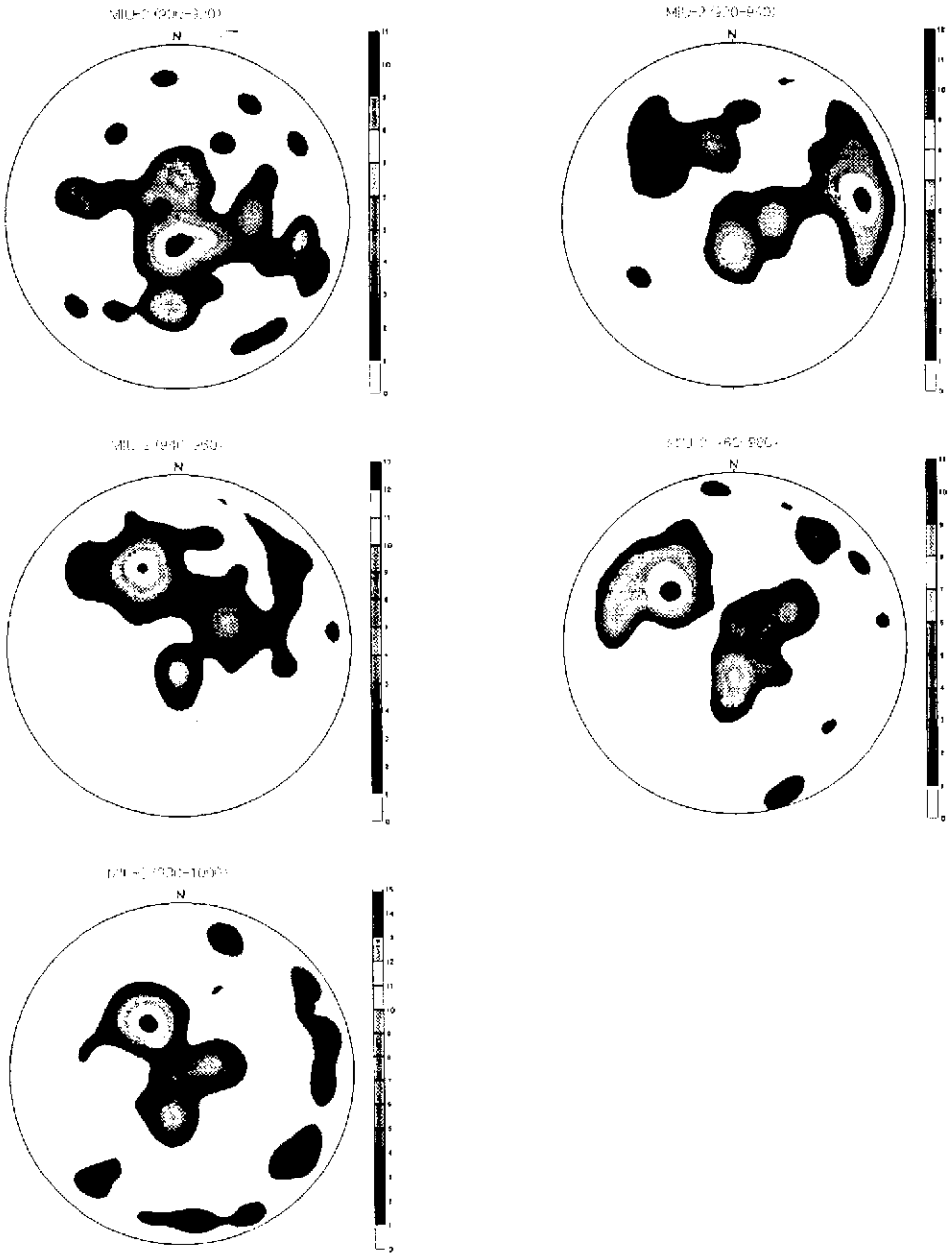

図 9.1.2　MIU-2 孔における割れ目分布（深度別）

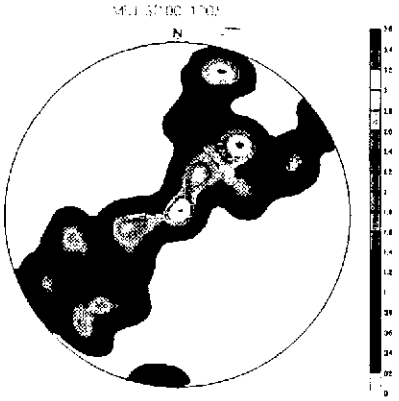
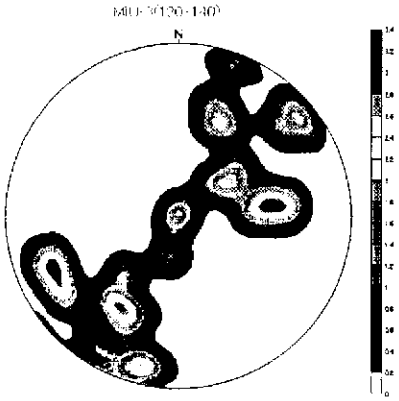
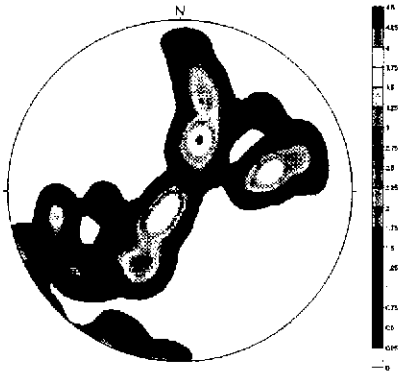
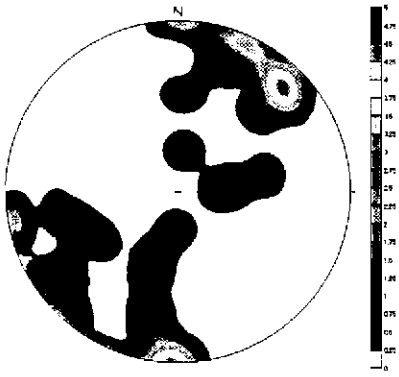
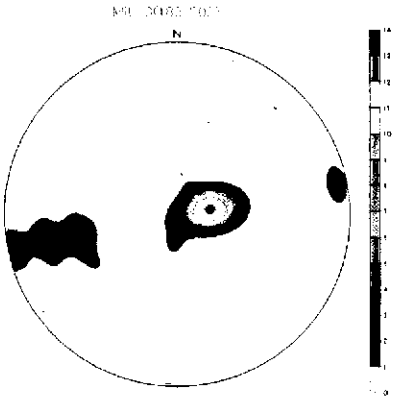
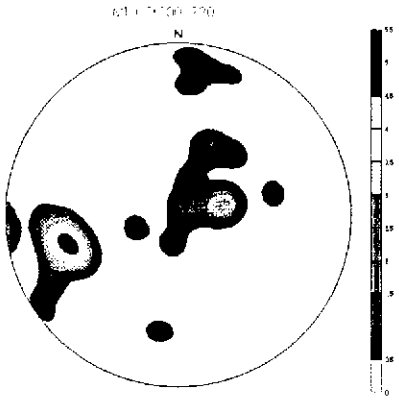
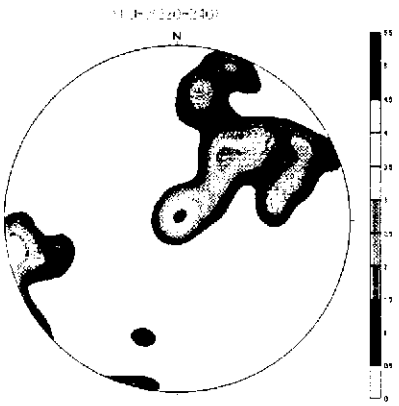
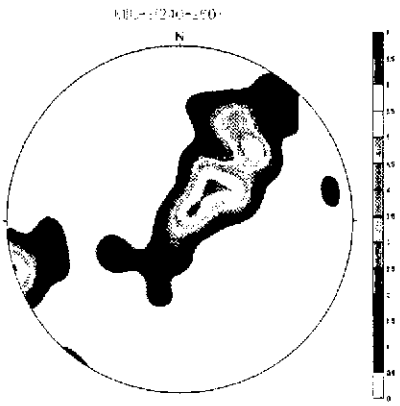

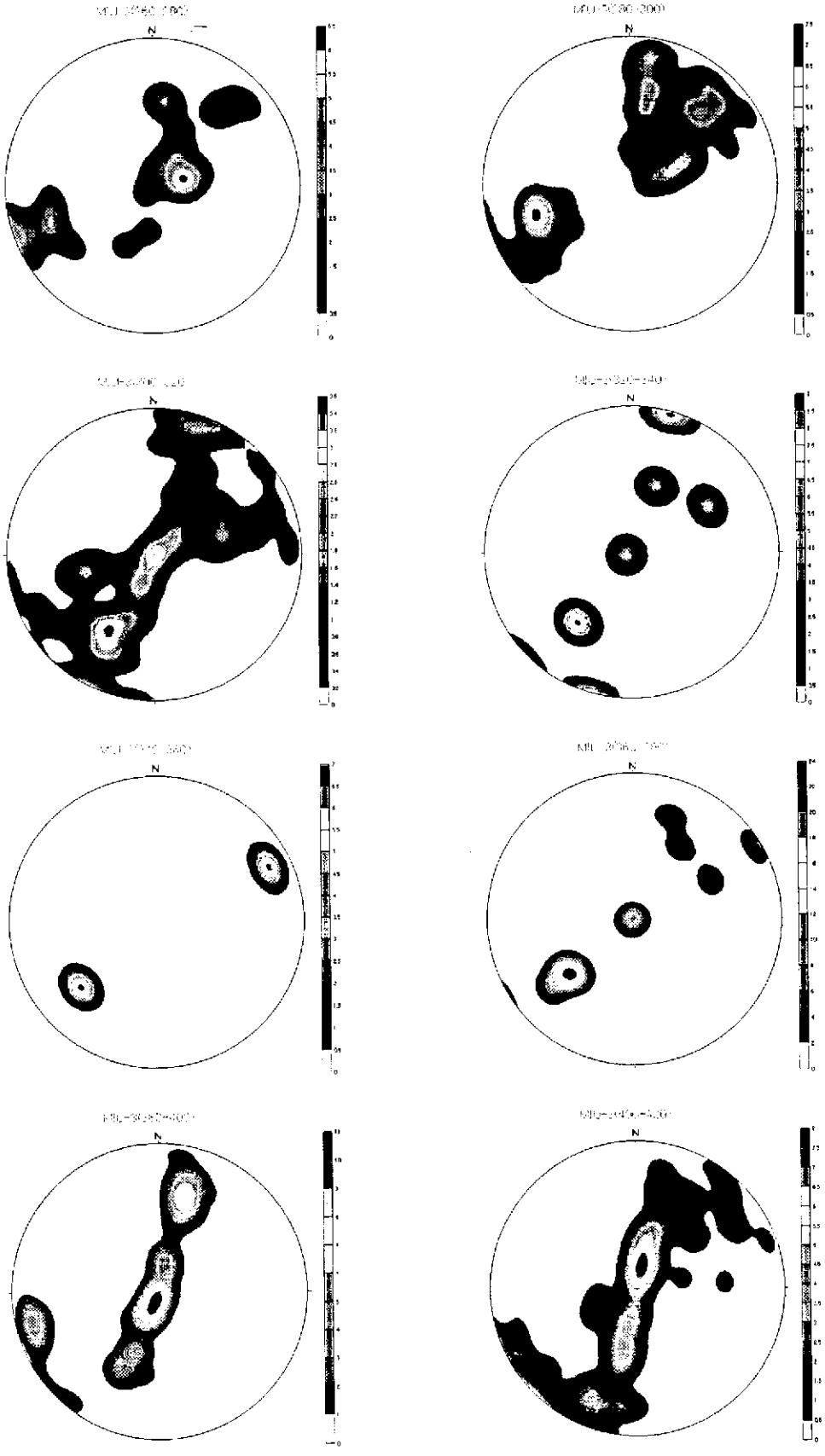

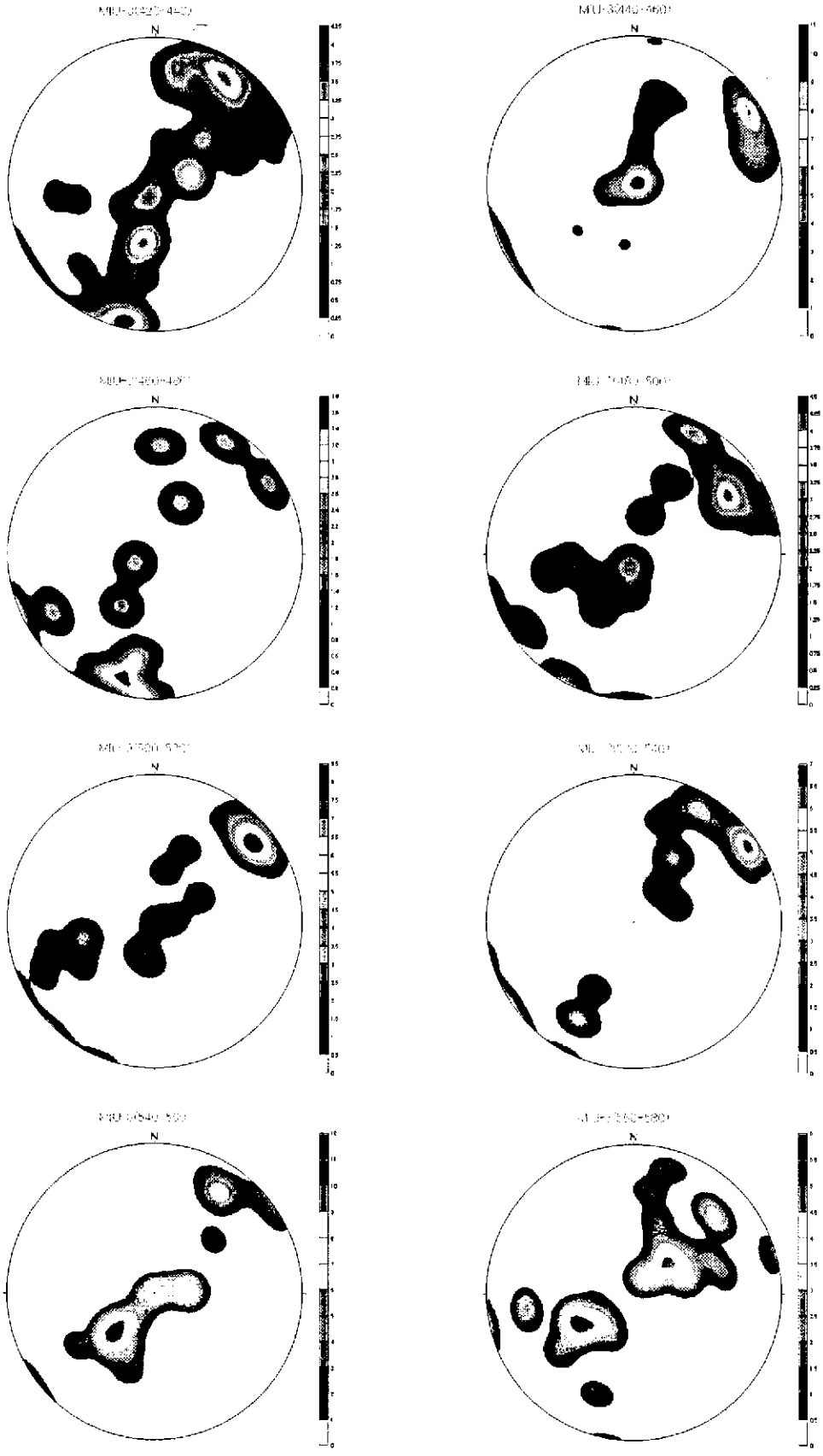

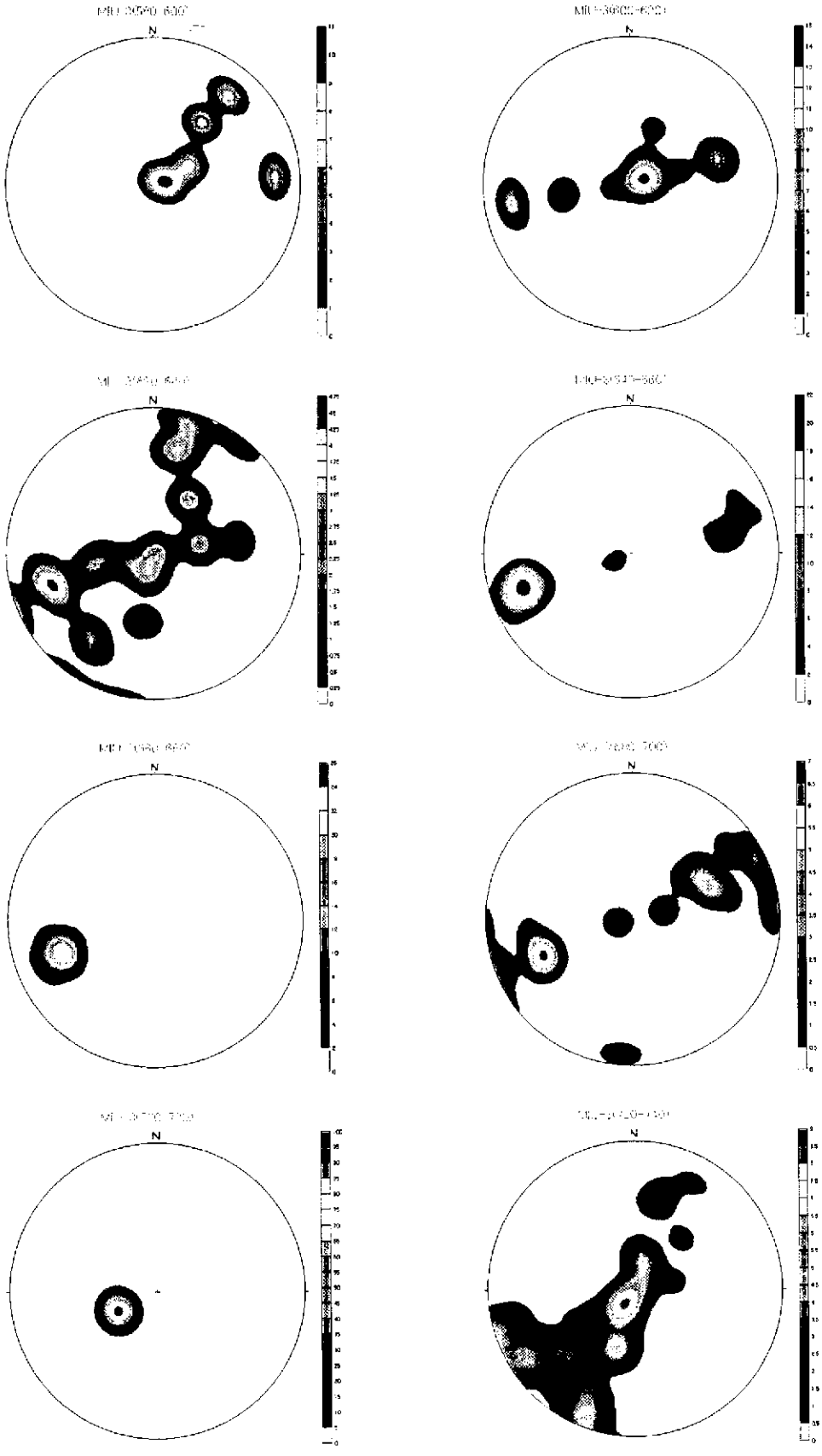

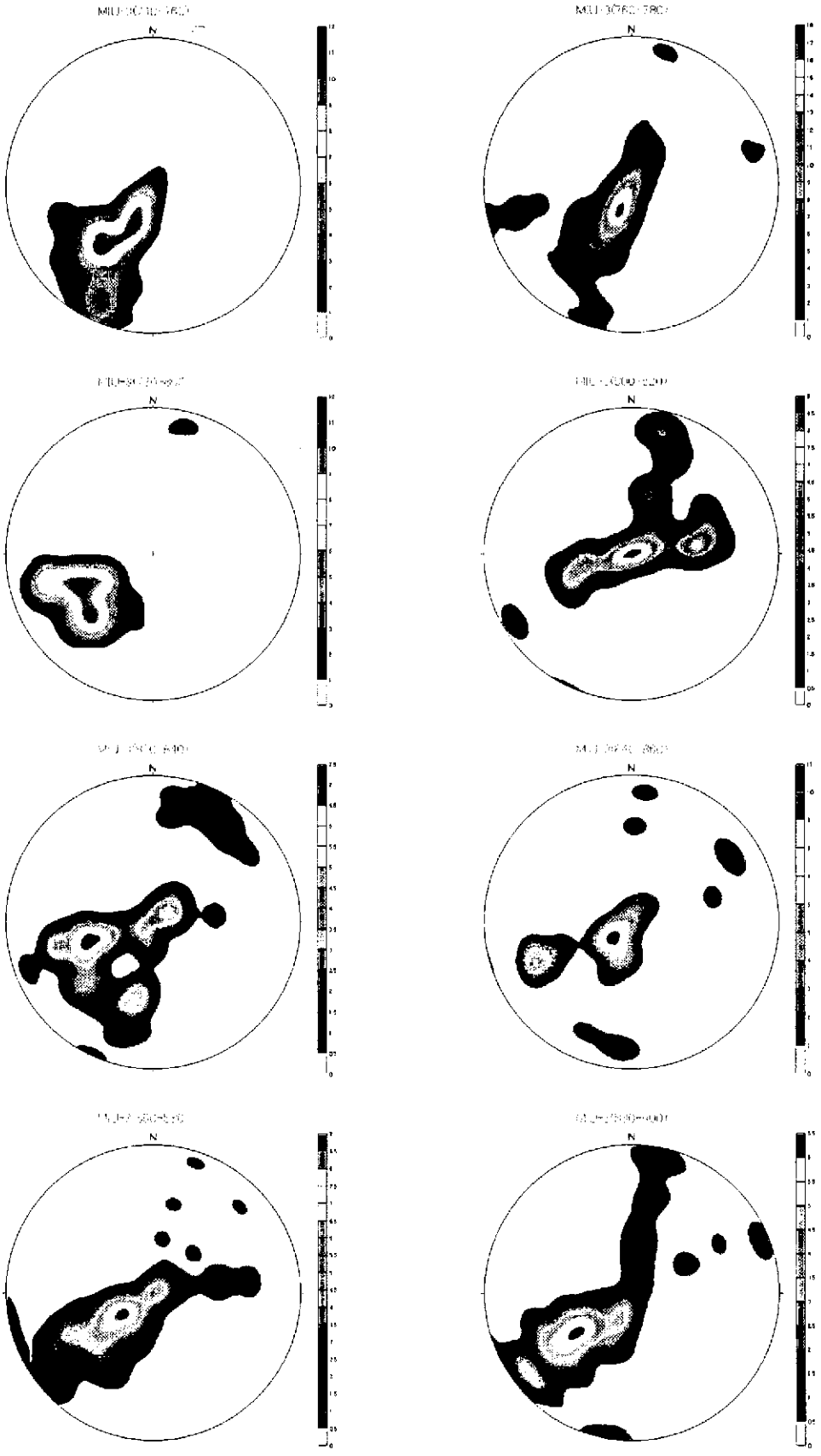

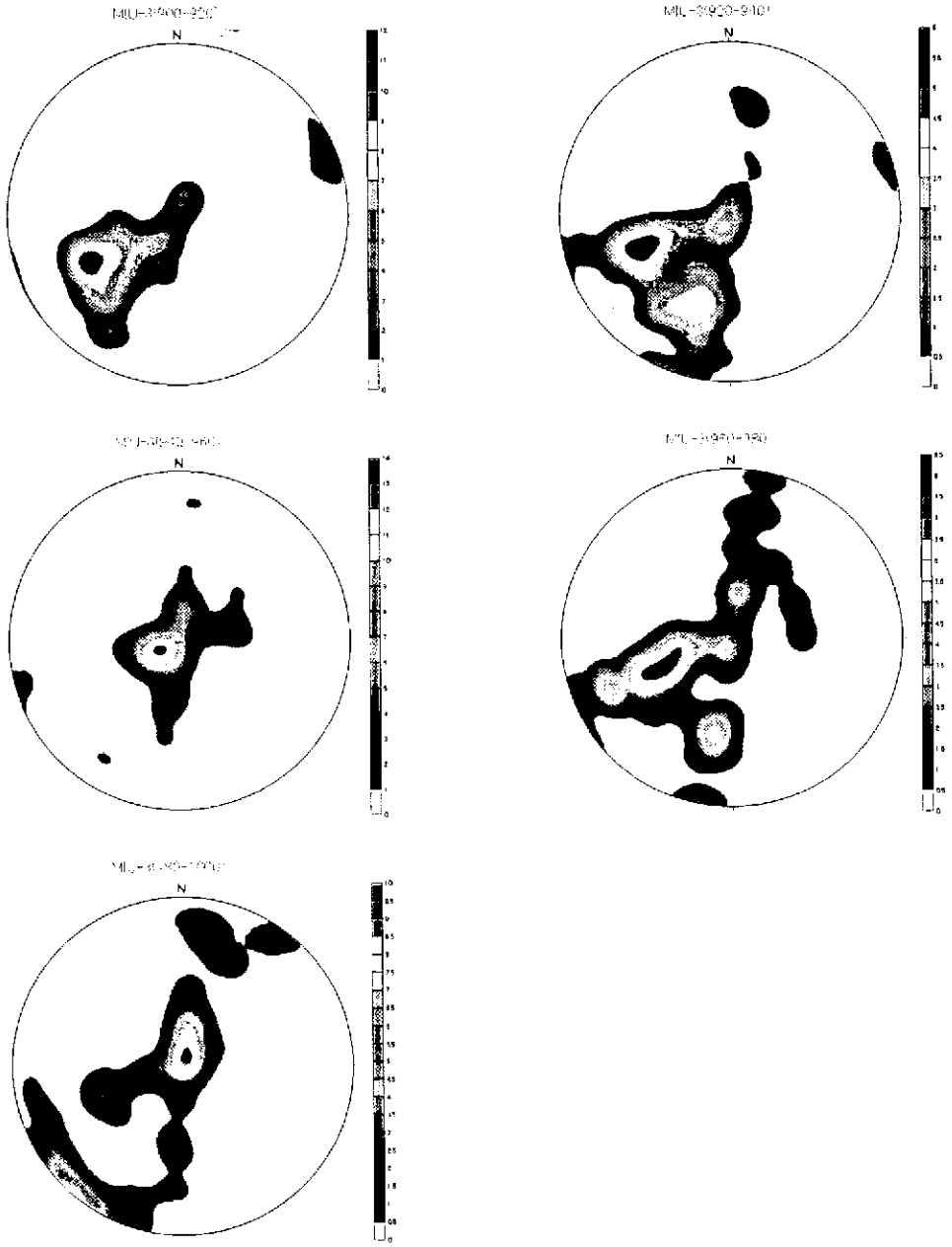

図 9.1.3　MIU-3 孔における割れ目分布（深度別）

以上の図をもとに，深度ごとに読み取れる情報をまとめると，以下のようである。

◆MIU-1 について

- 100m～180m に共通して見られる割れ目として NE 走向の高角度南傾斜の割れ目がある。
- 180m あたりから北傾斜の低角度割れ目が現われ、320m あたりから南傾斜へと変化していく。
- 360m～580m は割れ目の数が少ない。少ない中にも EW 走向の割れ目が目立つ。
- 580m～620m では EW 走向の南傾斜、北傾斜の 2 種類の割れ目が存在しているので、共役割れ目がある可能性が高い。また 700m～740m についても同じことが言える。
- 840m～980m では 2 つの割れ目集中点がありここでも共役割れ目があると考えられる。

◆MIU-2 について

- 160m～200m にかけて 2 つの集中点が見られる。
- 220m～380m では低角度割れ目が目立つ。
- 400m～720m にかけて割れ目の数が少ない。
- 560m～840m に NE 走向の高角度南傾斜の割れ目見られ深度の増加にともない EW 走向に変化していく。
- 840m～920m では EW 走向の北傾斜、南傾斜の割れ目が存在する。
- 920m～1000m にかけて NE 走向北傾斜の割れ目が共通している。

◆MIU-3 について

- 180m～280m にかけて EW 走向南傾斜の高角度と NE～NS 走向北西傾斜の低角度割れ目が共通している。300m 付近にも同じような集中が見られる。
- 320m～380m では割れ目の数が少なく方向もばらばらである。
- 380m～440m にかけて低角度の割れ目が目立ち、NW→NS→NE と走向が変わっていったと考えられる。
- 500m～560m にかけて 2 つの集中点が見られる。
- 600m～680m にかけて高角度南傾斜の割れ目が集中している。
- 720m～780m では NE 走向南傾斜の割れ目が共通している。
- 880m～920m の間で NE 走向の南傾斜、北傾斜の割れ目が共通する。

9.2 岩相による違い

岩相の違いによる割れ目の特徴を比較するために、MIU-1,2,3 孔の深度 100～1000mの区間を対象とし比較を行った。今回対象としている土岐花崗岩は大きく Biotite Granite、Felsic Granite の 2 岩相に分けられ、さらに Fine、Medium、Coarse と分けられている。

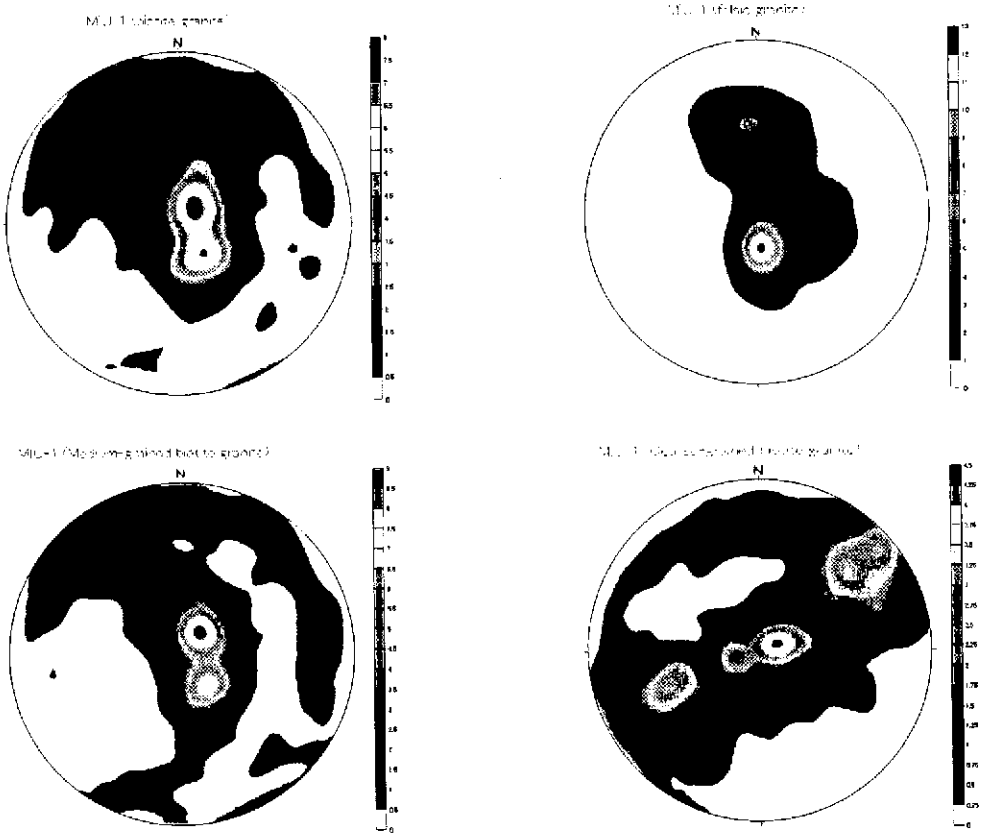

図 9.2.1　MIU-1 孔における割れ目分布　(岩相別)

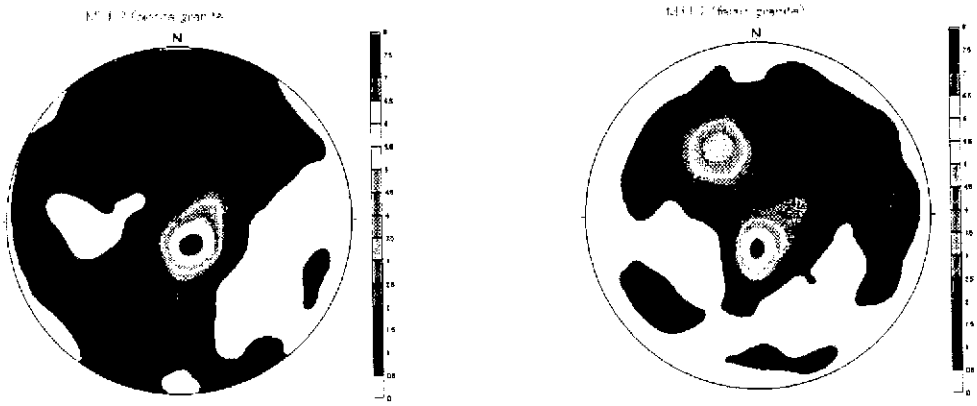

図 9.2.2　MIU-2 孔における割れ目分布　(岩相別)

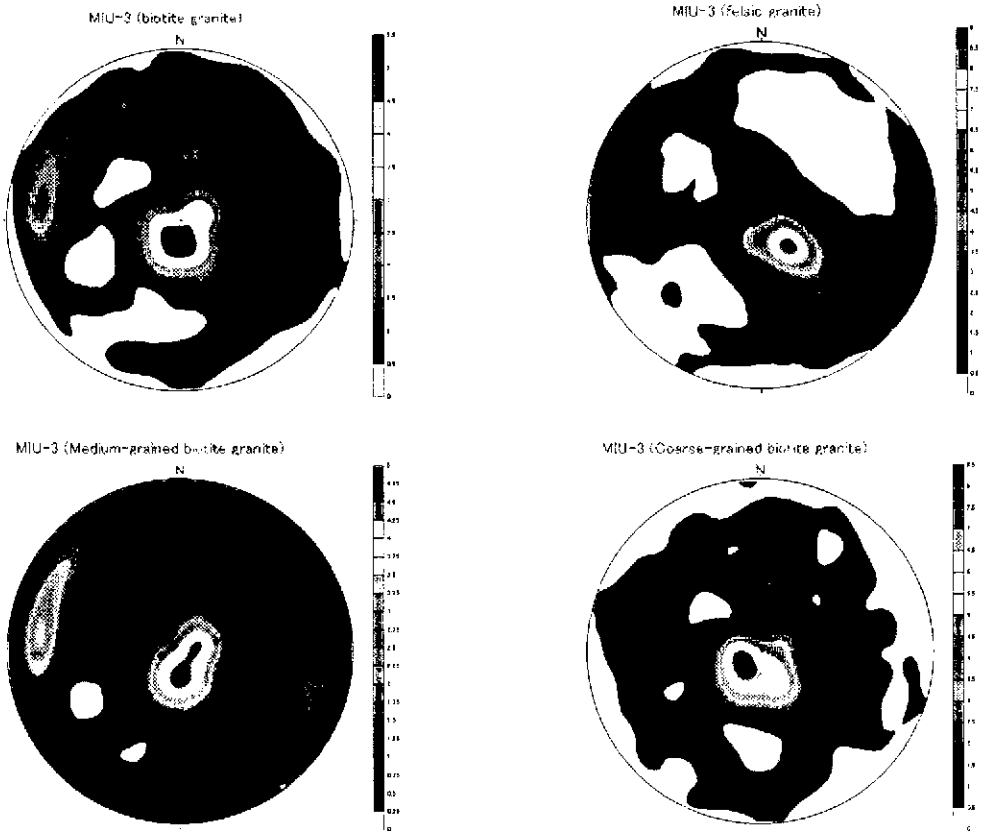

図 9.2.3　MIU-3 孔における割れ目分布　(岩相別)

表 9.2.1　岩相別割れ目密度（本／m）

	biotite granite	Medium-grained bi	Coarse-grained bi	felsic granite
MIU-1	2.638	3.246	2.097	3.506
MIU-2	3.181	4.294	1.602	10.408
MIU-3	3.925	4.531	2.985	7.921

以上の図表をもとに，岩層ごとに読み取れる情報をまとめると，以下のようである。

＜biotite Gr.＞

NE～EW 走向南傾斜の高角度割れ目が共通している。MIU-3 孔のみ NS～NE 走向北傾斜の低角度の割れ目の集中が見られる。

＜felsic Gr.＞

biotite Gr.と同様に NE～EW 走向南傾斜の高角度の割れ目が多い。MIU-1,2 孔に NE～EW 走向北傾斜の中角度の割れ目が見られる。biotite Gr.に比べ割れ目が発達している。

＜Medium grained biotite Gr.＞

前述の biotite Gr.全体の傾向とほぼ一致する。Coarse grained biotite Gr.に比べ割れ目が発達している。

＜Coarse grained biotite Gr.＞

MIU-1 では NW 走向の低角度割れ目の集中が見られるのに対し MIU-2,3 では見られない。NE 走向南傾斜の高角度割れ目が見られる点に関しては、全体の傾向と一致する。

9.3 構造的特徴を持った割れ目の分布

どのような構造を持った割れ目が水みちを形成するか考えた時、水は岩盤内の空隙を流れ、空隙が大きいほど流れやすいと考えられる。そのため水みちとなる部分では割れ目が開いていることが必要となる。つまり現在の応力場において、(1)引っ張り条件となる割れ目が集中する部分もしくは、(2)局所的に大きく開口した部分が水みちとなるはずである。前者については、単に、いろいろな方向の割れ目が集中しているところとも言える。それは、様々な方向の割れ目が集中している場合、そのうちのいくつかの割れ目には引張力が作用していると考えられるからである。しかし、古い時代に形成し、現在まで再動していない割れ目は、様々な充填鉱物により埋められ、現在では主要な透水経路とはなり得ない。このような原則を踏まえ、水みちとなる構造として図 9.3.1 に示すものをあげることができる。これらの割れ目に共通して言えることは、多少なりとも最近活動したということである。そこで図 9.3.1 に示したような構造の割れ目がBTVで見た場合、図 9.3.2 のように見えると予想し、図 9.3.3 のようなかたちで取り出し、その方向や割れ目密度が水みちと関係が無いか検討を行った。

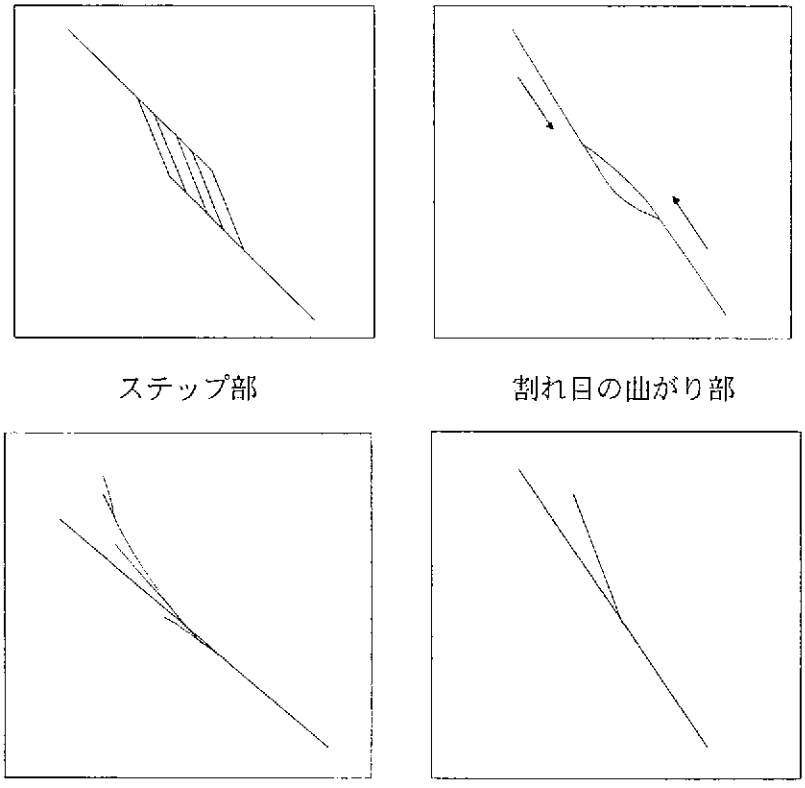

図 9.3.1　水みちを形成する可能性がある地質構造

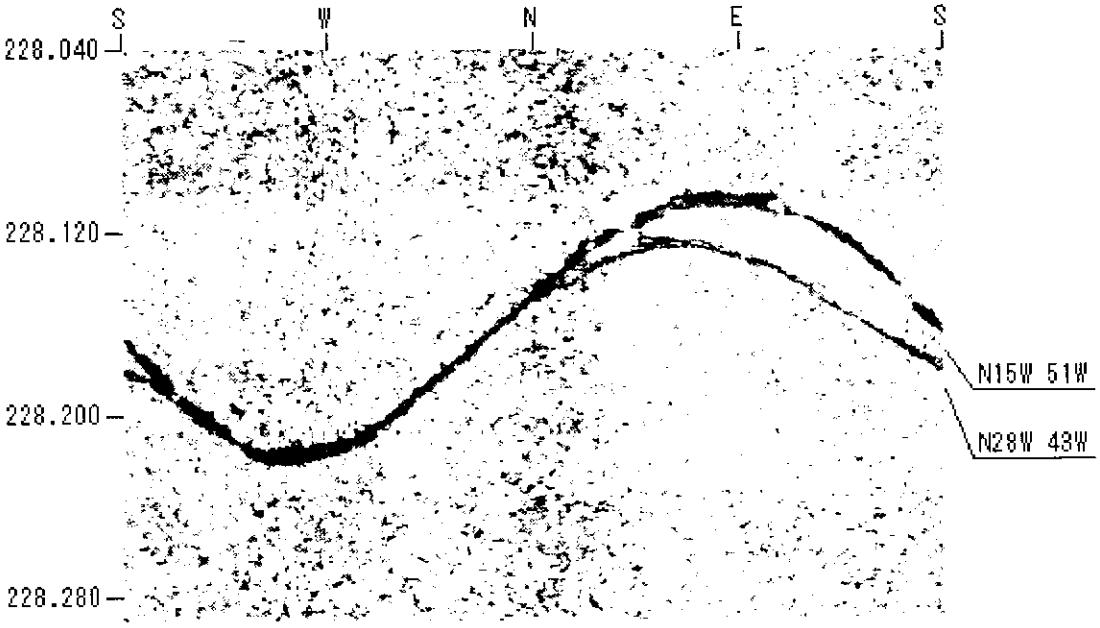

図 9.3.2　BTV 展開図

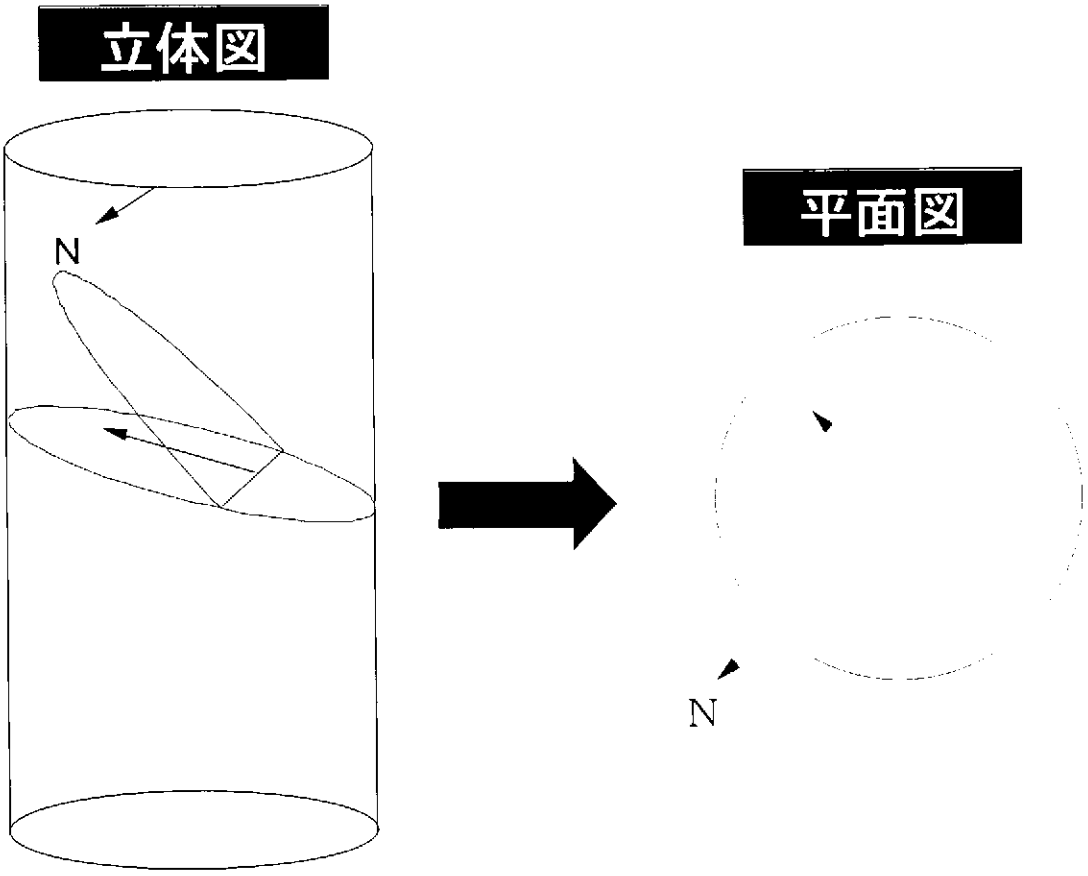

図 9.3.3　割れ目の方向の取り出し方　(模式図)

BTV による割れ目観察によって前述したような構造と予想される割れ目を取り出した。その割れ目の交線の法線方向（図 9.3.3 参照）を 10°ごとの区間に分け、さらに岩層ごとにわけたものを図 9.3.4、図 9.3.5、図 9.3.6 に示す。単位はパーセントである。

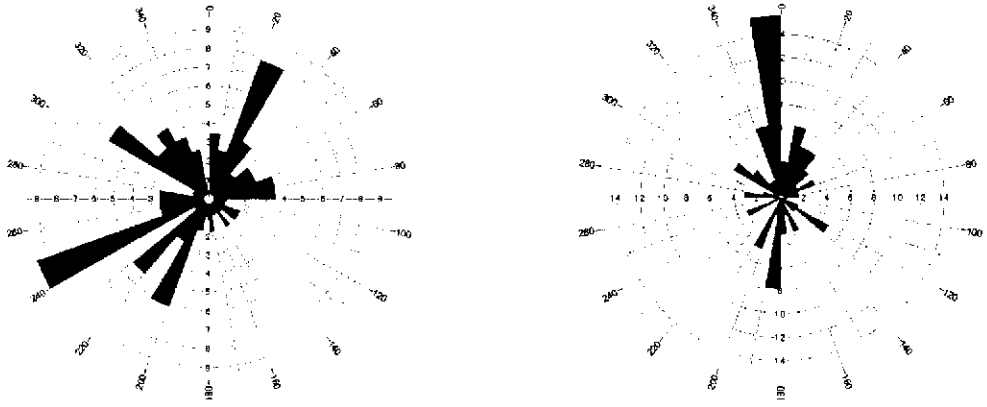

図 9.3.4　取り出した割れ目の方向　MIU-1（左 biotite Gr. 右 felsic Gr.）

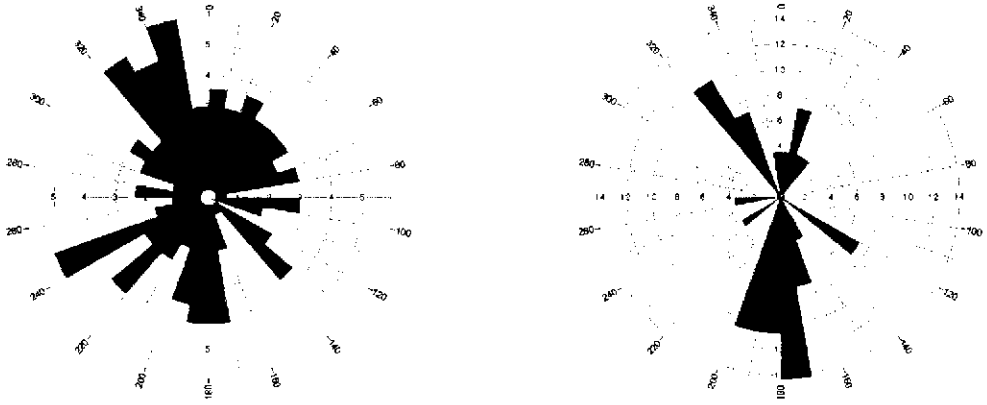

図 9.3.5　取り出した割れ目の方向　MIU-2（左 biotite Gr. 右 felsic Gr.）

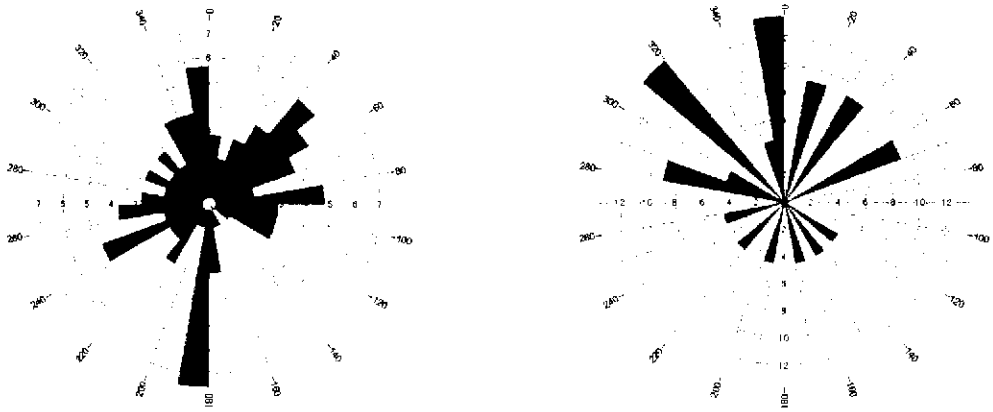

図 9.3.6　取り出した割れ目の方向　MIU-3（左 biotite Gr. 右 felsic Gr.）

表 9.3.1　本研究で取り上げた割れ目の割れ目密度（本／m）

	biotite granite	Medium-grained bi	Coarse-grained bi	
MIU-1	0.2	0.207	0.172	0.198
MIU-2	0.229	0.265	0.178	0.233
MIU-3	0.158	0.195	0.099	0.123

＜biotite Gr.＞

MIU-1 の 20° 200° 240° 方向への集中は、NW 走向北傾斜の割れ目から派生したと考えられる。また 300° 方向への派生は NE 走向の割れ目からの派生と考えられる。

MIU-2 の 180° 330° 方向への集中は、NE～EW 走向南傾斜の割れ目から派生したと考えられる。また図 9.3.5 からは NW 走向の割れ目の集中は確認できないが 240° 方向への集中が見られることから、NW 走向の割れ目が発達している可能性があると考えられる。

MIU-3 の 350° 180° 方向への集中は、EW 走向南傾斜の高角度割れ目から派生したと考えられる。また MIU-2 同様に図 9.3.6 からは NW 走向の割れ目の集中は確認できないが 40° 付近の方向への集中が見られることから、NW 走向の割れ目が発達している可能性があると考えられる。

＜felsic Gr.＞

MIU-1 の 350° 方向への集中は、EW 走向の割れ目から派生したと考えられる。

MIU-2 の 180° 付近への集中は、EW 走向南傾斜の高角度割れ目から派生したと考えられる。また 320° 方向への集中は、NE 走向北傾斜の割れ目から派生したと考えられる。

MIU-3 の 310° 350° 方向への集中は NE～EW 走向の割れ目から派生したと考えられる。

felsic Gr.は biotite Gr.に比べ割れ目密度が大きいが、本研究で取り上げた割れ目の密度を比較すると大きな差は見られない。従ってこの結果のみによって考えると、2 つの岩相を比べたとき岩相の違いにより水みちの発達の度合いが異なるとは言い難い。

次に本研究で取り上げた割れ目の深度と、実際に逸水が確認された深度の比較を行った。結果を図 9.3.7 に示す。矢印で示された箇所が逸水の確認された位置で、パーセント表示してあるものは大量逸水が確認された箇所である。大量逸水箇所付近の上下 10m 程度の範囲に割れ目が多くなっているのが確認できると思う。また他の逸水箇所でもいくつかそのような箇所が見られる。このことから BTV 観察により本研究で取り上げた割れ目と、水みちとなる割れ目との間に関係がある可能性が考えられる。

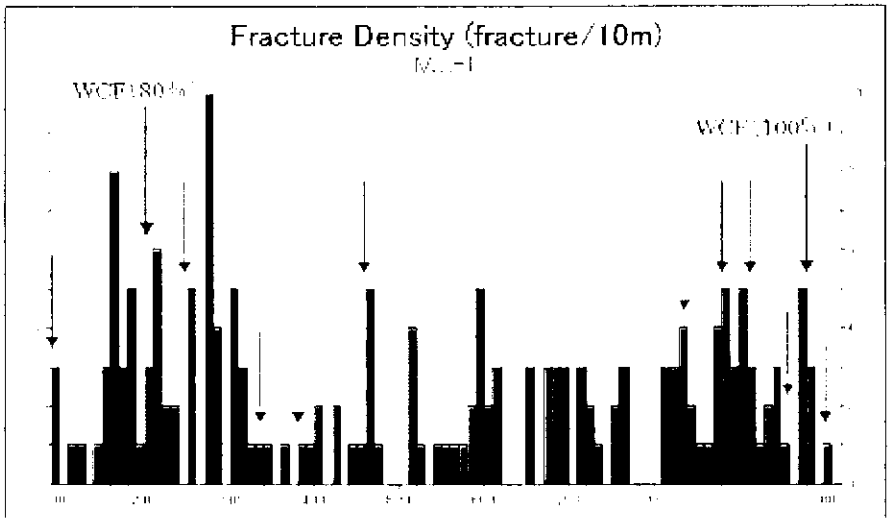

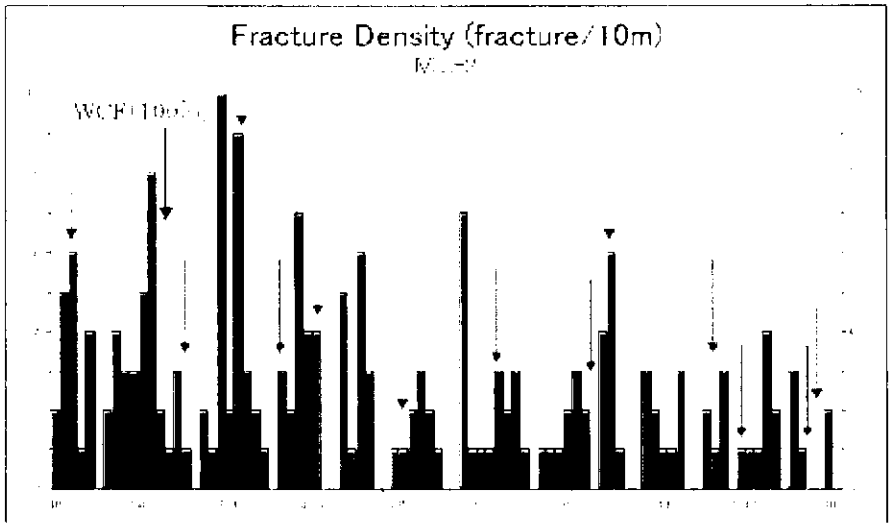

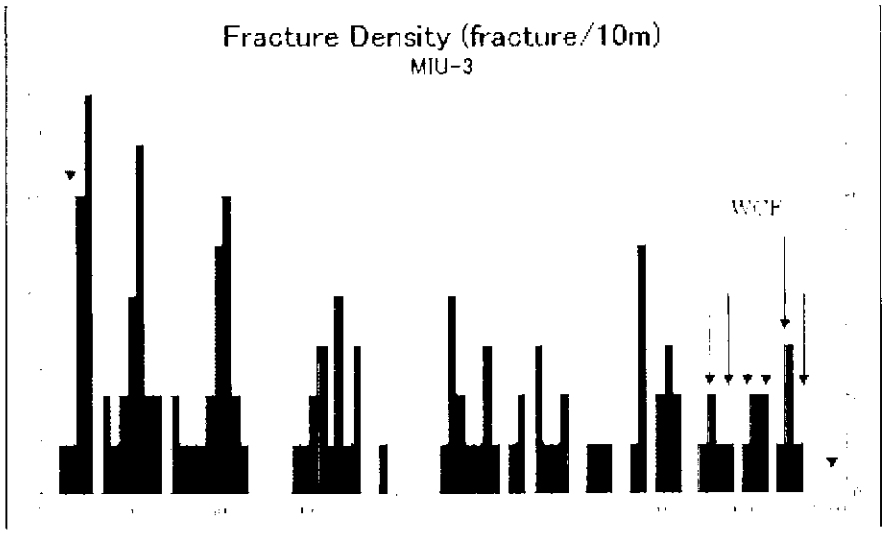

図 9.3.7　本研究で取り出した割れ目の割れ目密度と逸水割れ目の関係

第10章 エコーチップ反発硬度試験

10.1 試験目的

近年、エコーチップ反発硬度試験の岩石材料への適用性に関する研究が発表されている。そこで本試験機を用い、ボーリングコアに対して試験を行い、断層破砕帯付近および逸水割れ目付近で硬度の違いがあるかどうか検討を行った。

10.2 試験機

エコーチップ硬さ試験機　(株)富士物産

測定原理は、ばねの力でインパクトボディーを供試体に打ち付け、そのときの打撃速度に対する反発速度の比を計測するものである。硬さの指標値“L”として表示され、この“L”は反発速度を打撃速度で割った商を1000倍した値である。

また、この試験機は従来から提案されているシュミットハンマーやショアー硬度試験機に比べ、以下の利点を有している。

- 打撃エネルギーが11Nmmと小さく岩石供試体の非破壊試験として適用できる。
- データがデジタル値で自動収録されるため多量のデータを短時間で計測できる。
- 測定方法が簡単で個人差が少ない。
- 装置が小型軽量で携帯性に優れている。

10.3 供試体

核燃料サイクル開発機構、東濃地科学センター所有、ボーリングコア MIU-1(Intact, WCF)　MIU-2(Fault Zone, WCF)　MIU-3,4(Fault Zone)

10.4 試験方法

- コア箱に入った状態のコアの側面を計測
- 打撃方向がコアの中心を通るように試験機をしっかりと固定
- 測定点近傍で連続打撃を避け数回の測定を行い、最大値を記録
- 表面の凸凹の著しい箇所は避ける

10.5 結果

10.5.1 健岩部（Intact Rock）

まず始めに健全なコアの測定を行った。ここで言う健全なコアとは、1mごとに切断されてコア箱に入っているコアが、割れ目が無くつながっているもので、変質等も確認されないものである。Biotite Gr.は深度500m付近において、Felsic Gr.は深度750m付近において、それぞれ3本ずつ計6本の測定を2.5cm間隔で行った。図10.5.1と表10.5.1に結果を示す。Biotite Gr.とFelsic Gr.でL値を比較すると、Felsic Gr.の方が大きな値になった。またBiotite Gr.の方がL値のばらつきが大きくなった。図10.5.2からもわかるようにBiotite Gr.は表面の鉱物の分布がばらついているために、測定の際に叩いた鉱物の違いが、L値に反映したものと考えられる。健岩部での結果から〔健岩部でのL値の下限値＝平均値－標準偏差〕と考えて、健岩部の各岩相における下限値をBiotite Gr.でL＝803、Felsic　Gr.でL＝860と考えた。

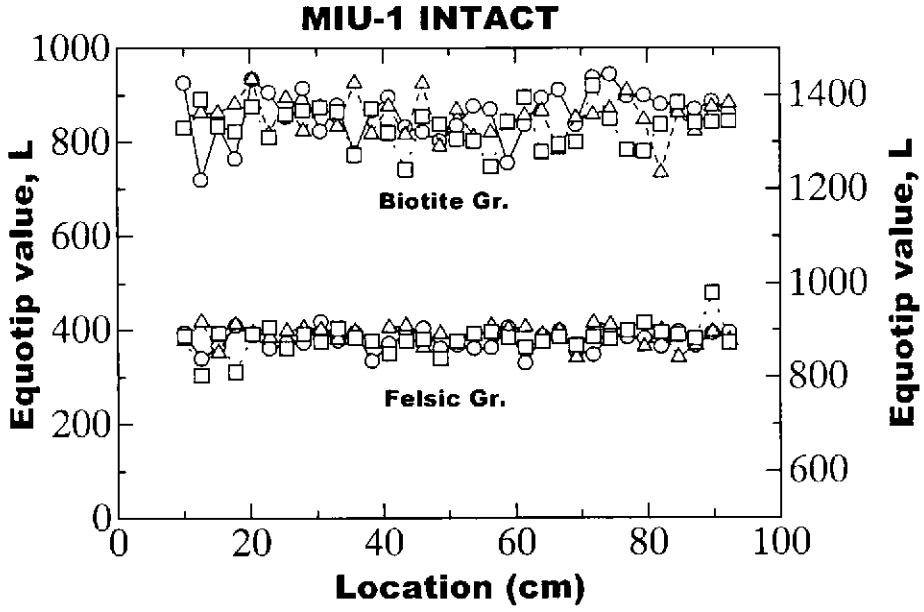

図10.5.1　健岩部でのL値分布

表 10.5.1　健岩部での L 値

MIU-1 Intact (L Values)

Biotite

depth(m)	490-491	496-497	503-504
average	863	855	835
std	54	43	43
Max	946	936	922
Min	721	737	744

TOTAL	Biotite
average	851
std	48

Felsic

depth(m)	744-745	745-746	747-748
average	883	892	879
std	30	21	22
Max	983	921	920
Min	806	843	832

TOTAL	Felsic
average	885
std	25

(std=標準偏差)

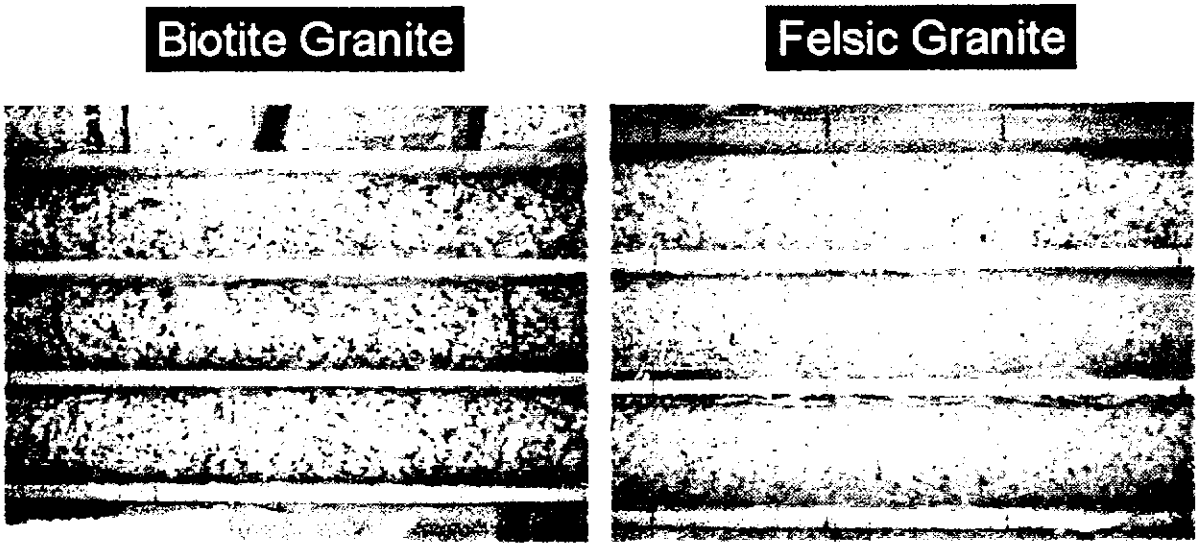

図 10.5.2　Biotite Granite と Felsic Granite

10.5.2 断層破砕帯（Fault Zone）

次に断層破砕帯付近での測定を行った。断層破砕帯ではコアの損傷が著しく、健岩部のように一定の間隔で測定することはできなかった。測定の対象としたコアは、(1)測定点からコアの端面方向にそれぞれ 2.5cm 以上の長さがあり、(2)コア側面が測定点から周方向に全て残っているものを条件とした。

MIU-2

MIU-2 での測定結果を図 10.5.3 に示す。断層破砕帯に近づくにつれて L 値が減少していった。断層破砕帯で L 値の平均が 498 になったのに対し、断層破砕帯を境に上盤側で 726、下盤側で 803 となった。これはやはり破砕帯において岩盤の硬度が低下しているものと考えられる。赤の実線で示している範囲が公表されている断層破砕帯の区間で、破線で示したものが本研究で行った測定によるものである。破砕帯の影響がもう少し広範囲にわたっているのではないかと考えられる。見た目では健全に見えるコアも実際に測定を行ってみると、断層破砕帯の近くで硬度の低下が見られた。断層の上盤側に比べ下盤側の方が、L 値のばらつきが小さく、健全なコアでの L 値に戻るのが早い。

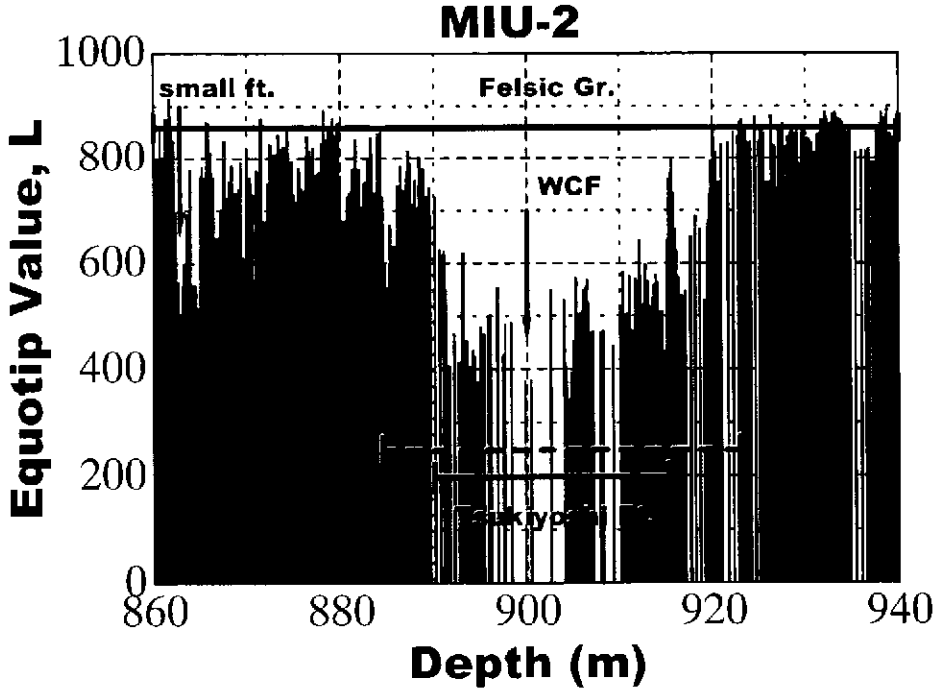

図 10.5.3　MIU-2 での L 値分布　（n=434）

MIU-3

MIU-3での測定結果を図10.5.4に示す。MIU-3においてもMIU-2同様、断層破砕帯でL値の低下が見られた。断層破砕帯でL値の平均が592になったのに対し、上盤側で769、下盤側で773となった。上盤側と下盤側のL値のばらつきを比べるとMIU-2同様、下盤側で健全なコアでのL値に戻るのが早いように思われる。

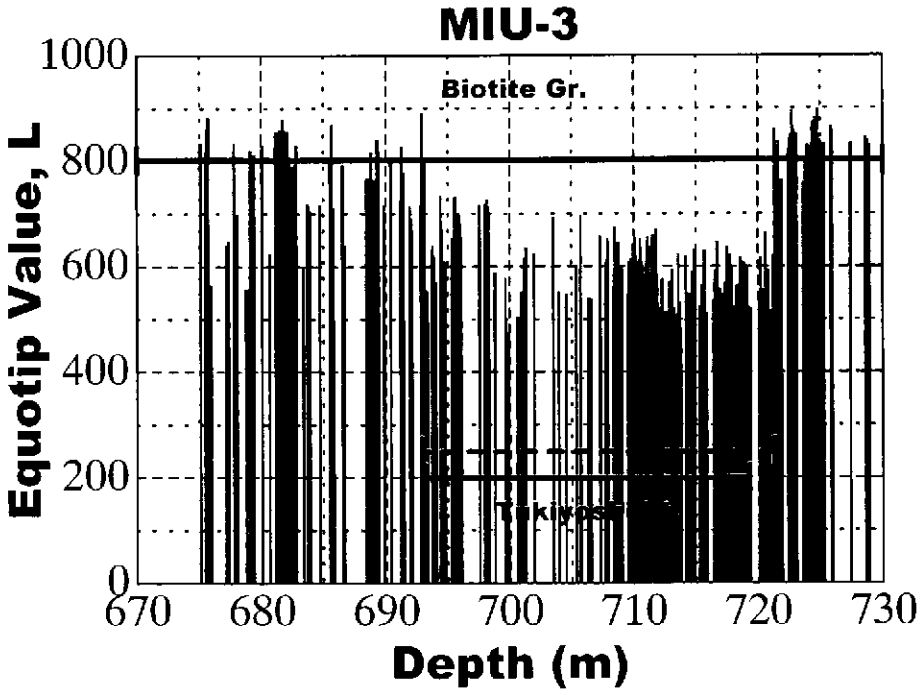

図10.5.4　MIU-3でのL値分布　（n=217）

MIU-4

MIU-4 での測定結果を図 10.5.5 に示す。MIU-4 のボーリングは最近終了したばかりで断層破砕帯区間の決定はなされていない。断層の上盤側が Felsic Gr.で下盤側が Biotite Gr.となっており、上盤側の方が下盤側に比べ L 値が高く、MIU-1 での測定結果と一致する。上盤側と下盤側との L 値のばらつきを比較すると MIU-2、MIU-3 とは違い下盤側でのばらつきが大きくなった。MIU-2、MIU-3 に比べ L 値のばらつきが全体的に大きく見えるのは測定が不慣れだった影響が出たものと考えられる。

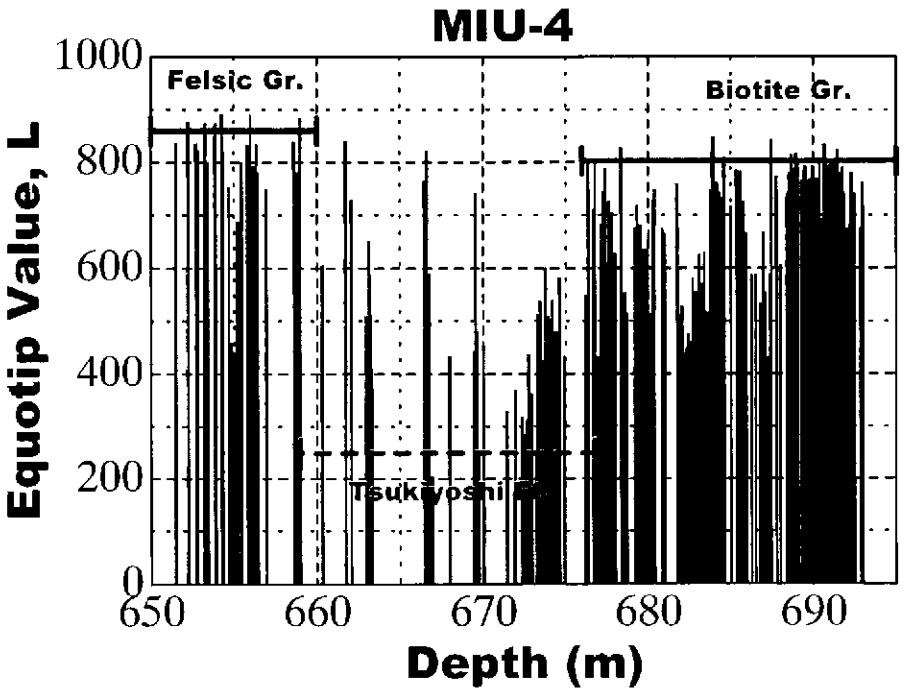

図 10.5.5　MIU-4 での L 値分布　（n=185）

今回の測定結果から、断層破砕帯では広範囲にわたって著しく硬度が低下していると言えると思う。現状では断層破砕帯の決定に多くの時間が費やされているが、測定精度を上げることで、エコーチップ反発硬度試験により短時間で決定が行える可能性が示せたと思う。

10.5.3 逸水割れ目付近（Water Conducting Fractures）

断層破砕帯での結果から、水みちとなっている割れ目付近で硬度の低下が見られないか検討するために、核燃料サイクル開発機構が行った試験により逸水が確認された位置で測定を行った。今回はその中でも大量の逸水が確認された付近で測定を行った。測定間隔は約 50cm である。

逸水箇所

- MIU-1　深度 201m（80％逸水）
- MIU-1　深度 980m（100％逸水）
- MIU-2　深度 223m（100％逸水）

MIU-1（201m）

MIU-1（201m）付近での測定結果を図 10.5.6 に示す。健岩部での L 値の平均値を茶色の線で示した。健岩部での L 値と比較すると逸水割れ目付近で L 値の低下は見られず、逆に高い値となった。深度によって若干 L 値が変化しているように思われる。

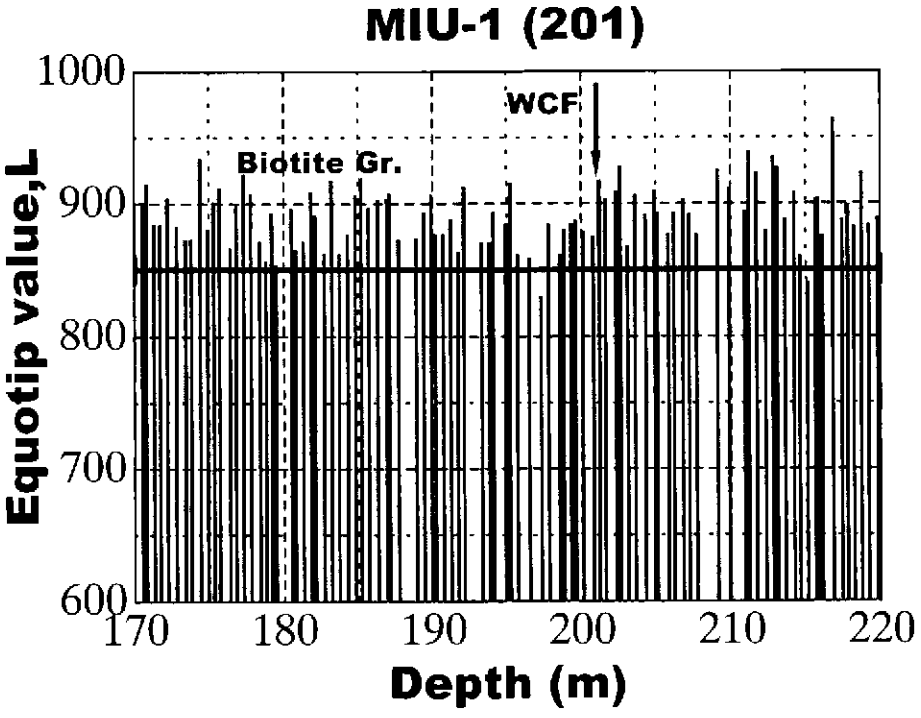

図 10.5.6　MIU-1（201m）付近での L 値分布　（n=95）

MIU-2（223m）

MIU-2（223m）付近での測定結果を図 10.5.7 に示す。グラフに Fr と示した箇所はコアに割れ目が確認された場所である。MIU-1（201m）での測定結果と同様に、逸水割れ目付近での L 値の低下は見られなかった。また健岩部での平均値より高い値となる傾向も見られた。健岩部でのデータは深度 500m 付近のものであるので、浅いところの Granite の方が L 値が大きい可能性があると考えられる。

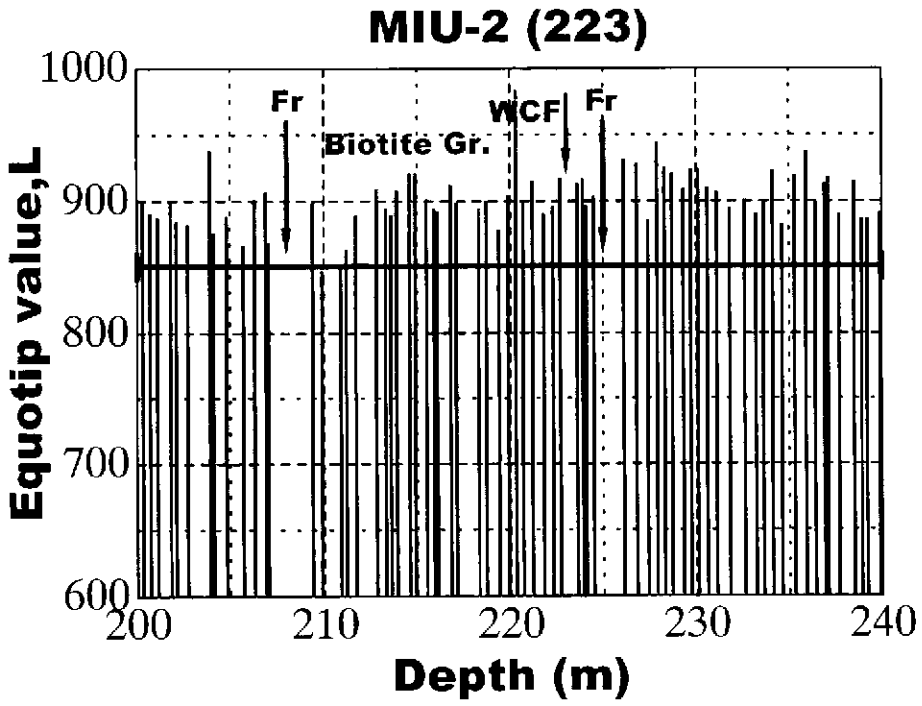

図 10.5.7　MIU-2（223m）付近での L 値分布　（n=70）

MIU-1（980m）

MIU-1（980m）付近での測定結果を図 10.5.8 に示す。前述の浅い場所での結果とは異なり、逸水割れ目付近でＬ値の低下が確認された。しかし、コアの損傷が著しく細かな測定を行うことができなかったため、この結果から逸水割れ目付近で硬度が低下していると判断するのは難しい。

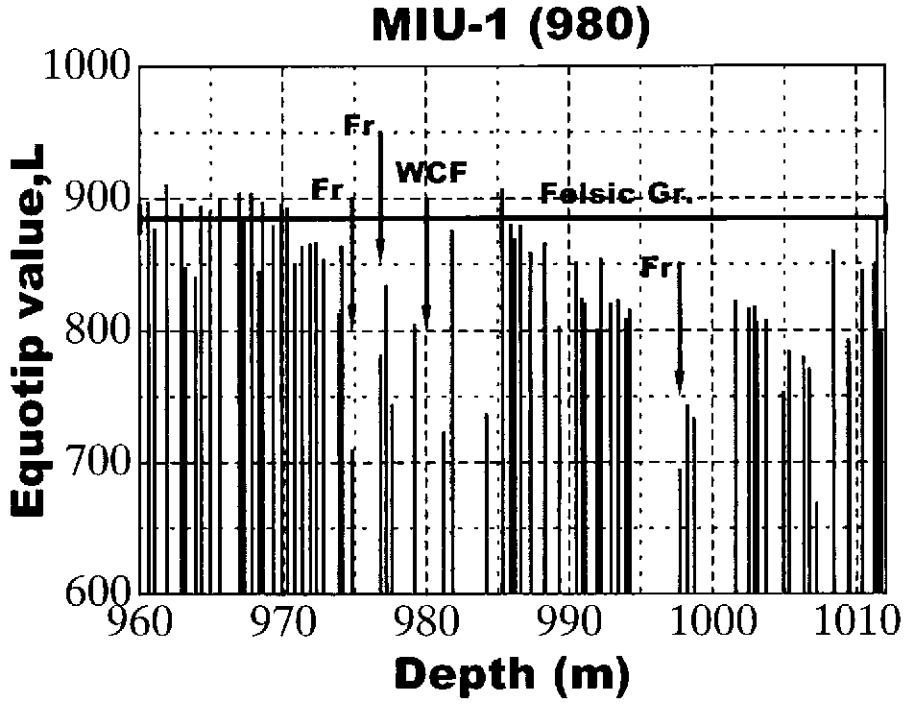

図 10.5.8　MIU-1（980m）付近でのＬ値分布　（n=69）

逸水割れ目付近で岩盤の硬度が低下していないか検討を行ったが、深度の浅いところではそのような結果は見られなかった。しかし、深いところでは硬度が低下している可能性が確認できた。また、浅いところにおいてＬ値が大きくなり、深度の増加に伴ってＬ値が若干ではあるが小さくなる傾向が見られた。

今回行った一連の測定から、エコーチップ反発硬度試験をボーリングコアの全ての深度において行ってみる価値は十分にあるのではないかと思う。

第 11 章　SEM（走査電子顕微鏡）による観察

MIU-3 孔、深度 697.3m（biotite granite）の断層破砕帯内において、条線が確認できた。そこで SEM を使い、より詳しい観察を行った。

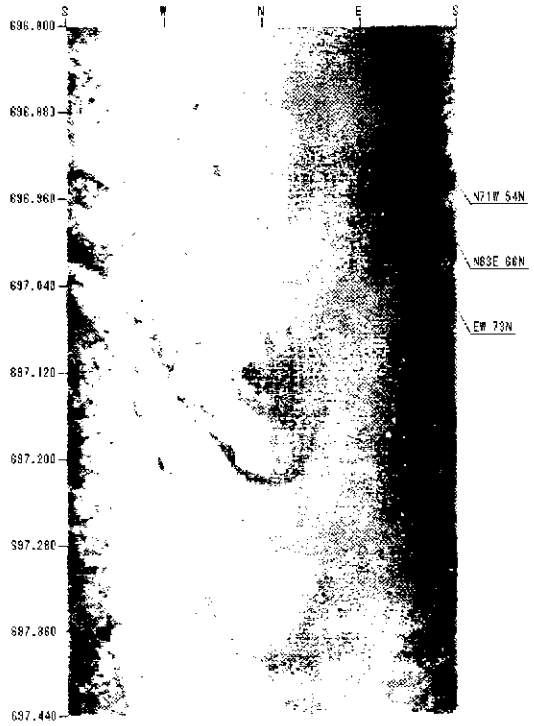

図 11.1　BTV で見た MIU-3 孔 697.3m 付近

図 11.2　MIU-3 孔 697.3m でサンプリングしたコア

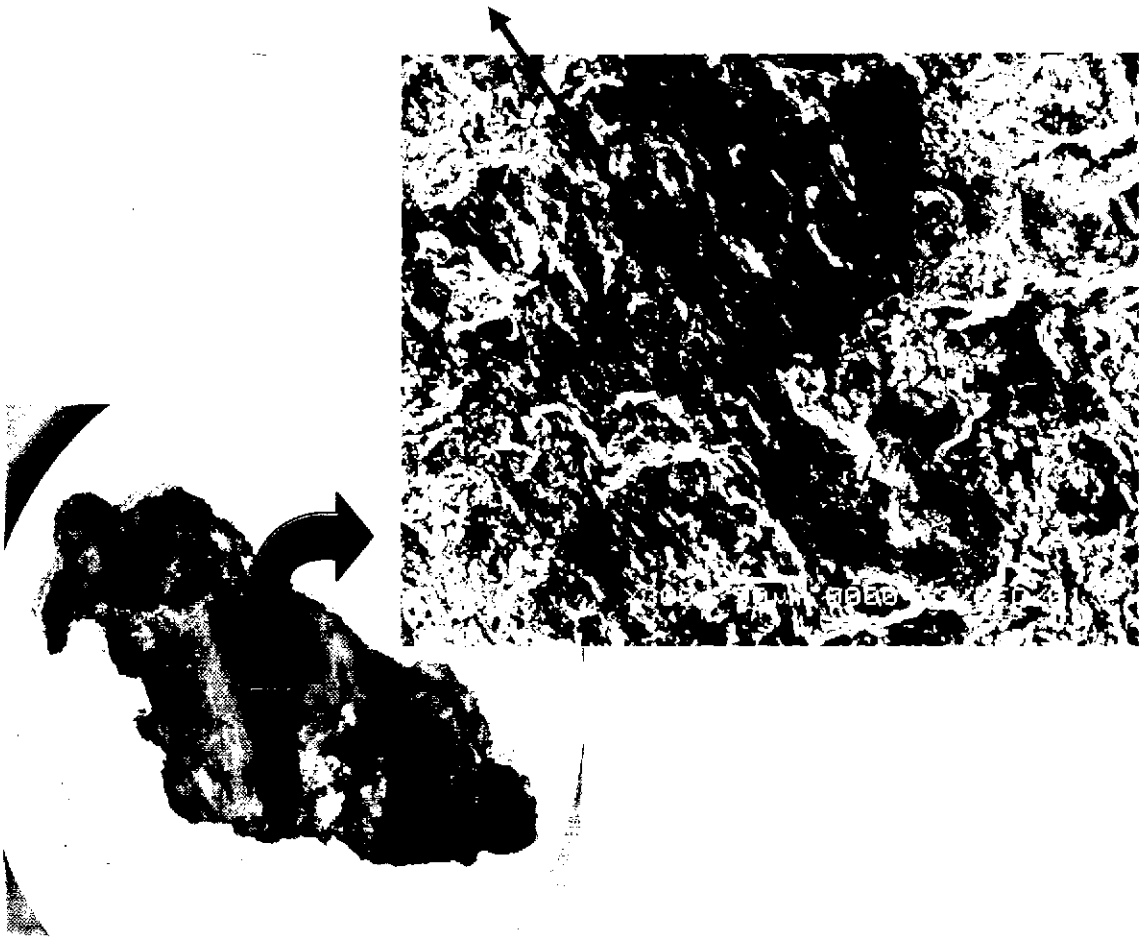

図 11.3　SEM で見た滑り面　(×300)

SEM によって詳しく観察をしてみると、条線の上で図 11.3 のような構造が数カ所確認でき、他では同じような構造は見られなかった。SEM による観察からこの面には Step が確認でき、写真でいうと左上に動いたと思われる。肉眼で確認できた方向と SEM によって見られる方向は一致する。また BTV（図 11.1）から、この滑り面は本研究で取り上げた構造を持った割れ目であることがわかる。したがって BTV 観察から水みちを形成する可能性が高い割れ目を抽出することは可能であると言える。

第12章　結論

1）　本研究で取り上げた構造の割れ目と水みちとなる割れ目とは、関連性があると考えられる。

2）　エコーチップ反撥硬度試験により断層破砕帯の影響範囲を簡便に測定できる可能性が示せた。

3）　深度の増加に伴って若干ではあるが L 値が低下している可能性があると考えられる。

4）　エコーチップ反撥硬度試験をボーリングコアへ行う有用性があると考えられる。

5）　本研究で取り上げた構造の割れ目の中に変位のあるものが確認され、SEM による観察で動いた方向が確認できた。

参考文献

1） 橋本　徹・片川　秀次・村上　弘行：エコーチップ硬さ試験器による岩石材料物性評価の試み：第 33 回地盤工学研究発表会（山口），pp.1231-1232，1998.

2） 大川　哲志・大岡　政雄・船戸　明雄：岩石試料への反発硬度試験機の適用性について：第 29 回岩盤力学に関するシンポジウム講演論文集，pp.256-260，1999.

3） 吉田　昌登・川崎　了・谷本　親伯・舛屋　直：エコーチップ反発硬度試験の岩石材料への適用性：第 30 回岩盤力学に関するシンポジウム講演論文集，pp308-312，2000.

4） 三枝　博光・渡辺　邦夫・大沢　英昭：釜石鉱山での割れ目系特性調査とスプレィ・ステップ構造：土木学会第 50 回年次学術講演会講演概要集，pp710-711，1995.